

# **Impact of cardiac stromal cells on Coxsackievirus B3-induced myocarditis**

vorgelegt von  
M. Sc.  
Muhammad El-Shafeey  
ORCID: 0000-0002-8345-0052

von der Fakultät III - Prozesswissenschaften  
der Technischen Universität Berlin  
zur Erlangung des akademischen Grades

Doktor der Naturwissenschaften  
- Dr. rer. nat.-

genehmigte Dissertation

Promotionsausschuss:

Vorsitzender: Prof. Dr. Juri Rappsilber

Gutachter: Prof. Dr. Jens Kurreck

Gutachter: Prof. Dr. Carsten Tschöpe

Gutachterin: PD Dr. Sophie Van Linthout

Tag der wissenschaftlichen Aussprache: 20. Mai 2019

Berlin 2019

## إهداء

إلى من أحمل اسمه بكل إفتخار..

والذي العزيز رحمه الله وجعل هذا العمل برأ له وفي ميزان حسناته ..

إلى عائلتي الكبيرة في مصر ..

إلى والدي العزيزة أمد الله في عمرها..

إلى سندی إخوتي و أخواتي..

إلى عائلتي الصغيرة في برلين..

إلى زوجتي الحبيبة بيداء وبنتي الحبيبة جويدان وابني الغالي إلياس بارك الله فيهم..

إلى الذين مهدوا لي سبيل العلم..

إلى أساتذتي..

(Dedication in Arabic language)

## Abstract

Myocarditis is an inflammatory cardiac disorder, which is characterized by cardiac inflammation and fibrosis, leading to left ventricular (LV) dysfunction. Most commonly, the inflammatory response of the heart is directed to viruses, of which most research has been done on Coxsackievirus B3 (CVB3). CVB3 can directly damage the cardiomyocytes and leads to the activation of a primary immune response, which can progress to inflammatory cardiomyopathy.

Despite extensive investigations, no specific treatment for myocarditis patients exists up to now. Under conventional heart failure therapy, inflammatory cardiomyopathy typically has a progressive course, indicating the need for alternative therapeutic strategies to improve long-term outcome.

At the Berlin-Brandenburg Center for Regenerative Therapies, a unique cell type has been isolated from human endomyocardial biopsies (EMB): cardiac-derived adherent proliferating cells (CardAPs), further abbreviated as (EMB-CardAPs). EMB-CardAPs are CD90<sup>low</sup> cells, low immunogenic and share many features with mesenchymal stromal cells. They have been proven to exert cardioprotective effects in different murine models of cardiac dysfunction. Though, they have not been compared *in vivo* so far with EMB-cardiac fibroblasts (EMB-CF), which, similar to EMB-CardAPs, are derived from EMB via outgrowth culture, be it in another medium. Furthermore, given the small EMB size, EMB-CardAPs can only be isolated and expanded for autologous use. In view of an allogeneic approach, CardAPs have been isolated from the right atrial appendage (RAA), which allows sufficient cells for the treatment of more than 250 patients. The cardioprotective potential of RAA-CardAPs has not been evaluated so far.

The overarching aim of this study is to get further insights into the cardioprotective potential of CardAPs. The first aim of this study was to further characterize EMB-CardAPs and to compare their cardioprotective potential with EMB-CF from the same patient in acute CVB3-induced myocarditis mice. The second aim of the study was to characterize the cardioprotective features of RAA-CardAPs. Therefore, their cardio(myocyte) protective effects were investigated *in vitro* on CVB3-infected HL-1 cardiomyocytes and *in vivo* in CVB3-induced acute and chronic myocarditis mice.

The first study demonstrated that EMB-CardAPs and EMB-CF improved LV function in mice. However, EMB-CardAPs, but not EMB-CF, reduced LV fibrosis, downregulated the expression of the chemokines CCL2, CCL7 and CX3CL1, decreased LV monocyte presence, reduced

CVB3 mRNA expression and upregulated the ratio of anti-apoptotic Bcl2 towards pro-apoptotic Bax in acute CVB3-induced myocarditis mice.

*In vitro*, the viability of RAA-CardAPs was not reduced by CVB3 and RAA-CardAPs decreased the CVB3-induced apoptosis of HL-1 cardiomyocytes. Following these promising findings, RAA-CardAPs were intravenously administered in acute CVB3-induced myocarditis mice. Similar to EMB-CardAPs, RAA-CardAPs improved systolic and diastolic function in acute CVB3-induced myocarditis mice. RAA-CardAPs reduced LV collagen I as well as the collagen I/collagen III ratio, but did not decrease cardiac inflammation (immune cell presence, chemokine and cytokine expression), nor CVB3 mRNA expression, neither did intravenous RAA-CardAPs application increase the Bcl2/Bax ratio in acute CVB3-induced myocarditis mice.

To assess the cardioprotective potential of RAA-CardAPs in a chronic setting of CVB3 myocarditis, myocarditis was induced with the 31-1-93 CVB3 virus strain in NMRI mice. The chronic stage was characterized by increased LV collagen I protein expression and collagen I/collagen III ratio and upregulated LV presence of immune cells, which was reflected by an impaired LV function. Intravenous application of RAA-CardAPs at day 10 post infection improved LV function, as shown by an increase in the ejection fraction as well as LV contractility in chronic CVB3-induced myocarditis NMRI mice. In parallel, RAA-CardAPs reduced LV collagen I expression and slightly decreased the LV presence of CD68<sup>+</sup> cells in chronic CVB3-induced myocarditis NMRI mice.

We conclude that EMB-CardAPs are unique cells with profound cardioprotective features. Though, the cardioprotective potential of RAA-CardAPs needs to be further explored.

## Zusammenfassung

Myokarditis ist eine entzündliche Herzerkrankung, die durch eine kardiale Entzündung und Fibrose charakterisiert ist, die zu einer linksventrikulären (LV) Dysfunktion führt. In den meisten Fällen, ist die kardiale Entzündungsreaktion auf eine virale Infektion zurückzuführen, wobei die meiste Forschung mit dem Coxsackievirus B3 (CVB3) betrieben wurde. CVB3 kann direkt die Kardiomyozyten schädigen und führt zur Aktivierung des primären Immunsystems, welches zum Fortschreiten der inflammatorischen Kardiomyopathie führen kann.

Trotz intensiver Forschung, gibt es bis lang keine spezifische Behandlung für Myokarditispatienten. Unter einer konventionellen Herzinsuffizienztherapie, hat eine inflammatorische Kardiomyopathie typischerweise einen progressiven Verlauf, wobei diese Tatsache die Notwendigkeit für alternative therapeutische Strategien zeigt, um somit den langfristigen Outcome zu verbessern.

Am Berlin-Brandenburg Centrum für Regenerative Therapien wurde ein einzigartiger Zelltyp aus humanen endomyokardialen Biopsien (EMB) isoliert: cardiac-derived adherent proliferating cells (CardAPs), weiter abgekürzt als (EMB-CardAPs). EMB-CardAPs sind CD90<sup>low</sup> Zellen, mit einer niedrigen Immunogenität und sie teilen viele Eigenschaften mit den mesenchymalen stromalen Zellen. In zahlreichen murinen Modellen mit kardialer Dysfunktion wurde deren kardioprotektive Eigenschaften nachgewiesen. Jedoch, wurden sie noch keinem *in vivo* Vergleich mit den EMB-kardialen Fibroblasten (EMB-CF) unterzogen, die ebenfalls, wie die EMB-CardAPs, mittels einer Auswuchskultur aus EMBs gewonnen werden, sei es nun in einem anderen Medium. Weiterhin können die EMB-CardAPs, aufgrund der kleinen Größe der EMBs, nur für den autologen Gebrauch isoliert und expandiert werden. Im Hinblick auf eine allogene Anwendung, wurden CardAPs aus dem rechten Vorhofanhang (right atrial appendage (RAA)) isoliert, mit ausreichender Zellanzahl, um mehr als 250 Patienten zu behandeln. Das kardioprotektive Potenzial von RAA-CardAPs wurde bislang noch nicht untersucht.

Das übergreifende Ziel dieser Studie ist, weitere Einblicke in das kardioprotektive Potential der CardAPs zu erhalten. Das erste Ziel der Studie war es, die EMB-CardAPs weiter zu charakterisieren und deren kardioprotektives Potential mit den EMB-CF, vom selben Patienten stammend, in CVB3 induzierten Myokarditis Mäusen zu vergleichen. Das zweite Ziel der Studie war es, die kardioprotektiven Eigenschaften von RAA-CardAPs zu charakterisieren. Dafür wurden deren kardio(myozyten)protektiven Effekte *in vitro* an CVB3 infizierten HL-1 Kardiomyozyten und *in vivo* in CVB3 induzierten akuten und chronischen Myokarditis Mäusen untersucht.

Die erste Studie zeigte, dass die EMB-CardAPs und EMB-CF die LV Funktion in den Mäusen verbesserten. Wobei, EMB-CardAPs jedoch nicht EMB-CF, die LV Fibrose reduzierten, die Expression der Chemokine CCL2, CCL7 und CX3CL1 runter regulierten, die LV Präsenz von Monozyten reduzierten, die CVB3 mRNA Expression verringerten und die Ratio vom anti-apoptotischen Bcl2 gegenüber dem pro-apoptotischen Bax in CVB3 induzierten Myokarditis Mäusen reduzierten.

*In vitro* war die Lebensfähigkeit von RAA-CardAPs durch CVB3 nicht reduziert und RAA-CardAPs reduzierten die CVB3 induzierte Apoptose von HL-1 Kardiomyozyten. Basierend auf diesen vielversprechenden Ergebnissen, wurden die RAA-CardAPs folglich in CVB3 induzierte Myokarditis Mäuse intravenös appliziert. Ähnlich wie die EMB-CardAPs, verbesserten RAA-CardAPs die systolische und diastolische kardiale Funktion in CVB3 induzierten Mäusen. RAA-CardAPs verminderten das LV Collagen I, sowie die Collagen I/Collagen III Ratio, jedoch wurde weder die kardiale Entzündung (Immunzellpräsenz, Chemokin -und Zytokinexpression) und die CVB3 mRNA Expression reduziert, noch wurde die Bcl2/Bax Ratio erhöht durch die intravenöse Applikation von RAA-CardAPs in akuten CVB3 induzierten Myokarditis Mäusen.

Um das kardioprotektive Potenzial von RAA-CardAPs im Rahmen einer chronischen CVB3 Myokarditis zu untersuchen, wurde eine Myokarditis mit dem 31-1-93 CVB3 Virusstamm in NMRI Mäusen induziert. Das chronische Stadium wurde an Hand einer erhöhten LV Collagen I Protein Expression charakterisiert, sowie einer erhöhten Collagen I/Collagen III Ratio und einer hochregulierten LV Präsenz von Immunzellen, welches durch eine verschlechterte LV Funktion wiedergespiegelt wurde. Eine intravenöse Applikation von RAA-CardAPs an Tag 10 nach der Infektion verbesserte die LV Funktion, dargestellt an Hand einer Erhöhung der Ejektionsfraktion und der LV Kontraktilität in chronischen CVB3 infizierten NMRI Mäusen. Gleichzeitig reduzierten die RAA-CardAPs die LV Collagen I Expression und erniedrigten leicht die LV Präsenz von CD68<sup>+</sup> Zellen in chronischen CVB3 induzierten Myokarditis NMRI Mäusen.

Wir schließen daraus, dass EMB-CardAPs einzigartige Zellen mit umfassenden kardioprotektiven Eigenschaften sind. Jedoch bedarf das kardioprotektive Potential von RAA-CardAPs weiterer Untersuchungen.

## Table of contents

Table of contents .....	v
Abbreviations .....	ix
1. Introduction .....	1
1.1 Cardiovascular diseases .....	1
1.2 Myocarditis .....	1
1.2.1 Definition .....	1
1.2.2 Epidemiology of myocarditis .....	1
1.2.3 Etiology of myocarditis .....	2
1.2.4 Pathophysiology of Coxsackievirus B3-induced myocarditis .....	2
1.3 Acute myocarditis .....	3
1.4 Chronic myocarditis .....	4
1.5 Dilated cardiomyopathy: .....	5
1.6 Treatment of myocarditis .....	5
1.7 Cell therapy for non-ischemic heart failure .....	6
1.8 Mesenchymal stromal cells .....	6
1.9 Human Cardiac-Derived Adherent Proliferating Cells in cardiomyopathy .....	7
1.9.1 Endomyocardial biopsy-derived cardiac adherent proliferating cells .....	7
1.9.2 Right atrial appendage-derived cardiac adherent proliferating cells .....	10
2. Aim of the study .....	12
3. Materials and methods .....	13
3.1 Materials .....	13
3.2 Methods .....	21
3.2.1 Cardiac cells isolation and culture .....	21
3.2.1.1 Endomyocardial biopsy-derived cardiac adherent proliferating cells .....	21
3.2.1.2 Endomyocardial biopsy-derived cardiac fibroblasts .....	21
3.2.1.3 Right atrial appendage-derived cardiac adherent proliferating cells .....	21
3.2.1.4 Evaluation of impact of Coxsackievirus B3 infection on viability of right atrial appendage-derived cardiac adherent proliferating cells .....	22
3.2.1.5 Evaluation of cardiomyocyte-protective potential of RAA-CardAPs .....	23
3.2.1.5.1 Co-culture of RAA-CardAPs with DiO-labeled HL-1 cardiomyocytes .....	23
3.2.1.5.2 Annexin V/7AAD flow cytometry .....	23
3.2.2 Experimental design of <i>in vivo</i> experiments .....	24
3.2.2.1 Evaluation of intravenous application of endomyocardial biopsy-derived cardiac adherent proliferating cells versus endomyocardial biopsy-derived cardiac fibroblasts in acute Coxsackievirus B3 myocarditis mice .....	24
3.2.2.2 Evaluation of intravenous application of right atrial appendage-derived cardiac adherent proliferating cells in acute Coxsackievirus B3 myocarditis mice .....	25

3.2.2.3	Assessment of the chronic Coxsackievirus B3 myocarditis mouse model .....	25
3.2.2.4	Evaluation of intravenous application of right atrial appendage-derived cardiac adherent proliferating cells in chronic Coxsackievirus B3 myocarditis mice .....	26
3.2.3	Measurement of hemodynamic parameters using the PV loop method .....	26
3.2.3.1	Principle.....	26
3.2.3.2	Preparation .....	27
3.2.3.3	Anesthesia.....	28
3.2.3.4	Mechanical ventilation .....	28
3.2.3.5	Surgical procedure.....	28
3.2.3.6	Data acquisition .....	29
3.2.4	Total ribonucleic acid isolation and DNase treatment .....	31
3.2.4.1	RNA isolation .....	31
3.2.4.2	DNase treatment.....	32
3.2.5	Reverse transcription .....	33
3.2.6	Real-time PCR .....	33
3.2.7	Immunohistochemistry .....	35
3.2.7.1	Background.....	35
3.2.7.2	Tissue cutting using cryostat .....	35
3.2.7.3	Immunohistochemistry .....	36
3.2.7.3.1	The Avidin-Biotin Complex .....	36
3.2.7.3.2	The Envision™ method.....	37
3.2.8	Statistical analysis.....	38
4.	Results .....	39
4.1.	Comparison of EMB-CardAPs versus EMB-cardiac fibroblasts in acute Coxsackievirus B3-induced myocarditis mice .....	39
4.1.1.	EMB-CardAPs and EMB-Cardiac fibroblasts improve the systolic and diastolic function in acute Coxsackievirus B3-induced myocarditis mice .....	39
4.1.2.	EMB-CardAPs but not EMB-cardiac fibroblasts reduce left ventricular fibrosis in acute Coxsackievirus B3-induced myocarditis mice.....	40
4.1.3.	EMB-CardAPs but not EMB-cardiac fibroblasts modulate left ventricular chemokine mRNA expression in acute Coxsackievirus B3-induced myocarditis mice .....	42
4.1.4.	EMB-CardAPs but not EMB-cardiac fibroblasts reduce left ventricular mRNA levels of chemokine receptors in acute Coxsackievirus B3-induced myocarditis mice.....	43
4.1.5.	EMB-CardAPs but not EMB-cardiac fibroblasts reduce left ventricular monocyte and pro-inflammatory cell presence in acute Coxsackievirus B3-induced myocarditis mice .....	43
4.1.6.	EMB-CardAPs but not EMB-Cardiac fibroblasts reduce left ventricular mRNA levels of inflammatory cytokines in acute Coxsackievirus B3-induced myocarditis mice...45	45
4.1.7.	EMB-CardAPs but not EMB-cardiac fibroblasts modulate markers of left ventricular apoptosis in acute Coxsackievirus B3-induced myocarditis mice .....	46
4.1.8.	EMB-CardAPs but not EMB-cardiac fibroblasts reduce left ventricular Coxsackievirus B3 mRNA expression in acute Coxsackievirus B3-induced myocarditis mice.....	46

4.2.	<i>In vitro</i> evaluation of RAA-CardAPs.....	48
4.2.1.	Impact of Coxsackievirus B3 infection on the viability of RAA-CardAPs.....	48
4.2.2.	Impact of RAA-CardAPs on apoptosis of Coxsackievirus B3-infected HL-1 cardiomyocytes.....	48
4.2.3.	Impact of RAA-CardAPs on CVB3 mRNA expression in HL-1-RAA-CardAPs co-culture.....	49
4.3.	Allogenic CardAPs in acute Coxsackievirus B3-induced myocarditis mice .....	50
4.3.1.	RAA-CardAPs improve left ventricular function in acute Coxsackievirus B3-induced myocarditis mice .....	50
4.3.2.	RAA-CardAPs reduce left ventricular fibrosis in acute Coxsackievirus B3-induced myocarditis mice .....	51
4.3.3.	RAA-CardAPs did not change the left ventricular chemokine mRNA expression in acute Coxsackievirus B3-induced myocarditis mice .....	52
4.3.4.	RAA-CardAPs have no effect on the expression of left ventricular chemokine receptors in acute Coxsackievirus B3-induced myocarditis mice.....	52
4.3.5.	RAA-CardAPs had no effect on the left ventricular immune cell presence- in acute Coxsackievirus B3-induced myocarditis mice.....	53
4.3.6.	RAA-CardAPs did not modulate left ventricular mRNA levels of pro- and anti-inflammatory and anti-viral cytokines in acute Coxsackievirus B3-induced myocarditis mice .....	55
4.3.7.	RAA-CardAPs did not change the left ventricular mRNA expression of markers of cardiac apoptosis in acute Coxsackievirus B3-induced myocarditis mice.....	56
4.3.8.	RAA-CardAPs did not change the left ventricular Coxsackievirus B3 mRNA expression in acute Coxsackievirus B3-induced myocarditis mice .....	56
4.4.	Assessment of the chronic Coxsackievirus B3-induced myocarditis model .....	58
4.4.1.	Coxsackievirus B3 infection of NMRI mice impairs left ventricular function at day 28 post infection.....	58
4.4.2.	Coxsackievirus B3 infection of NMRI mice leads to left ventricular fibrosis at day 28 post infection.....	58
4.4.3.	Coxsackievirus B3 infection of NMRI mice does not change the left ventricular chemokine mRNA expression at day 28 post infection.....	59
4.4.4.	Coxsackievirus B3 infection of NMRI mice modulates left ventricular mRNA expression of chemokine receptors at day 28 post.....	60
4.4.5.	Coxsackievirus B3 infection of NMRI mice increases left ventricular monocyte and pro-inflammatory cell presence at day 28 post infection .....	61
4.4.6.	Coxsackievirus B3 infection of NMRI mice induces left ventricular inflammation at day 28 post infection.....	62
4.4.7.	Coxsackievirus B3 infection of NMRI mice does not change left ventricular mRNA expression of factors indicative for cardiac apoptosis at day 28 post infection .....	63
4.4.8.	Coxsackievirus B3 infection of NMRI mice is associated with low Coxsackievirus B3 mRNA expression at day 28 post infection.....	63
4.5.	Allogenic CardAPs in chronic Coxsackievirus B3-induced myocarditis mice .....	65
4.5.1.	RAA-CardAPs moderately improve left ventricular function in chronic Coxsackievirus B3-induced myocarditis mice .....	65
4.5.2.	RAA-CardAPs reduced left ventricular fibrosis in chronic Coxsackievirus B3-induced myocarditis mice .....	66

4.5.3.	RAA-CardAPs did not change the left ventricular chemokine mRNA expression in chronic Coxsackievirus B3-induced myocarditis mice .....	66
4.5.4.	RAA-CardAPs have no effect on the left ventricular mRNA expression of chemokine receptors in chronic Coxsackievirus B3-induced myocarditis mice .....	67
4.5.5.	RAA-CardAPs reduce the left ventricular presence of monocytes in chronic Coxsackievirus B3-induced myocarditis mice.....	68
4.5.6.	RAA-CardAPs modulate the left ventricular mRNA levels of cytokines in chronic Coxsackievirus B3-induced myocarditis mice.....	69
4.5.7.	RAA-CardAPs did not change left ventricular mRNA expression of factors indicative for cardiac apoptosis in chronic Coxsackievirus B3-induced myocarditis mice .....	70
4.5.8.	RAA-CardAPs did not affect left ventricular Coxsackievirus B3 mRNA expression in chronic Coxsackievirus B3-induced myocarditis mice .....	70
5.	Discussion.....	72
5.1.	EMB-CardAPs versus EMB-CF in acute Coxsackievirus B3-induced myocarditis mice .....	72
5.2.	RAA-CardAPs in acute Coxsackievirus B3-induced myocarditis mice .....	75
5.3.	Assessment of the chronic Coxsackievirus B3-induced myocarditis model .....	78
5.4.	RAA-CardAPs in chronic Coxsackievirus B3-induced myocarditis mice .....	79
6.	References.....	81
7.	List of Figures.....	90
8.	List of Tables.....	93
9.	Complete list of publications.....	94
10.	Acknowledgments .....	96
11.	Declaration.....	97

## Abbreviations

Abbreviation	Explanation
ABC	avidin-biotin complex
bFGF	basic fibroblast growth factor
BSA	bovine serum albumin
BW	body weight
CAR	Coxsackie- and adenovirus receptor
CardAPs	cardiac-derived adherent proliferating cells
CF	Cardiac fibroblast
CSC	cardiac stem cells
CVB3	coxsackievirus B3
CVD	cardiovascular disease
DAF	decay accelerating factor
DCM	dilated cardiomyopathy
ECM	extra cellular matrix
EF	ejection fraction
EGF	epidermal growth factor
EMB	endomyocardial biopsy
EPC	endothelial progenitor cells
FBS	fetal bovine serum
HLA	human leukocyte antigen
HSC	human hematopoietic stem cells
i.p.	intraperitoneal(ly)
i.v.	intravenous(ly)
IFN- $\beta$	interferon-beta
IFN- $\gamma$	interferon-gamma
IHC	immunohistochemistry
IL	Interleukin
LAS	Leica Application Suite
LV	left ventricular
MSCs	mesenchymal stem cells

NMRI	Naval Medical Research Institute
NO	nitric Oxide
p.f.u.	plaque forming units
PCR	polymerase chain reaction
TBS	tris buffered saline
TGF- $\beta$	transforming growth factor- $\beta$
TNF- $\alpha$	tumor necrosis factor-alpha
Treg	T regulatory
VCAM1	vascular cell adhesion molecule1
VEGF	vascular endothelial growth factor
VMC	viral myocarditis
WHO	World health organization

## **1. Introduction**

### **1.1 Cardiovascular diseases**

People, who experience symptoms like chest pain or discomfort that don't go away after a few minutes, are suspected to have cardiovascular disease (CVD). CVDs include coronary heart disease, cerebrovascular disease, peripheral arterial disease, and congenital heart diseases<sup>1</sup>. CVDs are considered the first cause of death worldwide<sup>2</sup>. They are much higher in many of the developing countries of Asia, Africa and South America than in those developed ones of Europe, North America and Australia<sup>3</sup>. CVDs are responsible for the death of an estimated over 17 million until 2017, according to the world health organization (WHO)<sup>4</sup>. Near half a million of these patients are affected by myocarditis, of which 30% may develop a dilated cardiomyopathy (DCM)<sup>5</sup>.

### **1.2 Myocarditis**

#### **1.2.1 Definition**

Myocarditis is a heart disease associated with inflammation and injury of the myocardium, necrosis and degeneration of cardiomyocytes, caused by different infectious and non-infectious agents, but the main studied trigger is coxsackievirus<sup>6</sup>. When the disease is associated with virus persistence, it is defined as viral cardiomyopathy<sup>5</sup>.

#### **1.2.2 Epidemiology of myocarditis**

Viral myocarditis (VMC) can happen in different age groups, from infants to adults, but it mainly occurs in children and adults under the age of 40, with approximately one third of patients being between 10 and 30 years old. Due to the variety of VMC viruses and their epidemic law, there are differences in the main viruses of different regions and in different years within the same region. Lack of virological examinations resulted in few representatives, high-value epidemiological reports, while the exact incidence and prevalence of VMC are still unknown<sup>7</sup>.

Myocarditis usually results from infectious agents such as viruses including enteroviruses especially coxsackievirus B3 (CVB3)<sup>8</sup>, adenoviruses<sup>9</sup>, and parvovirus B19<sup>10</sup>, or non-viral protozoan *Trypanosoma cruzi* (Chagas disease)<sup>11</sup> or *Toxoplasma gondii*<sup>12</sup>.

### 1.2.3 Etiology of myocarditis

The cardiotropic CVB3 is the dominant studied etiological agent, which could be detected, either by analysis of serum or using molecular techniques such as the polymerase chain reaction (PCR)<sup>13</sup>. There is a temporal variation in the most common pathogens that lead to myocarditis. For long time ago (**Figure 1.1.**), enteroviruses were the prevalent viruses involved in myocarditis, especially coxsackievirus<sup>14</sup>.

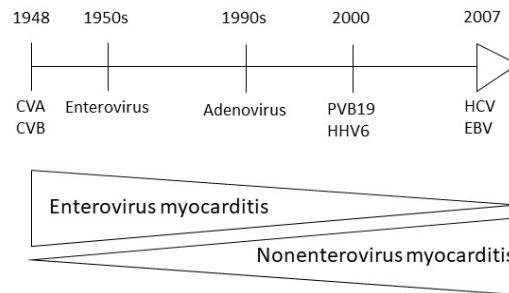


**Figure 1.1. Development of viral causes of myocarditis over time.** CVA = Coxsackievirus A; CVB = Coxsackievirus B; EBV = Epstein-Barr virus; HCV = hepatitis C virus; HHV6 = human herpesvirus 6; PV-B19 = parvovirus B19 (Schultz et al.<sup>15</sup>).

Myocarditis is characterized by cardiac inflammation<sup>16</sup> and fibrosis<sup>17</sup>, leading to left ventricular (LV) dysfunction. Other forms of myocarditis also have been reported including, eosinophilic myocarditis which is characterized by the presence of eosinophils in the histology and is clinically supposed to be caused by hypersensitivity to some drugs<sup>18</sup>, and giant cell myocarditis, which is associated with high inflammation and necrosis<sup>19</sup>.

### 1.2.4 Pathophysiology of Coxsackievirus B3-induced myocarditis

CVB3 uses two main receptors on the membrane of invaded cells to complete its productive infectious cycle. The first one functions as a primary attachment protein, which is called decay accelerating factor (DAF), whereas the second one functions as an internalization receptor, which is named Coxsackie- and adenovirus receptor (CAR)<sup>20</sup>. The underlying pathology in viral myocarditis results from the common work between viral processes of propagation and the host immune responses trying to resist and fight against the virus. Infection of the myocardial tissue by CVB3 develops in three stages (**Figure 1.2.**)<sup>20</sup>. When cardiomyocytes get infected with the virus, type 1 interferons are secreted, and cardiomyocytes go to death by apoptosis<sup>21</sup>. In the second stage of viral entry and the activation of primary immune responses, different immune mediators are released which trigger the third phase, as represented by cellular infiltrates<sup>22</sup>. Both innate and adaptive immune responses are crucial indications of the severity of myocardial damage, often associated with autoimmune responses to the cardiac tissue antigens<sup>23</sup>. The overwhelming immune response contributes to the development of chronic

myocarditis and DCM, a condition for which the only treatment option at end-stage is heart transplantation<sup>24</sup>.

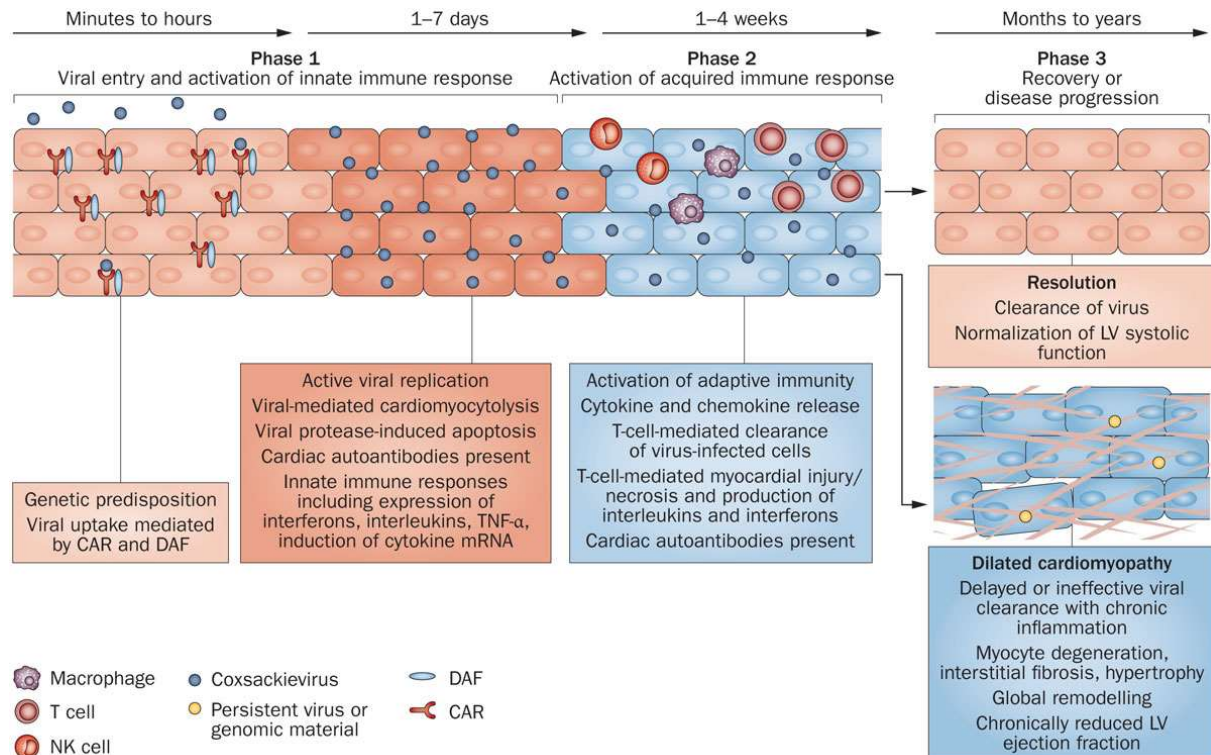


**Figure 1.2. Different phases of Coxsackievirus-mediated myocarditis.** Phase 1 starts with the viral entry into the cell and transit to the myocardium using the DAF and CAR receptors. When the virus enters the cell, it triggers the innate immune response in the first week. The cells start the lysis process due to virus replication and consequently release cytokines. In phase 2, both innate and adapted responses are present in the autoimmune-mediated injury, including the recruitment of the first lineage of the immune cells, i.e. NK cells, monocytes and T cells, which increased markedly in the second week showing the most severe phase of the disease. In phase 3, when the viral load decreases, some individuals show complete clearance of the virus. However, the viral genome persists in other patients (from Pollack *et al.*<sup>20</sup>).

### 1.3 Acute myocarditis

The diagnosis of the disease may be suspected by clinical and non-invasive measurements. However, the endomyocardial biopsy (EMB), using histopathologic criteria, is the gold standard for diagnosing myocarditis<sup>6</sup>. Acute myocarditis manifests with different clinical presentations, ranging from chest pain or mild dyspnea to acute cardiogenic shock<sup>25</sup>. Studying viral myocarditis in animal models facilitated the understanding of the underlying mechanism of the disease. The CVB3 mouse model is considered the most common model to investigate the different stages of myocarditis<sup>26</sup>.

Acute viral myocarditis is characterized by necrosis or fibrosis associated with cellular infiltrates including T cells of CD4<sup>+</sup> and CD8<sup>+</sup> surface markers, monocytes, natural killer cells, dendritic cells and mast cells<sup>17</sup>. There is growing evidence that T helper cells, monocytes/macrophages and B cells get infected during the viral phase, which suggests

incidental transport of virus particles into organs and subsequent infection of the resident cells<sup>27</sup>. It was reported in different induced myocarditis transgenic mice models that there is an increase in the gene expression of pro- and anti-inflammatory cytokines, which could be observed in the acute phase after 3-4 days post infection<sup>28</sup>.

In acute myocarditis, many cytokines are secreted as an acquired immune response. These inflammatory cytokines in patients with cardiac dysfunction were first described in 1990<sup>29</sup>. The most common and relevant pro-inflammatory cytokine, associated with inflammatory heart disease, is tumor necrosis factor-alpha (TNF- $\alpha$ ). The expression of high concentrations of TNF- $\alpha$  in the blood of patients with congestive heart failure has been confirmed by some clinical studies<sup>30</sup>. Beyond TNF- $\alpha$ , also interleukin (IL)-1 $\beta$  and IL-10 are increased in myocarditis as follows from both clinical and pre-clinical studies<sup>31-33</sup>.

Another main feature indicated in acute myocarditis is fibrosis, which is attributed to the production of the pro-fibrotic transforming growth factor (TGF)- $\beta$ , the proliferation of fibroblasts and subsequent the secretion of collagen<sup>34</sup>. Collagen is the most abundant element of the extracellular matrix of the cardiac tissue. There are no less than eighteen different forms of collagen of which five types (I, III, IV, V and VI) have been identified in the myocardial region<sup>35</sup>. The main components are type I and type III, sharing around 75% and 15% of total collagen, respectively<sup>36</sup>. The collagen network present in the myocardial tissue is important for the mechanical movement of the cardiac muscle, in both systolic and diastolic processes<sup>37</sup>. There are clear evidences of elevated collagen in acute myocarditis animal models<sup>17</sup>.

#### **1.4 Chronic myocarditis**

In some cases of viral myocarditis, if the host does not eliminate the virus successfully, a chronic disease develops. Moreover, the inflammation can be detected even though the infectious agent has been eradicated<sup>38</sup>. According to the Dallas criteria<sup>39</sup>, the chronic stage of viral myocarditis is characterized by chronic inflammation and sometimes by accumulation of collagen in cardiac tissue, i.e. fibrosis which may lead to heart dysfunction and may progress to DCM<sup>40</sup>. To understand the underlying molecular mechanisms of chronic viral myocarditis, researchers established different experimental animal models using the CVB3 virus at different end time points, i.e. 28 days<sup>41</sup>, 31 days<sup>42</sup>, 34 days<sup>43</sup>, 35 days<sup>44</sup>, 45 days<sup>45</sup>, 56 days<sup>40</sup>, and 70 days<sup>46</sup>.

In an experimental murine model, it has been shown that acute CVB3 myocarditis leads to chronic myocardial damage<sup>47</sup>. In another experiment, three mice strains have been used to investigate the chronic development of viral myocarditis. All animals clearly showed cardiac

inflammation at day 56 post infection, with no detectable virus in the cardiac tissue<sup>48</sup>. However, with the advent of the PCR technology, studies on the human myocardium did show evidence that the infectious agent was detectable in chronic myocarditis<sup>49</sup>.

Different murine models of induced CVB3 chronic myocarditis explained the pathogenesis of clinical chronic myocardial injury<sup>50</sup>. The direct injury to the cardiac cells due to viral infection on the one hand and the autoimmune response triggered by the initial infection on the other hand, are supposed to be the pathophysiological mechanism of chronic myocarditis<sup>42</sup>. However, the exact mechanism underlying this process still needs to be examined.

### **1.5 Dilated cardiomyopathy:**

DCM is one of the most known causes of heart failure, associated with the main mortality rate of cardiomyopathy<sup>51</sup>. Although the application of conventional heart failure therapy has led to an improved death rate, only half of the patients survive within five years after diagnosis<sup>52</sup>.

### **1.6 Treatment of myocarditis**

No specific treatment for myocarditis patients exists up to now. Though, extensive investigations of therapeutic perspectives have been performed<sup>21</sup>. Typically, myocarditis patients are treated with conventional heart failure therapy:  $\beta$ -blockers, diuretics, angiotensin converting enzyme inhibitors or angiotensin-receptor blockers<sup>21</sup>. In addition, three to six months' abstinence from competitive sports after myocarditis diagnosis is recommended by expert consensus to decrease risk of remodeling and sudden death<sup>53</sup>.

Treatment of myocarditis patients depends on the medical situation and the presence or absence of inflammation and viral infection in the EMB<sup>21, 54</sup>. Immunosuppressive agents have been/are used for the treatment of patients with high cardiac inflammation and idiopathic DCM with no viral infection<sup>54, 55</sup>. However, for viral-positive patients, antiviral agents like interferon-beta (IFN- $\beta$ ), have been shown to eradicate the enterovirus<sup>21</sup>.

Other therapeutic options for the treatment of myocarditis, including anti-inflammatory drugs such as colchicine and canakinumab, or cell therapy such as the use of MSCs<sup>6</sup> are in preclinical evaluation or are entering clinical trials. Novel therapeutics have been tested for the treatment of cardiovascular disorders, such as the immunomodulatory compound paquinimod and the IL-1 receptor antagonist anakinra. However, the potential of those drugs has not been investigated so far in the context of viral myocarditis<sup>6</sup>.

## 1.7 Cell therapy for non-ischemic heart failure

Cardiomyocytes rarely regenerate<sup>56</sup>, so it was a challenge to find a kind of cell, which can differentiate into cardiomyocytes or to repair the impaired cardiac tissue, or to find cells, which have a cardioprotective effect. The use of cell therapy for treating heart failure emerged three decades ago<sup>57</sup>. However, it has only been used for non-ischemic cardiomyopathy since the late 1990s<sup>58</sup> and in the beginning of the 21<sup>st</sup> century<sup>59</sup>. In view of finding a cell therapy to improve cardiac function, scientists have used many different cell sources and different routes for administration in different animal models<sup>57</sup>.

For the treatment of ischemic and non-ischemic cardiomyopathy models<sup>60, 61</sup>, cells of cardiac origin<sup>62</sup>, bone marrow mesenchymal stromal cells<sup>63</sup>, adipose mesenchymal stromal cells<sup>64</sup>, bone marrow mononuclear cells<sup>64</sup>, human umbilical cord-derived mesenchymal stromal cells<sup>65</sup> and the novel recent cell type, human cardiac-derived adherent proliferating cells (CardAPs)<sup>66</sup>, which share most of the mesenchymal stromal cell characteristics, have been used.

Our laboratory investigated the beneficial effect of different cell types for heart diseases in different experimental models. In a murine model of CVB3-induced myocarditis, MSCs improved the injured cardiac tissue when injected intravenously (i.v.) one day after the CVB3 infection<sup>63</sup>. Similarly, i.v. injection of CardAP cells also improved cardiac function in acute CVB3-induced myocarditis mice<sup>66</sup>. Savvatis and his colleagues<sup>67</sup> compared the administration of MSCs versus human cardiac fibroblasts (CF) in a murine model of acute myocarditis and they concluded that MSCs had a beneficial effect on the impaired heart function via immunomodulatory and anti-apoptotic effects, but not the CFs. Further evaluation of MSCs application in acute CVB3-induced myocarditis mice illustrated a MSC-mediated suppression of pro-inflammatory monocytes infiltration in the heart<sup>68</sup> and a reduction in the activation of cardiac and systemic (NOD)-like receptor pyrin domain-containing 3 (NLRP3) inflammasome, which is assumed to play an important role in the pathogenesis of acute myocarditis<sup>69</sup>.

The therapeutic effect of the T regulatory (Treg) cells, which were formerly known as T suppressor cells, in CVB3-induced acute myocarditis model has been investigated. Adoptive transfer of Treg in the viral acute phase showed an improvement in cardiac function involving the reduction in inflammatory damage and fibrosis<sup>70</sup>.

## 1.8 Mesenchymal stromal cells

MSCs are multipotent stem cells, which are present in adult tissue and have the ability to differentiate into different cell lineages of mesenchymal origin, including cardiomyocytes<sup>71</sup>. Besides their multilineage potential, main characteristics of MSCs are: 1) their adherence and

growth to plastic and 2) their expression of the surface markers CD44, CD73, CD90, CD105, CD106, CD166 and Stro-1, but negativity for the hematopoietic markers such as CD45, CD34, and CD14<sup>72</sup>.

MSCs can be isolated from many adult tissues including adipose tissue<sup>65</sup>, placenta<sup>73</sup>, heart<sup>74</sup>, but their main source of isolation is the bone marrow<sup>75</sup>. MSCs are distinguished by their simple isolation, tendency of expansion and their unique low immunogenicity, which allows their allogenic use for tissue repair<sup>76</sup>.

Besides their ability to differentiate into cardiomyocytes<sup>77-79</sup>, MSCs are particularly known for their paracrine, cardioprotective effects. MSCs secrete a variety of angiogenic<sup>80</sup>, anti-apoptotic<sup>63, 81</sup>, anti-fibrotic<sup>67, 82</sup>, and proangiogenic<sup>83</sup> factors. The cardioprotective potential of MSCs follows from a plethora of experimental studies in models of myocardial infarction<sup>84</sup>, viral myocarditis<sup>63, 68, 85</sup>, autoimmune myocarditis<sup>86</sup>, diabetic cardiomyopathy<sup>87</sup>, and non-ischemic dilated cardiomyopathy<sup>88, 89</sup>, showing improvement in cardiac dysfunction after MSCs application. Related to myocarditis and non-ischemic DCM, MSCs have been shown to improve cardiac function in preclinical and clinical trials<sup>88</sup>.

## **1.9 Human Cardiac-Derived Adherent Proliferating Cells in cardiomyopathy**

### **1.9.1 Endomyocardial biopsy-derived cardiac adherent proliferating cells**

CardAP cells (previously known as CAP cells) are cardiac-derived cells, which are isolated and efficiently expanded from EMB<sup>90</sup>. In this study, CardAP cells will be abbreviated as EMB-CardAPs. EMB-CardAPs are generated via outgrowth culture using a specific cell culture medium, containing human serum, basic fibroblast growth factor (bFGF) and epidermal growth factor (EGF)<sup>90</sup>. Morphologically, outgrowing adherent EMB-CardAPs are detected at day 3-5, displaying a fibroblast-like shape. After further subculture, and at passage 3, the cells are stretched and exhibit a stable fibroblast-like phenotype<sup>90</sup>.

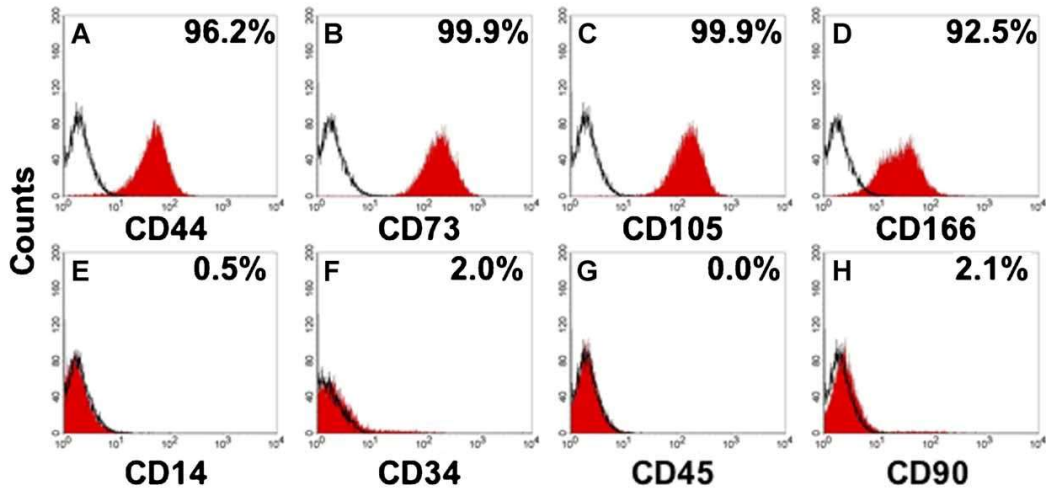


**Figure 1.3. Specific surface antigen expression of EMB-CardAPs.** EMB-CardAPs are positive for the surface markers CD44, CD73, CD105, CD166, and negative for CD14, CD34, CD45, and CD90 (from Haag *et al.*<sup>90</sup>)

EMB-CardAPs are positive for the surface markers CD44, CD73, CD105, CD166, and negative for the hematopoietic markers CD14, CD34, and CD45. Although EMB-CardAPs have initially been suspected to be cardiac MSCs, lack of CD90, vascular cell adhesion molecule-1 (VCAM-1) and desmin cell surface markers, proved them to be uniquely different from MSCs as well as from CF<sup>90</sup> (**Figure 1.3.**). Moreover, they do not possess the multilineage potential of MSCs<sup>90</sup>. Expression profiling of EMB-CardAPs and subsequent principle component analysis further illustrated that EMB-CardAPs have an unique expression profile different from MSCs, human hematopoietic stem cells (HSC) and different cell types residing in the heart such as endothelial progenitor cells (EPC), cardiac stem cells (CSC), and CF<sup>90</sup> (**Figure 1.4.**).

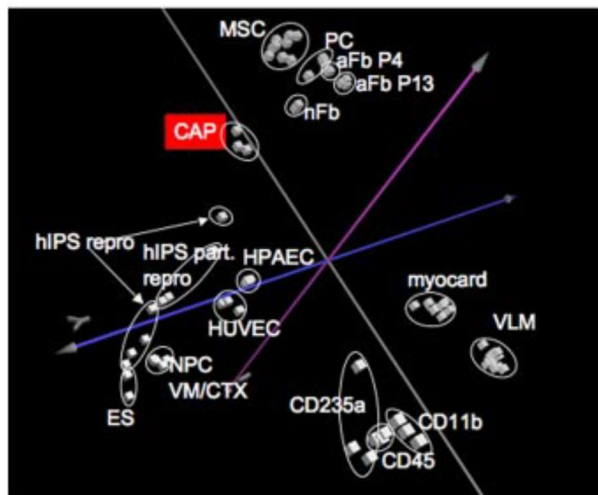


**Figure 1.4. Three-dimensional blot showing the principal component analysis of EMB-CardAPs.** EMB-CardAPs from three donors formed a separate cluster. EMB-CardAPs shifted to the progenitor cells but not to the muscle or hematopoietic stem cells, indicating that they have their own characteristics. (from Haag *et al.*<sup>90</sup>).

In comparison to CSC, the hampered therapeutic candidate of heart disease due to the complexity of its isolation and expansion, EMB-CardAPs have a relatively high proliferation capacity with a mean cell doubling time of 49.9 h and a cellular density as high as  $2.54 \times 10^7$  cells in passage 3<sup>90</sup>.

Similar to MSCs, EMB-CardAPs are low immunogenic. This follows from the finding that EMB-CardAPs failed to express human leukocyte antigen (HLA)-DR, an antigen presenting molecule expressed on immune cells and indicator of induced immunogenicity<sup>91</sup>, in the presence or absence of inflammatory conditions<sup>92</sup>.

Since EMB-CardAPs are isolated from cardiac biopsies, it has been postulated that being primed by their cardiac-specific niche, they are potentially superior over cells of different ontology<sup>90</sup>. EMB-CardAPs cannot induce myogenesis and cannot differentiate into cardiomyocytes<sup>93</sup>. However, they exert pro-angiogenic effects, involving the secretion of the pro-angiogenic factors, IL-8 and vascular endothelial growth factor (VEGF)<sup>94</sup>. Like MSCs<sup>81</sup>, EMB-CardAPs also exert anti-apoptotic effects in an nitric oxide- (NO)<sup>95</sup> and IL-10<sup>96</sup>-dependent manner<sup>66</sup>. In frame with the anti-apoptotic properties of EMB-CardAPs on CVB3-infected HL-1 cardiomyocytes and the relevance of apoptosis on viral progeny release, EMB-CardAPs reduce viral progeny release and the CVB3 viral titer<sup>66</sup>.

In parallel to the pro-angiogenic, anti-apoptotic and anti-viral effects, EMB-CardAPs have also been shown to exert immunomodulatory effects, which further confirms their similarity with MSCs<sup>97, 98</sup>. EMB-CardAPs induce the production of Treg cells in CVB3-infected mice<sup>92, 98</sup>, decrease the CVB3-induced proliferation/activity of cardiac mononuclear cells<sup>66</sup> and induce the apoptosis of CD4<sup>+</sup> and CD8<sup>+</sup> T cells in the spleen of CVB3-infected mice<sup>66</sup>.

Another main beneficial activity of EMB-CardAPs is their anti-fibrotic potential, which has been proven in an experimental angiotensin II (Ang II)-induced heart failure model<sup>98</sup>. Intramyocardial injection of EMB-CardAPs reduced the Ang II-induced cardiac fibrosis, which follows from the lower LV collagen mRNA expression in Ang II EMB-CardAPs versus Ang II mice<sup>98</sup>. Additionally, EMB-CardAPs exert direct anti-fibrotic effects, as shown by *in vitro* experiments illustrating that co-culture of Ang II-stimulated cardiac fibroblasts with EMB-CardAPs leads to lower expression of Ang II type I receptor (AT1R) expression on cardiac fibroblasts, as well as lower myofibroblast differentiation and proliferation<sup>98</sup>. Similar to their anti-apoptotic<sup>66</sup>, anti-viral<sup>66</sup>, and immunomodulatory properties<sup>66</sup>, EMB-CardAPs exerted these anti-fibrotic effects in an NO- and IL-10-dependent manner<sup>98</sup>. Furthermore, EMB-CardAPs diminished cardiac hypertrophy in the Ang II-induced heart failure mice<sup>98</sup>.

In summary, EMB-CardAPs exert cardioprotective effects, which follows from the improvement in cardiac function following EMB-CardAPs application in experimental models of CVB3-induced myocarditis<sup>66</sup> and Ang II-induced heart failure<sup>98</sup>.

EMB-CardAPs have originally been isolated for autologous use<sup>66, 90, 92, 98</sup>. Given the exposure of the cells to the patients risk factors<sup>99</sup> and the limited availability<sup>100</sup>, a new cell fraction has recently been isolated with assumed similar features of EMB-CardAPs for allogenic cell-based cardiac regeneration<sup>100</sup>. In contrast to autologous cells, allogenic cell sources allow immediate availability and off-the shelf therapy, for acute and chronic cardiac dysfunction<sup>99, 101</sup>. Hereto, CardAP cells were isolated from the right atrial appendage (RAA) of the heart: RAA-CardAPs<sup>100</sup>.

### **1.9.2 Right atrial appendage-derived cardiac adherent proliferating cells**

Similar to EMB-CardAPs, RAA-CardAPs are harvested via outgrowth culture be it from the RAA instead of the EMB<sup>100</sup>. RAA-CardAPs are next sorted with CD90 microbeads to obtain a CD90<sup>low</sup> cell population, and expanded in a specific culture medium, containing human serum, bFGF and EGF<sup>100</sup>. Morphologically, outgrowing RAA-CardAPs have been detected on day 6-8, showing a fibroblast-like shape<sup>100</sup>. RAA-CardAP cells display a high proliferation capacity with a mean cell doubling time of 37.94 h and cellular density as high as  $3.42 \times 10^9$  cells in passage 3 and  $3.23 \times 10^{10}$  in passage 4. This number is sufficient for the treatment of more than 250 patients<sup>100</sup>. Similar to EMB-CardAPs, RAA-CardAPs are characterized by their 1) positivity for CD44, CD73, CD105 and CD166 surface markers; 2) negativity for the hematopoietic markers CD14, CD34 and CD45; and 3) low expression of CD90<sup>100</sup>. A brief comparison between EMB-CardAPs and RAA-CardAPs is summarized in **Table 1.1**.

**Table 1.1. Comparison of EMB-CardAPs and RAA-CardAPs.**

<b>Criteria</b>	<b>EMB-CardAPs</b>	<b>RAA-CardAPs</b>
CD90 surface marker	Low	Low
Morphology	Fibroblast-like	Fibroblast-like
Isolation region	Out growth culture from endomyocardial biopsy	Out growth culture from right atrial appendage
Cell detection	At day 3-5	At day 6-8
Growth kinetics	Doubling time 49.9 h Cell count $2.54 \times 10^7$ in passage 3	Doubling time 37.94 h Cell count $3.42 \times 10^9$ cells in passage 3
Cardioprotective effect	Pro-angiogenic, anti-apoptotic, anti-fibrotic, anti-viral, and immunomodulatory effects	Pro-angiogenic effect, Other cardioprotective effects still to be investigated

So far, only the pro-angiogenic potential of RAA-CardAPs has been demonstrated *in vitro*. RAA-CardAPs express the pro-angiogenic factors VEGF and IL-8<sup>100</sup> and conditioned medium of RAA-CardAPs increases tube formation, indicating that these cells exert pro-angiogenic effects in a paracrine manner.

The *in vivo* therapeutic potential of RAA-CardAPs is still obscure. Hence, the anti-apoptotic, anti-viral, anti-fibrotic, and immunomodulatory effects of RAA-CardAPs will be investigated in the current study.

## 2. Aim of the study

The overarching aim of this study is to get further insights into the cardioprotective potential of CardAP cells. The study is divided into two arms:

1. The first arm aims to further characterize EMB-CardAP cells and to compare them with EMB-derived cardiac fibroblasts (EMB-CF) from the same patient i.e. based on a one-by-one comparison of EMB-CardAPs and EMB-CF from the same patient, showing differences in proteoform expression between EMB-CardAPs and EMB-CF (**Figure 2.1.**), the cardioprotective potential of EMB-CardAPs versus EMB-CF were evaluated in murine acute CVB3-induced myocarditis mice;

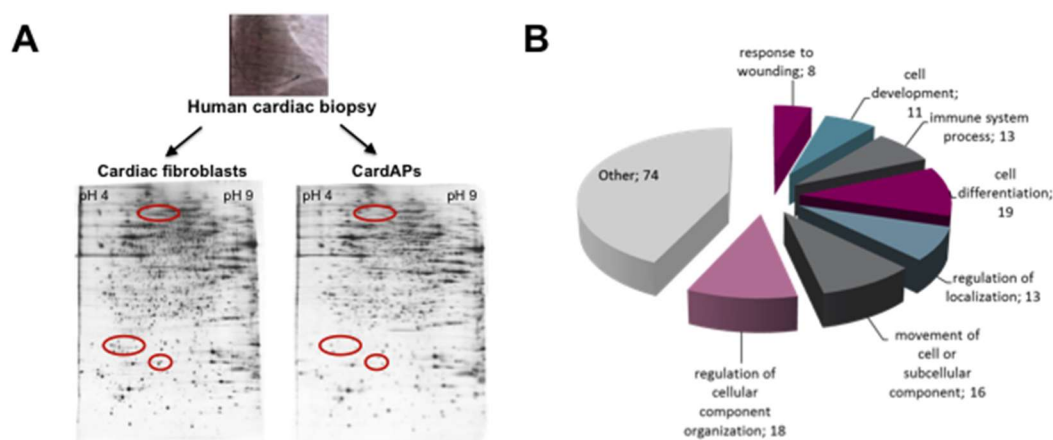


**Figure 2.1. EMB-CardAPs and EMB-CF differ in their proteoform expression. A.** 2D gels illustrate differences in the intact proteoform (isoform) expression between EMB-CF and EMB-CardAPs. **B.** The different regulated proteoforms comprise proteins involved in response to wounding, cell development, immune system processes, cell differentiation, regulation of localization, movement of cell or subcellular components and regulation of cellular component organization (Unpublished results / cooperation partner Dr. Oliver Klein).

2. The second arm aims to characterize the cardioprotective potential of RAA-CardAP cells. Therefore, their cardio(myocyte) protective effects were investigated
  - 2.1. *In vitro* on CVB3-infected HL-1 cardiomyocytes and in
  - 2.2. acute and
  - 2.3. chronic CVB3-induced myocarditis mice.

### 3. Materials and methods

#### 3.1 Materials

**Table 3.1. Laboratory equipment**

Article	Company
Balance-EMB 1200-I	KERN & SOHN GmbH, Balingen, Germany
Centrifuge 5415 R	Eppendorf, Hamburg, Germany
Centrifuge-Microfuge 22R	Beckman Coulter GmbH, Krefeld, Germany
CO <sub>2</sub> Incubator-HERACell 240i	Thermofisher Scientific, Darmstadt, Germany
Conductance catheter 1.2F	Scisense Inc., Ontario, Canada
Conductance catheter 1.4F (4.5 mm)- model SPR-893	Millar Instruments, Inc., The Hague, The Netherlands
Eppendorf MasterCycler RealPlex	Eppendorf AG, Hamburg, Germany
Flow Cytometer-MACSQuant analyzer	Miltenyi Biotec, Bergisch Gladbach, Germany
Freezer -20°C-Comfort	Thermofisher Scientific, Darmstadt, Germany
Freezer -80°C	Thermofisher Scientific, Darmstadt, Germany
Homogenizer	IKA®T25 digital ULTRA-TURRAX®, Staufen, Germany
Horizontal shaker SM-25	Edmund Bühler, Tübingen, Germany
Ice maker	Scotsman AF80, Suffolk, UK
Leica Microscope- DM2000 LED	Leica Microsystems GmbH, Wetzlar, Germany
Microscope-Primovert	Carl Zeiss microimaging GmbH, Göttingen, Germany
Minilys homogenizer	Bertin GmbH, Frankfurt am Main, Germany
Nanodrop™ 2000 spectrophotometer	Thermofisher Scientific, Darmstadt, Germany
pH meter-PB-11	Sartorius GmbH, Göttingen, Germany
Pipettes variable volumes	Eppendorf, Hamburg, Germany
Quant Studio 6 Flex TaqMan	Life Technologies GmbH, Darmstadt, Germany

SpectraMax Gemini microplate reader	Molecular Devices, Inc. Sunnyvale, CA, USA
Thermocycler	Eppendorf AG, Hamburg, Germany
Ventilator	MiniVent Type 845, Harvard Apparatus, D-79232 March-Hugstetten, Germany
Vortex-Genie 2	Scientific industries Inc., USA

**Table 3.2. Laboratory consumables**

<b>Article</b>	<b>Company</b>
Cell strainer 40 µm	BD Biosciences, New Jersey, USA
Cell strainer 70 µm	BD Biosciences, New Jersey, USA
Coverslips 50x24mm	R. Langenbrinck, Emmendingen, Germany
Cryotubes	Greiner, Solingen-Wald, Germany
Falcon tubes	Sarstedt, Nürnberg, Germany
MicroAmp Optical 384-well plate	Applied Biosystems, Darmstadt, Germany
Microtome blades	Feather, Köln, Germany
Multiply PCR 96-well plate	Sarstedt, Nürnberg, Germany
PCR tubes	ThermoFisher Scientific, Darmstadt, Germany
Pipette tips	Sarstedt, Nürnberg, Germany

**Table 3.3. Chemicals and reagents**

<b>Article</b>	<b>Company</b>
3-Amino-9-ethylcarbazole	Sigma, Steinheim, Germany
ABC Blocking Kit	Vector Labs/Biozol, Eching, Germany
ABC Kit Standard	Vector Labs/Biozol, Eching, Germany
Absolute ethanol	Carl Roth GmbH, Karlsruhe, Germany
Acetic acid (96-100%)	Carl Roth GmbH, Karlsruhe, Germany

Bovine serum albumin (BSA) Fraction V	Carl Roth GmbH, Karlsruhe, Germany
Buprenorphine 0,324 mg/ml-Tamgesic	Indivior UK limited, Slough, United Kingdom
CellTiter 96® AQueous One Solution Reagent	Promega, Madison, USA
Dimethyl sulfoxide (DMSO)	Merck, Darmstadt, Germany
di-Sodium hydrogen phosphate dihydrate	Merck, Darmstadt, Germany
Eosin	Sigma, Steinheim, Germany
Ethanol 96%	Carl Roth GmbH, Karlsruhe, Germany
Formalin solution 10%	Sigma, Steinheim, Germany
Goat Serum	Sigma, Steinheim, Germany
Hydrogen peroxide solution (H <sub>2</sub> O <sub>2</sub> )	Carl Roth GmbH, Karlsruhe, Germany
Ionomycin	Sigma, Steinheim, Germany
Isopropanol	Carl Roth GmbH, Karlsruhe, Germany
Kaiser's glycerol gelatin, phenol-free	Carl Roth GmbH, Karlsruhe, Germany
Mayer's hemalum solution	Merck, Darmstadt, Germany
N, N-Dimethylformamide	Carl Roth GmbH, Karlsruhe, Germany
Phenol/chloroform/isoamyl alcohol	Carl Roth GmbH, Karlsruhe, Germany
Phosphate buffered saline (PBS)	Biochrom, Berlin, Germany
Potassium chloride	Merck, Darmstadt, Germany
Potassium dihydrogen phosphate	Merck, Darmstadt, Germany
Sodium acetate	Merck, Darmstadt, Germany
Sodium acetate trihydrate	Merck, Darmstadt, Germany
Sodium chloride salt	VWR Merck, Darmstadt, Germany
Sodium chloride solution 0.9%	B. Braun Melsungen AG, Hessen, Germany

Sodium Chloride solution 10%	Fresenius Kabi AG, Bad Homburg, Germany
Sodium Dodecyl Sulfate	Sigma, Steinheim, Germany
Tissue-Tek OCT	Sakura, Zoeterwoude, Netherlands
Trichloromethan/Chloroform	Carl Roth GmbH, Karlsruhe, Germany
Tris-Base	Sigma, Steinheim, Germany
Tris-HCl	VWR Merck, Darmstadt, Germany
Trizol™ Reagent	Invitrogen/ThermoFisher Scientific, Darmstadt, Germany
Tween20	Sigma, Steinheim, Germany
Urethane	Sigma, Steinheim, Germany
Vitro-Clud	R. Langenbrinck, Emmendingen, Germany
Vybrant® DiO Cell-labeling	Invitrogen, Heidelberg, Germany
N, N Dimethylformamide	Sigma, Steinheim, Germany
Xylene	Carl Roth GmbH, Karlsruhe, Germany

**Table 3.4. Reporter assays**

Gene name	Gene Symbol	Catalogue Number
Bcl-2-associated X protein	BAX	Mm00432050_m1
B cell leukemia/lymphoma 2	Bcl-2	Mm00477631_m1
Chemokine (C-C motif) ligand 2	CCL2	Mm00441242_m1
Chemokine (C-C motif) ligand 7	CCL7	Mm00443113_m1
Chemokine (C-C motif) receptor 2	CCR2	Mm00438270_m1
Chemokine (C-X3-C motif) ligand 1	CX3CL1	Mm00436454_m1
Chemokine (C-X3-C motif) receptor 1	CX3CR1	Mm02620111_s1
Cyclin-dependent kinase inhibitor 1b	CDKN1b	Mm00438167_g1
Glyceraldehyde-3-phosphate dehydrogenase	GAPDH	Mm99999915_g1

Interferon-beta	IFN- $\beta$	Mm00439546_s1
Interferon-gamma	IFN- $\gamma$	Mm00801778_m1
Interleukin-1 $\beta$	IL-1 $\beta$	Mm00434228_m1
Interleukin-6	IL-6	Mm00446190_m1
Interleukin-10	IL-10	Mm00439616_m1
Lymphocyte antigen 6 complex, locus C	Ly6c	Mm03009946_m1
Tumor necrosis factor- $\alpha$	TNF- $\alpha$	Mm00443258_m1

**Table 3.5. Coxsackievirus B3 primers**

Gene name	Sequence 5'– 3'
Coxsackievirus B3	Forward: 5'-CCCTGAATGCGGCTAATCC-3' Reverse: 5'-ATTGTCACCATAAGCAGCCA-3' Probe: 5'-FAM-TGCAGCGGAACCG-TAMRA-3'

**Table 3.6. Kits**

Article	Company
High Capacity cDNA Reverse Transcriptase Kit	Applied Biosystems, Darmstadt, Germany
NucleoSpin RNA II Kit	Macherey-Nagel, Düren, Germany
qPCR™ MasterMix Plus for SYBR® Green I – Dttp	Eurogentec GmbH, Köln, Germany
Taqman® Universal Master Mix II	Applied Biosystems, Darmstadt, Germany

**Table 3.7. Cell culture media and reagents**

Article	Company
ACK lysis buffer	Gibco BRL, Karlsruhe, Germany
Basic fibroblast growth factor (bFGF)	PeptoTech GmbH, Hamburg, Germany

Claycomb medium	Sigma, Steinheim, Germany
Dulbecco Modified Early Medium (DMEM)	Biochrom, Berlin, Germany
DMEM 11966	Biochrom, Berlin, Germany
Epidermal growth factor (EGF)	PeptoTech GmbH, Hamburg, Germany
Fetal bovine serum (FBS)	Gibco BRL, Karlsruhe, Germany
Glucose	Sigma, Steinheim, Germany
Glutamine	Biochrom, Berlin, Germany
Ham's F12	Biochrom, Berlin, Germany
Human allogenic serum	German Red Cross, Berlin, Germany
Iscove's Modified Dulbecco's Medium (IMDM)	Biochrom, Berlin, Germany
Norepinephrine	Sigma, Steinheim, Germany
Penicillin/Streptomycin	Invitrogen, Grand Island, USA
Phosphate buffered saline (PBS)	Biochrom, Berlin, Germany
RPMI 1640	Gibco BRL, Karlsruhe, Germany
Trypsin/EDTA	Biochrom, Berlin, Germany

**Table 3.8. Cell culture medium composition**

<b>Cell type</b>	<b>Medium composition</b>
Endomyocardial Biopsy-Cardiac-derived adherent proliferating cells (EMB-CardAPs)	1/3 IMDM; 1/3 DMEM; 1/3 Ham's F12 Medium 5% human allogenic serum 1% penicillin/streptomycin 20 ng/ml bFGF 10 ng/ml EGF
Endomyocardial Biopsy-Cardiac-derived fibroblasts (EMB-CF)	Iscove's medium 10% human allogenic serum 10% FBS

	1% penicillin/streptomycin
HL-1 cardiomyocytes	Claycomb medium 10% FBS 1% penicillin/streptomycin 1 % norepinephrine 2mM glutamine
Right Atrial Appendage-derived-CardAPs (RAA-CardAPs)	1/3 IMDM; 1/3 DMEM; 1/3 Ham's F12 Medium 5% human allogenic serum 1% penicillin/streptomycin 100 ng/ml bFGF 100 ng/ml EGF

**Table 3.9. Antibodies for immunohistochemistry**

1. AB	Company
Anti-CD4	BD/Pharmingen, Heidelberg, Germany
Anti-CD68	Abcam, Cambridge, UK
Anti-CD8	BioLegend, Koblenz, Germany
Anti-Collagen I	Chemicon, Nuremberg, Germany
Anti-Collagen III	Calbiochem, Darmstadt, Germany

**Table 3.10. Antibodies/kits for flow cytometry**

Antibody/kit	Company
Annexin V apoptosis detection kit	BD sciences, Franklin Lakes, USA

**Table 3.11. Coxsackievirus B3**

Virus	Provider
CVB3 (Nancy strain)	Kindly provided by Prof. U. Rauch, Charité
CVB3 batch 31-1-93/SAP	Kindly provided by Dr. Fechner, TU Berlin

**Table 3.12. Software**

<b>Software</b>	<b>Software developer</b>
Circlab 2004	Paul Steendijk, GTX Medical Software, Belgium
FlowJo 8.7. software	Tree Star, Ashland, USA
GraphPad Prism 7.0 software	GraphPad Software, La Jolla, USA
IOX 1.8.9	EMKA Technologies, Falls Church, USA
Labchart 8.1.10	ADInstruments Ltd., Oxford, UK
Leica Application Suite (LAS) V4.4	Leica Microsystems GmbH, Wetzlar, Germany
PV Loop 2.4	ADInstruments Ltd., Oxford, UK

## 3.2 Methods

### 3.2.1 Cardiac cells isolation and culture

The donation of cardiac tissue was approved by the ethical committee of the Charité-Universitätsmedizin Berlin (No 225-07) and by the patients, who provided written consent.

#### 3.2.1.1 Endomyocardial biopsy-derived cardiac adherent proliferating cells

EMB-CardAPs were isolated by outgrowth culture from the EMB and expanded in 1/3 IMDM, 1/3 DMEM, and 1/3 Ham's F12 Medium, supplemented with 5% human allogenic serum, 1% penicillin/streptomycin, 20 ng/ml bFGF and 10 ng/ml EGF, according to Haag *et al.*<sup>90</sup> (**Figure 3.1.**). Cells were passaged until passage 4, trypsinized and collected for cell injection. Therefore, a cell suspension in PBS was prepared with a concentration of  $12.5 \times 10^5$  cells in 250  $\mu$ l PBS.

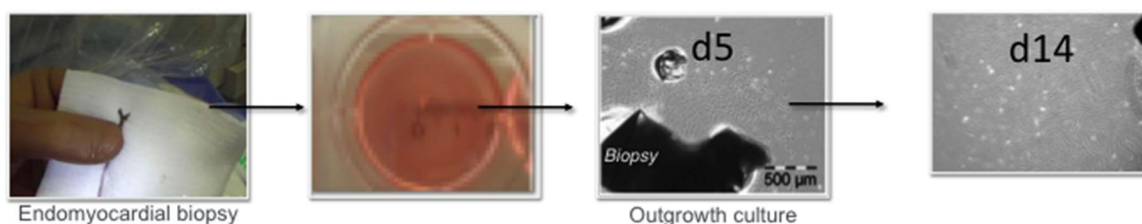


**Figure 3.1.** Isolation of CardAPs from an endomyocardial biopsy via outgrowth culture.

#### 3.2.1.2 Endomyocardial biopsy-derived cardiac fibroblasts

Similar to EMB-CardAPs, EMB-CF of the same patient were isolated by outgrowth culture from the EMB. In contrast to EMB-CardAPs, which are cultured in 1/3 IMDM, 1/3 DMEM, 1/3 Ham's F12 Medium, supplemented with 5% human allogenic serum, 1% penicillin/streptomycin, 20 ng/ml bFGF and 10 ng/ml EGF, EMB-CF were obtained by outgrowth in Iscove's medium containing 10% human allogenic serum, 10% FBS and 1% penicillin/streptomycin, as described previously.<sup>102, 103</sup> Cells were passaged until passage 4, trypsinized and collected for cell injection. Therefore, a cell suspension in PBS was prepared with a concentration of  $12.5 \times 10^5$  cells in 250  $\mu$ l PBS.

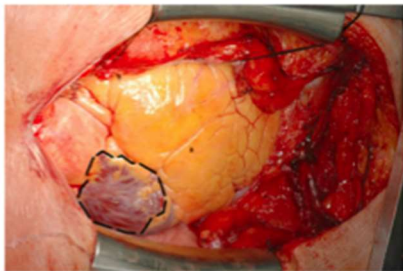
#### 3.2.1.3 Right atrial appendage-derived cardiac adherent proliferating cells

RAA-CardAPs were isolated by outgrowth culture from the right atrial appendage (RAA) according to Detert *et al.*<sup>100</sup> (**Figure 3.2.**). In brief, the RAA was cut in pieces of approximately 1 mm<sup>3</sup>. Next, the pieces were mechanically fixed to the bottom of a 6-well using a sterile scalpel. Following outgrowth culture, CD90<sup>low</sup> RAA cells were gained via negative CD90

immunomagnetic sorting. CD90<sup>low</sup> cells were next seeded in cell culture flasks at a density of 6,000 cells/mm<sup>2</sup> and further expanded under standard cell culture conditions in full medium comprising 1/3 IMDM; 1/3 DMEM; 1/3 Ham's F12 Medium, supplemented with 5% human allogenic serum, 1% penicillin/streptomycin, 100 ng/ml bFGF and 100 ng/ml EGF

RAA-CardAPs were kindly provided by Dr. Marion Haag (Charité, BCRT, Berlin) in passage 1 and further propagated to passage 4 for subsequent *in vitro* experiments (see supra) or cell injection in CVB3 C57BL/j and NMRI mice.

A.



B.

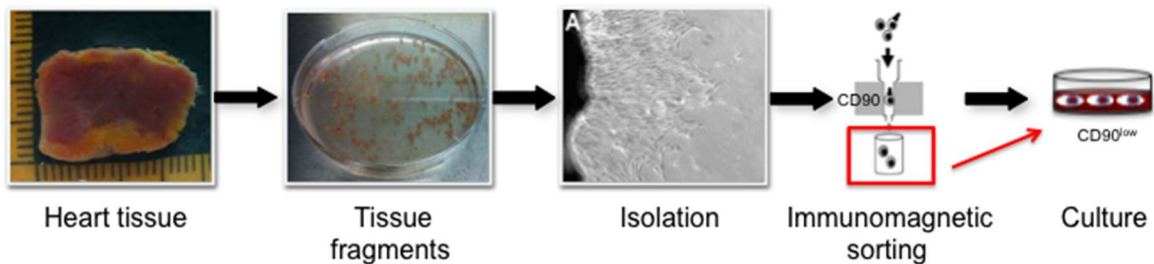


**Figure 3.2. Isolation of CardAPs from the right atrial appendage via outgrowth culture and subsequent immunomagnetic sorting.** A. Intraoperative view of the heart. The dotted line indicates the right atrial appendage (RAA), which is removed when the atrium is opened for insertion of the venous cannula (from Detert *et al.*<sup>100</sup>). B. Fragments of  $\approx 1 \text{ mm}^3$  from the RAA were cut and mechanically fixed to the bottom of a petridish using a sterile scalpel. Following outgrowth culture, CD90<sup>low</sup> RAA cells were gained via negative CD90 immunomagnetic sorting. CD90<sup>low</sup> cells were next seeded in cell culture flasks at a density of 6,000 cells/mm<sup>2</sup> and further expanded.

#### 3.2.1.4 Evaluation of impact of Coxsackievirus B3 infection on viability of right atrial appendage-derived cardiac adherent proliferating cells

10,000 RAA-CardAPs were plated per well of a 96-well plate. After 24 h of culture, cells were serum starved or incubated with CVB3 in serum starvation medium (DMEM 11966, 5 mM glucose and 0.01% FBS) at a multiplication of infection (m.o.i.) of 2 for 1 hour (h). Next, cells were washed 2 times in PBS (Biochrom) and 100  $\mu\text{l}$  of full medium was added. 4 h, 12 h, 24 h, and 48 h after serum starvation or CVB3 infection, 20  $\mu\text{l}$  of the CellTiter 96® AQueous One Solution Reagent (Promega, Madison, USA) was added to the culture wells, and incubated for

2 h in full medium. The absorbance was recorded at 490 nm with a SpectraMax Gemini microplate reader (Molecular Device Inc. Sunnyvale, CA, USA).

### **3.2.1.5 Evaluation of cardiomyocyte-protective potential of RAA-CardAPs**

#### **3.2.1.5.1 Co-culture of RAA-CardAPs with DiO-labeled HL-1 cardiomyocytes**

To assess whether RAA-CardAPs can reduce the CVB3-induced apoptosis of HL-1 cardiomyocytes, RAA-CardAPs were co-cultured with HL-1 cells. To be able to detect apoptosis specifically in HL-1 cells in the HL-1/RAA-CardAPs co-cultures, HL-1 cells were labeled with Vybrant® DiO Cell-labeling (Invitrogen, Heidelberg, Germany) before plating.

Before cell plating, 6-wells plates were first coated with 0.02% Gelatin (Sigma-Aldrich Chemie, Steinheim, Germany) for 30 minutes (min) at 37°C. Afterwards, 250,000 DiO-labeled HL-1 cells were plated per well in Claycomb medium (Sigma-Aldrich Chemie) supplemented with 10% FBS (Biochrom, Berlin, Germany), 1% penicillin/streptomycin (P/S, Life Technologies, Carlsbad, Ca, USA), 0.1 mmol/L norepinephrine (Sigma-Aldrich Chemie), and 2 mmol/L L-glutamine (Biochrom). 24 h later, HL-1 were infected with CVB3 (Nancy Strain) at a m.o.i. of 2 in serum starvation medium, or incubated with serum starvation medium, both for 1h. One hour post CVB3 infection or serum starvation, RAA-CardAPs were added to HL-1 cells at a ratio of 1 RAA-CardAP to 10 HL-1. After 24h of CVB3 infection, cells were collected for subsequent Annexin V/7AAD flow cytometry analysis.

The same experiment was performed for collection of the cells for subsequent RNA isolation and quantification of CVB3 mRNA expression via real-time PCR.

#### **3.2.1.5.2 Annexin V/7AAD flow cytometry**

Flow cytometry was performed to assess the % of early apoptotic DiO-labeled HL-1 cells following CVB3 infection and culture in the presence or absence of RAA-CardAPs.

Cells were harvested and washed twice with cold cell staining buffer (Biolegend, Koblenz, Germany). After the last washing step, cells were re-suspended in 100 µL Annexin-binding buffer (BioLegend). Next, 5 µL anti-Annexin V and 5 µL of anti-7AAD were added and incubated at RT for 15 min in the dark. After incubation, 400 µL Annexin-binding buffer was added for measurement of early apoptotic, Annexin V<sup>+</sup>/7AAD<sup>-</sup> cells. All samples were measured on a MACSQuant Analyzer (Miltenyi Biotec, Bergish Gladbach, Germany) and analyzed via the FlowJo software version 8.8.6. (Tree Star Inc., Ashland, VI, USA). Data are expressed as Annexin V<sup>+</sup>/AAD<sup>-</sup> cells (% DiO<sup>+</sup>).

### 3.2.2 Experimental design of *in vivo* experiments

All experiments were performed according to the European legislation for the Care and Use of Laboratory Animals (Directive 2010/63/EU) and approved by the local ethics committee (Landesamt für Gesundheit und Soziales, Berlin, G0094/11 (acute myocarditis) and G0186/15 (chronic myocarditis)). Male C57BL6/j mice were used for the acute CVB3 myocarditis model, whereas male Naval Medical Research Institute (NMRI) mice were used for the chronic CVB3 myocarditis experiments.

#### 3.2.2.1 Evaluation of intravenous application of endomyocardial biopsy-derived cardiac adherent proliferating cells versus endomyocardial biopsy-derived cardiac fibroblasts in acute Coxsackievirus B3 myocarditis mice

Eight-weeks-old C57BL/6 mice were purchased from Charles Rivers (Sulzfeld, Germany) and randomly divided into four groups: control, CVB3, CVB3+EMB-CardAPs and CVB3+EMB-CF. To induce acute CVB3 myocarditis, mice were intraperitoneally (i.p.) injected with  $1 \times 10^5$  plaque forming units (p.f.u) of CVB3 virus (Nancy strain). Control mice received PBS instead of CVB3. To study the effect of EMB-CardAPs and EMB-CF on the progression of acute CVB3-induced myocarditis,  $1 \times 10^6$  EMB-CardAPs or EMB-CF in 200  $\mu$ l PBS were i.v. administered via the tail vein into C57BL/6 mice, one day after CVB3 viral infection. Seven days after CVB3 infection, all mice were hemodynamically characterized and subsequently sacrificed (**Figure 3.3.**)<sup>1</sup>

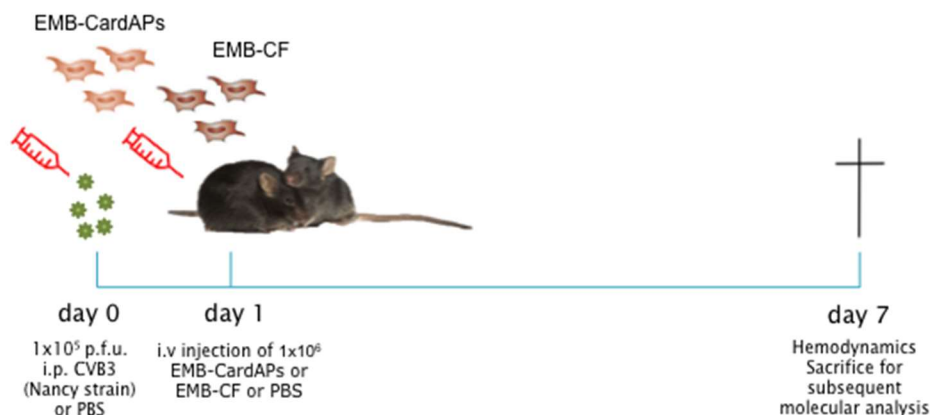


**Figure 3.3. Experimental design for the evaluation of EMB-CardAPs and EMB-CF in acute Coxsackievirus B3-induced myocarditis mice.**

<sup>1</sup> The comparison of EMB-CardAPs versus EMB-CF in acute CVB3-induced myocarditis mice was part of an experimental study comparing EMB-CardAPs versus EMB-CF of different patients. This Dr. thesis only comprises the comparison of EMB-CardAPs versus EMB-CF of one patient. The comparison of EMB-CardAPs of different patients was the topic of another thesis.

### 3.2.2.2 Evaluation of intravenous application of right atrial appendage-derived cardiac adherent proliferating cells in acute Coxsackievirus B3 myocarditis mice

Eight-week-old male C57BL6/j mice were purchased from Charles Rivers (Sulzfeld, Germany) and randomly divided into three groups: control, CVB3, and CVB3+RAA-CardAPs. To induce viral myocarditis, mice were i.p. injected with  $1 \times 10^5$  p.f.u. CVB3 (Nancy strain) in 200  $\mu$ l PBS. Control mice were injected with the same volume of PBS. One day after infection, mice were i.v. injected with  $1 \times 10^6$  RAA-CardAPs in 200  $\mu$ l PBS or solely with PBS for the control CVB3 mice. Seven days after CVB3 infection, all mice were hemodynamically characterized and subsequently sacrificed (Figure 3.4.).

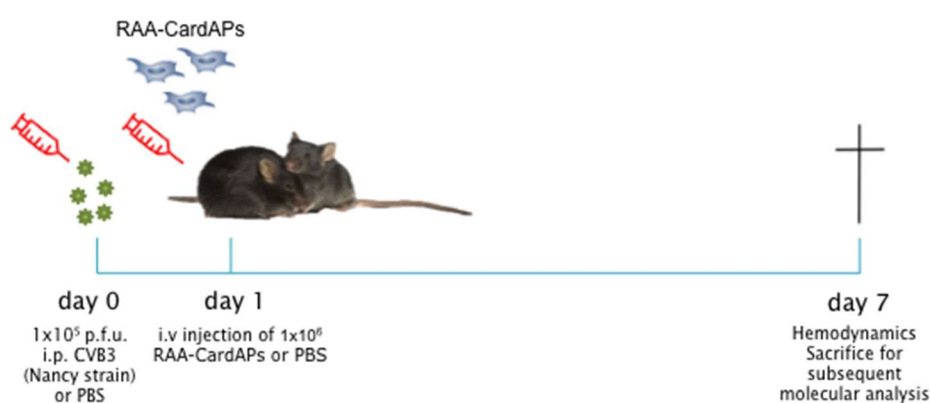


Figure 3.4. Experimental design for the evaluation of RAA-CardAPs in acute Coxsackievirus B3-induced myocarditis mice.

### 3.2.2.3 Assessment of the chronic Coxsackievirus B3 myocarditis mouse model

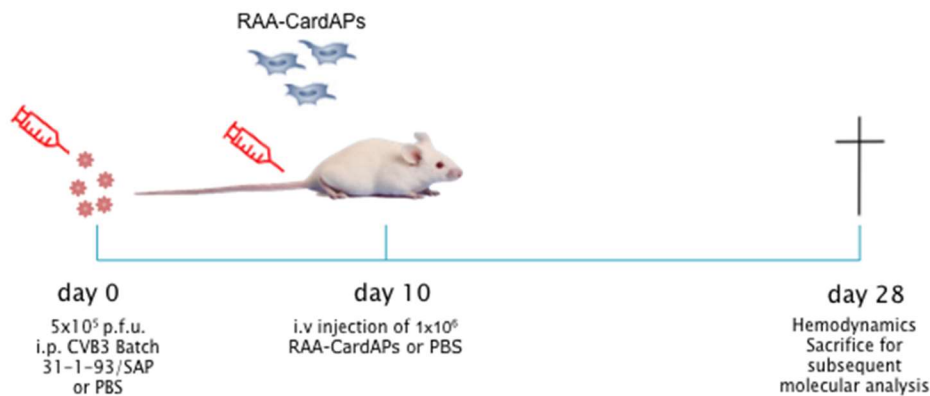
Seven-week-old male NMRI mice were purchased from Charles Rivers (Sulzfeld, Germany) and divided into two groups: control and CVB3. To induce CVB3 chronic myocarditis, mice were i.p. injected with  $5 \times 10^5$  p.f.u. of the CVB3 batch, 31-1-93/SAP. Control mice were injected with the same volume of sole PBS. Twenty-eight days after CVB3 infection, all mice were hemodynamically characterized and subsequently sacrificed (Figure 3.5.).



Figure 3.5. Experimental design for the chronic Coxsackievirus B3-induced myocarditis model.

### 3.2.2.4 Evaluation of intravenous application of right atrial appendage-derived cardiac adherent proliferating cells in chronic Coxsackievirus B3 myocarditis mice

Seven-week-old male NMRI mice were purchased from Charles Rivers (Sulzfeld, Germany) and divided into four groups: control, control+RAA-CardAPs, CVB3 and CVB3+RAA-CardAPs. To induce CVB3 chronic myocarditis, mice were i.p. injected with  $5 \times 10^5$  p.f.u. CVB3 batch 31-1-93/SAP. Control mice were injected with the PBS instead of CVB3. To study the effect of RAA-CardAPs on the progression of chronic CVB3-induced myocarditis,  $1 \times 10^6$  RAA-CardAPs in 200  $\mu$ l PBS were i.v. injected via the tail vein in to NMRI mice, 10 days after CVB3 viral infection. Twenty-eight days after CVB3 infection, all mice were hemodynamically characterized and sacrificed (**Figure 3.6.**).



**Figure 3.6.** Experimental design for the evaluation of RAA-CardAPs in chronic Coxsackievirus B3-induced myocarditis mice.

### 3.2.3 Measurement of hemodynamic parameters using the PV loop method

#### 3.2.3.1 Principle

Pressure-volume measurements rely on the quantification of the intrinsic cardiovascular condition by the assessment of ventricular systolic and diastolic cardiac function, using a conductance catheter, containing one pressure sensor and 4 or more electrodes for volume measurement (**Figure 3.7.**) in a continuous and on-line fashion. This method was developed by Baan *et al.*<sup>104</sup>. Briefly, it is based on measuring the electrical conductance of the blood contained in the LV cavity. The pressure (on Y axis) and volume (on X axis) records are represented by a loop, which reflect a complete cardiac cycle. The catheter measures the total conductance of the blood plus the surrounding tissues. The latter is referred as parallel conductance. To obtain the volume of the LV in an accurate way, this parallel conductance should be subtracted from the total conductance. To calculate the parallel conductance, 5-10  $\mu$ l saline solution of 10% was injected in the jugular vein.

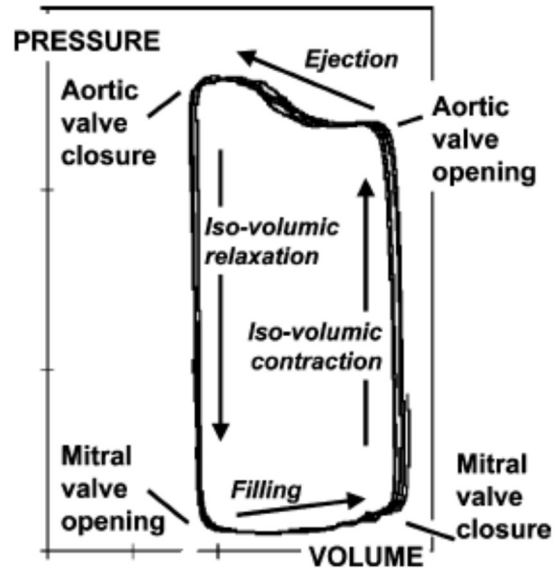
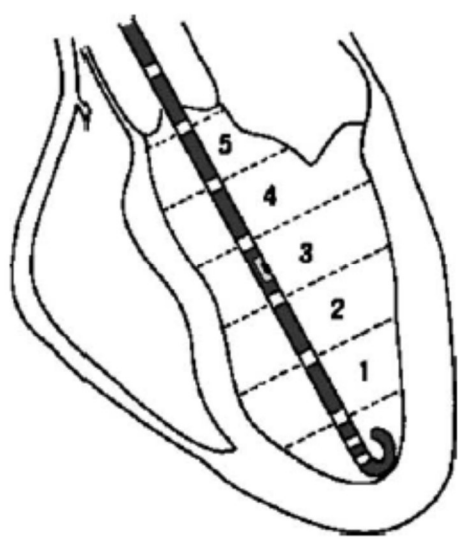


Figure 3.7. Left panel depicts the left ventricle and the correct position of the conductance catheter, whereas the right panel illustrates the complete cardiac cycle represented by the pressure volume loop showing the points of opening and closing of the aortic and mitral valves.<sup>105</sup>

### 3.2.3.2 Preparation

The complete system for acquiring hemodynamic data consists of 1) a computer, which has a windows system with the software installed for data acquisition and analysis, and 2) the conductance catheter, which must be connected to the PV amplifier and to the computer. The conductance catheter should be positioned in a 0.9% sodium chloride solution for 20-30 min before use (**Figure 3.8.**). Each study has three main parts. The first is to create a configuration file with calibrated volume. Calibration of the pressure occurs before measuring every mouse by adjusting the pressure transducer of the PV amplifier to zero. The second part is the surgical part and the hemodynamic data acquisition, and the third part is the analysis of the data.

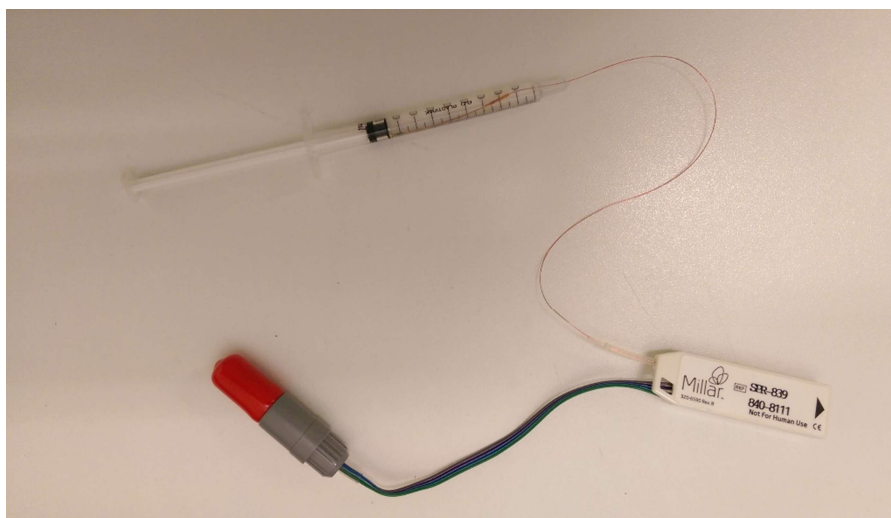


Figure 3.8. Figure illustrates a conductance catheter of Millar system positioned in a 0.9% saline solution.

### **3.2.3.3 Anesthesia**

Animals were anesthetized with a mixture of 0.8-1.2g/kg body weight (BW) urethane and 0.05 mg/kg BW buprenorphine 20-30 min before the hemodynamic measurement, followed by artificial ventilation. The volume of the injected anesthesia from the above-mentioned concentrations should be prepared for every mouse according to their respective weight.

### **3.2.3.4 Mechanical ventilation**

Anaesthetized mice were supported by mechanical ventilation using special MiniVent 845 apparatus, which is designed for mice artificial ventilation and is connected to a 1.3 mm outer diameter tracheotomy cannula. After switching on the ventilator, the respiratory rate is adjusted according to recommended values provided by the manufacturer manual, and tidal volume (on the device termed stroke volume), which is approximately 6.5-6.8 ml/kg BW.

Immediately after the mouse is completely anaesthetized, the mouse is positioned on a surgical platform laying on the dorsal side, fixed with surgical tape mainly on the tail, the fore legs and one through the teeth to fix the head (**Figure 3.9. A**). A small cut is carefully performed in the neck, showing clearly the trachea to allow another cut for insertion of the ventilation cannula (**Figure 3.9. B**).

### **3.2.3.5 Surgical procedure**

The assessment of the cardiac function via hemodynamic parameters occurs at the day of sacrificing the experimental animals after proper anesthesia. We hereby use an open chest or also called apex approach, by which the conductance catheter enters the LV from the apex. With a sharp scissor, the abdomen area is cut at a little distance under the middle. Then, we use the bipolar electrocautery (**Figure 3.9. C**) to stop the bleeding before going further with the cutting. With a surgical needle, we insert the surgical line from the xiphoid cartilage making the diaphragm area clearer (**Figure 3.9. D**). Carefully, we open the diaphragm with the scissors and make the heart and the ventricular apex clear. With a curved (90°) 12mm needle, we make a small puncture at the ventricular apex (**Figure 3.9. E**) and carefully insert the catheter in the LV to start the recording of the measurements (**Figure 3.9. F**).

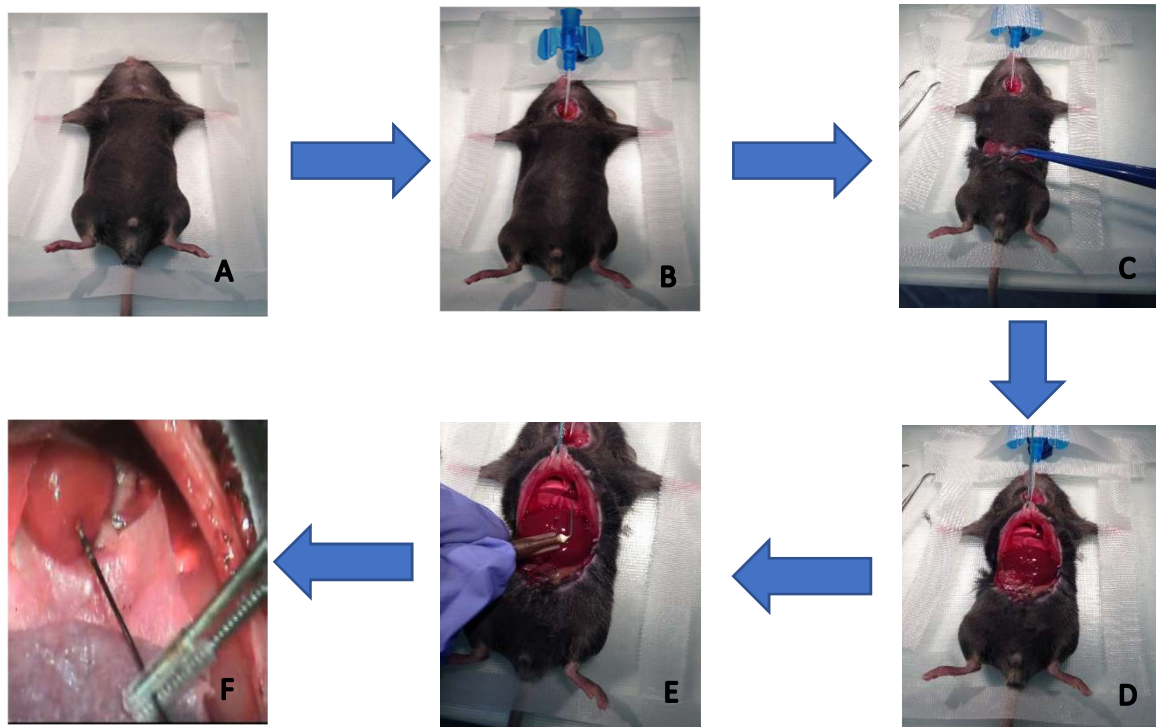


**Figure 3.9.** Scheme illustrating the surgical procedure of the PV loop catheterization in an open chest mouse showing, **A.** the fixation of the mouse, **B.** the cannulation for the mechanical ventilation, **C.** the opening of the abdomen and the electrical cautery, **D.** the pulling the xiphoid cartilage, **E.** the performance of a small puncture at the apex of LV, and **F.** the insertion of the conductance catheter.

### 3.2.3.6 Data acquisition

To avoid the effect of artificial ventilation, data were always recorded at apnea. Therefore, the ventilator was always switched off. The protocol for recording the hemodynamic data using the conductance catheter can be divided in three steps:

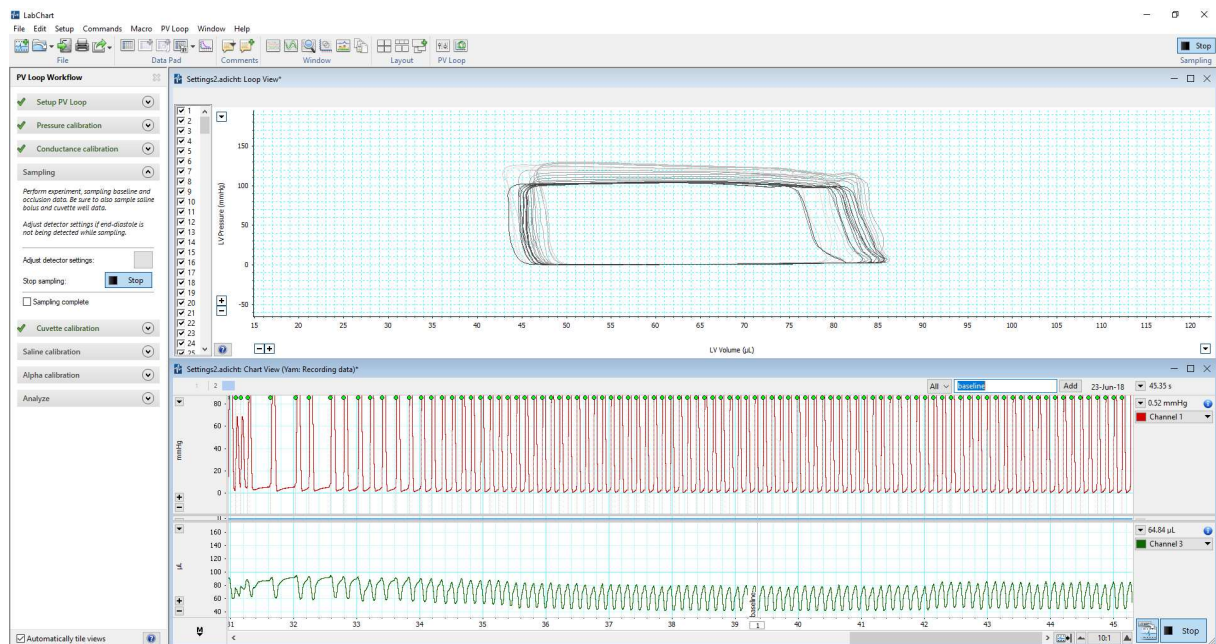


**Figure 3.10.** Hemodynamic analysis at baseline.

**Baseline:** after the insertion of the conductance catheter and observation of a PV loop view on the screen with a good rectangular loop, which confirms the right position of the catheter (**Figure 3.10.**), the ventilator was switched off for approximately 5 seconds and the baseline was recorded. Baseline was recorded for a total of three times.

**Saline:** a very important step for correct hemodynamic measurements, which – as previously mentioned – is done for calculating the parallel conductance. Therefore, a 12mm needle connected to a syringe with 10% sodium chloride solution is carefully inserted into the jugular vein. Then, 5-10  $\mu$ l of saline solution is injected after switching off the ventilator for approximately 5 seconds. Saline is then recorded (**Figure 3.11.**). Saline was three times recorded.

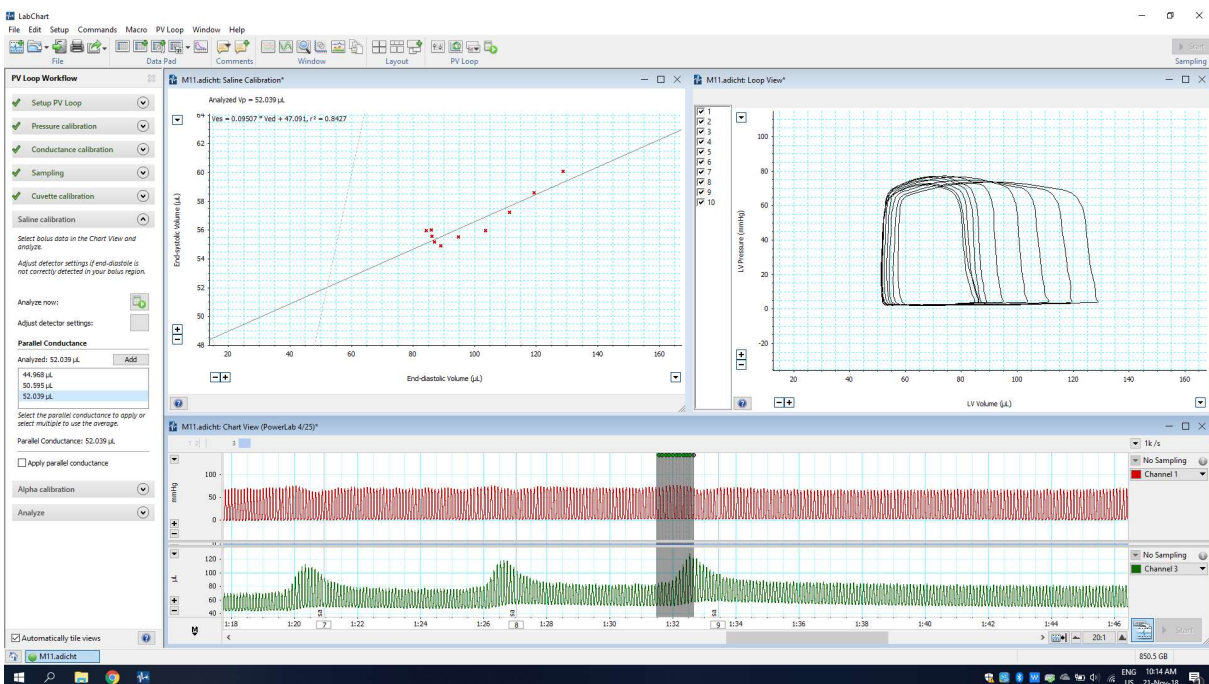


**Figure 3.11. Hemodynamic analysis of saline.**

**Inferior vena cava (IVC) occlusion:** the last step for recording, which is important to determine the end systolic and end-diastolic pressure volume relationship. After switching off the ventilator for approximately 5 seconds, occlusion was performed with a straight and a relatively thin tip forceps by a quick press on the inferior vena cava. The occlusion was immediately recorded (**Figure 3.12.**).

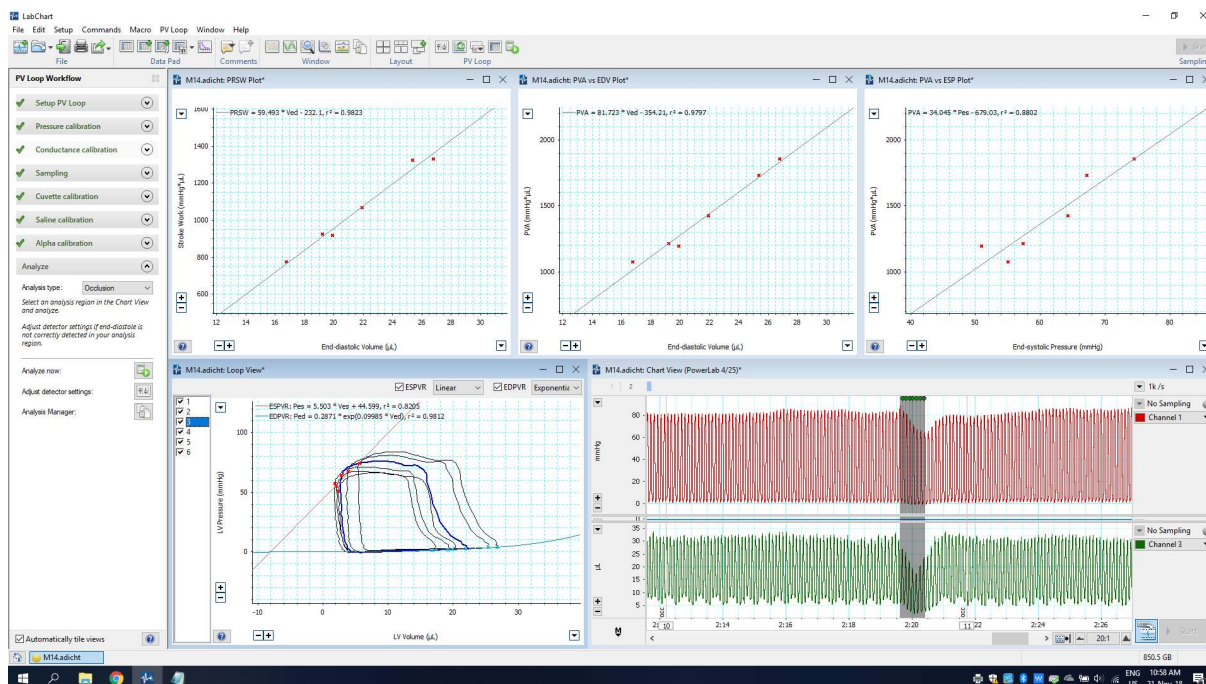


Figure 3.12. Hemodynamic analysis of occlusion.

Table 3.13. Measured hemodynamic parameters

Parameter	Unit
<b>Global cardiac function</b>	
Ejection fraction (EF)	%
<b>Systolic parameters</b>	
Maximum left ventricular pressure ( $P_{max}$ )	mmHg
LV End-systolic pressure (LVESP)	mmHg
Maximum LV pressure rise ( $dP/dt_{max}$ )	mmHg/s
<b>Diastolic parameters</b>	
Minimum LV pressure decay rate ( $dP/dt_{min}$ )	mmHg/min
LV relaxation time Tau ( $\tau$ )	ms

## 3.2.4 Total ribonucleic acid isolation and DNase treatment

### 3.2.4.1 RNA isolation

High quality RNA was isolated using a ready-to-use TRIzol™ reagent. TRIzol™ is a rose-coloured monophasic reagent, which mainly contains phenol and guanidine thiocyanate. TRIzol™ maintains the integrity of the RNA because of its high potential to inhibit the RNase activity.

A small frozen piece of LV of approx. 50 mg was put in 1ml of TRIzol™ and homogenized for 30 sec using a mechanical homogenizer. If the sample was not completely homogenized, the process was performed for an additional 30 sec. Next, 200 µl of chloroform were added to

each eppendorf tube containing the homogenate for phase separation. The tubes were vigorously shaken for 15 sec. by hand and incubated for 2 min at RT. Samples were afterwards centrifuged for 15 min at 4°C at 14,000 rpm. The homogenate was separated in three layers: 1) the top layer, which is a clear aqueous phase containing RNA, 2) the middle layer, which is a white cloudy phase containing DNA, and 3) the bottom layer, which is a red phenol phase containing protein. The upper aqueous layer, which contains the RNA, was next transferred to a clean eppendorf tube and 500 µl of isopropanol were added for RNA precipitation. The solution was shaken, up and down, and incubated for 10 min at RT. RNA was precipitated by centrifugation at 4°C for 10 min at 14,000 rpm. After centrifugation, the supernatant was removed. Next, the pellet was washed by addition of 500 µl of 70% ethanol and shortly vortexed, followed by centrifugation at 4°C for 10 min at 7,500 rpm. The supernatant was carefully and completely removed. Finally, the pellet was dissolved in 50µl of RNase free water.

#### **3.2.4.2 DNase treatment**

50µl of RNase free water were added to the eluted RNA, leading to a total volume of 100µl. Subsequent purification of the isolated RNA and DNase treatment were performed with the NucleoSpin RNA II Kit (Macherey-Nagel, Düren, Germany). Briefly, 600 µl of prepared RA1 buffer (RA1 buffer+Ethanol 96%, 1:1) were added to 100 µl of RNA. The solution was mixed thoroughly by pipetting, transferred to a column (blue ring) and centrifuged at 11,000 xg at RT for 30 sec. The column containing the RNA was moved on a new collection tube and 350 µl of MDB buffer were added on top of the columns to desalt the silica membrane. Then, the columns were centrifuged at 11,000 xg at RT for 1 min. 95 µl of DNase working solution (10% of reconstituted rDNase + 90% of rDNase reaction buffer) were added on the column and incubated at RT for 15 min. Next, 200 µl of RA2 buffer were added to the column and the columns were centrifuged at 11,000 xg at RT for 30 sec. Then, 600 µl of RA3 were added to the column and centrifuged for 30 sec. at 11,000 xg followed by adding 250 µl of RA3 buffer to the column and centrifuged for 2 min at 11,000 xg.

The columns were transferred onto newly labeled 1.5 ml eppendorf tubes and 30 µl RNase free water was directly added on the membranes and incubated at RT for 1-2 min. The tubes were centrifuged at 11,000 xg at RT for 1 min and were transferred on ice. Then, 20 µl of RNase free water was added and columns were incubated for 5 min. Finally, the tubes were centrifuged at 11,000 xg at RT for 1 min. Next, the RNA concentration was measured via Nanodrop. RNA samples were kept on ice during the measurement. 1µl of sterile RNase free water was used as a blank and 1µl of the RNA samples was used for the measurement. A ratio of the absorbance at wavelength 260 and 280 (A260/A280) of approximately 2 is accepted as (pure) for RNA.

### 3.2.5 Reverse transcription

Single-stranded complementary DNA (cDNA) is synthesized from RNA, using the high capacity cDNA reverse transcription kit (Applied Biosystems, Darmstadt, Germany). cDNA will be used to investigate the gene expression of target samples using quantitative real-time PCR. Briefly, 1µg of RNA was used for reverse transcription, followed by adding 10µl RNase free water, leading to a total volume of RNA of 11µl. After preparation of the RNA samples, two master mixtures were prepared. The first mixture comprises random primers and dNTPs, and the second mixture reaction buffer, reverse transcriptase enzyme and RNase free water. Both mixtures were prepared according to **Table 3.14**.

**Table 3.14. Reaction mixtures for cDNA reverse transcription.**

Mixture	µl	Sample (n)
<b>Mix 1</b>		
random primer	2	....
dNTP	0.8	....
<b>Mix 2</b>		
Buffer	2	....
RT enzyme	1	....
RNase free water	3.2	....

RNA should be denatured allowing annealing of primers and dNTPs. Therefore, a 5 min heating step was performed at 70°C, using a thermal cycler (Eppendorf AG, Hamburg, Germany), after addition of the first mixture of 2.8 µl. Next, samples were directly put on ice for at least 1 min, which helps efficient primer annealing to the target. The second mixture of 6.2µl was added to the tubes, leading to a total reaction volume of 20 µl. The program of the reverse transcription was run as following: 25°C for 10 min, 37°C for 2 hours, 85°C for 5 min, and 4°C. Afterwards, cDNA samples were taken out and RNase free water was added up to a volume of 50 µl and stored at -20°C until analysis.

### 3.2.6 Real-time PCR

Real-time PCR is an advanced technique based on monitoring the amplification of a target sequence in real-time. This monitoring is estimated via fluorescent signals emitted during the amplification. To avoid the background fluorescence, which occurs during most real-time PCR experiments, two values are considered, the threshold line and the Ct value. The threshold line is the point at which a reaction reaches a fluorescent intensity above background levels, and the Ct value or the cycle quantification value is the PCR cycle number at which a reaction curve intersects the threshold line (**Figure 3.13. A**).

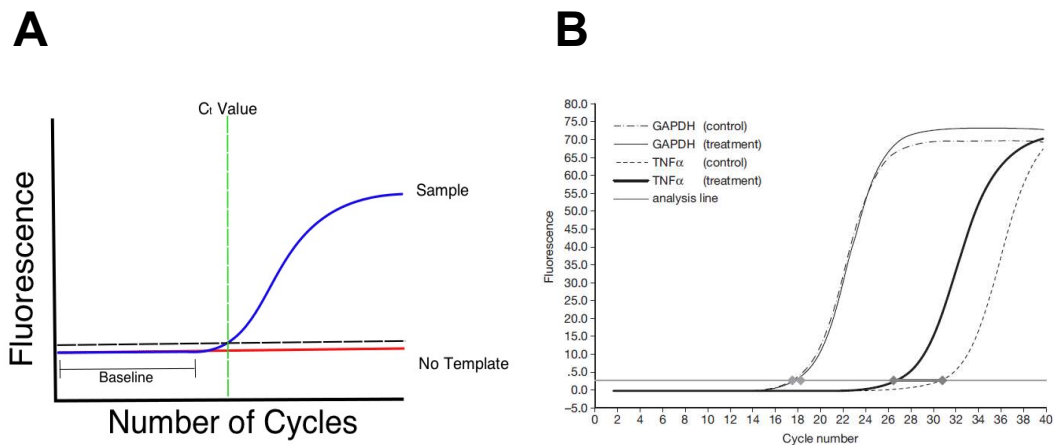


**Figure 3.13. Illustration of A. the amplification curve for real-time PCR showing the threshold line and the Ct value and B. The delta C method for normalization (from Pfaffl *et al.* <sup>106</sup>).**

For accurate gene expression results, the Ct values of target sequences were normalized to Ct values of endogenous controls or housekeeping genes, which should not be biologically changed due to any treatment. The common used housekeeping genes include GAPDH, 18S, and CDKN1b. The normalization method is named delta ( $\Delta$ ) Ct, since the Ct of the specific housekeeping gene is subtracted from the Ct of the target sequence to calculate the relative gene expression (**Figure 3.13. B**).

In general, real-time PCR was conducted with the Taqman universal PCR master mix of Applied Biosystems (Darmstadt, Germany) using reporter assays, which are all purchased from Applied Biosystems (Darmstadt, Germany) **Table 3.4**. The reaction mixture was performed as outlined in **Table 3.15**. For the evaluation of CVB3 mRNA expression, a Taqman universal master mix was used, CVB3 forward and reverse primers (TIB MOLBIOL GmbH, Berlin, Germany; **Table 3.5**), and a probe designed for CVB3 (ThermoFisher Scientific, Darmstadt, Germany). The reaction mixture was performed as outlined in **Table 3.16**. 1  $\mu$ l or 3  $\mu$ l of the cDNA were used, depending on the reporter assay, in a total volume of 10  $\mu$ l. In case of using CVB3, 2  $\mu$ l of cDNA were used, in a total volume of 12.5  $\mu$ l. Quantitative real-time PCR was performed at a Quant Studio 6 Flex (Life Technologies GmbH, Darmstadt, Germany). After pipetting the mixture and the samples in all wells, the plate was covered using a transparent adhesive film. Next, the plate was centrifuged for 1 min at 1,000 rpm. The program of the PCR started with an incubation of 2 min at 50°C, followed by 10 min at 95°C for denaturation. Afterwards, 45 PCR cycles were performed, which consisted of 15 sec denaturation at 95°C, and 1 min annealing at 60°C. The resulted Ct values were analyzed at a definite threshold. In this study, a threshold of 0.2 was used. Gene expression was normalized with the control group set as 1 (relative expression;  $\Delta\Delta$ Ct), with the exception of CVB3 for which the  $\Delta$ Ct formula was used.

**Table 3.15. Real-time PCR reaction mixture with Taqman Universal PCR master mix.**

Reagent	1 Reaction $\mu$ l	1 Reaction $\mu$ l	Sample (n)
Reporter assay	0.5	0.5	....
cDNA	1	3	-
Taqman Universal PCR Master Mix (2x)	5	5	....
Nuclease-free water	3.5	1.5	....
Final volume	10	10	....

**Table 3.16. Coxsackievirus B3 Real-time PCR reaction mixture with Taqman Universal PCR master mix.**

Reagent	1 Reaction $\mu$ l	Sample (n)
Forward primer	0.5	....
Reverse primer	0.5	
Probe	0.5	
cDNA	2	-
Taqman Universal PCR Master Mix (2x)	6.25	....
Nuclease-free water	2.75	....
Final volume	12.5	....

### 3.2.7 Immunohistochemistry

#### 3.2.7.1 Background

Immunohistochemistry (IHC) is defined as the *in situ* detection of antigens in tissue sections and cells using monoclonal or polyclonal antibodies. Visualization takes place through a conversion of a substrate into a color, which can be detected using a microscope. A complete immunohistochemical method comprises five main steps, starting with 1) tissue acquisition from the experimental animal, 2) tissue processing and embedding, 3) tissue sectioning, 4) tissue staining and ending by 5) screening and analysis.

#### 3.2.7.2 Tissue cutting using cryostat

At the end of the animal experiment, a relatively big ring was cut from the LV, snap frozen in liquid nitrogen and then positioned at  $-80^{\circ}\text{C}$ . LV samples were transferred to  $-20^{\circ}\text{C}$  one day before cutting. LV rings were embedded in Tissue-Tek OCT (Sakura, Zoeterwoude, NL). Afterwards, transverse sections of  $5\mu\text{m}$  thickness were cut using the cryostat (Microm,

Minnesota, USA). Subsequently, the sections were immersed in ice-cold acetone for 10 min. After drying, the slides were immediately ready for staining or stored at -20°C.

### 3.2.7.3 Immunohistochemistry

There are numerous IHC methods, which can be used to localize and quantify antigens. The selected method should include consideration of different factors, including the specimen types of the antibodies and assay sensitivity. In this work two methods were used, the avidin-biotin complex (ABC) method and the EnVision method.

#### 3.2.7.3.1 The Avidin-Biotin Complex

The ABC method was developed at the beginning of 1980s. It relies on the strong affinity of avidin for the vitamin, biotin (**Figure 3.14.**). Biotin is simply conjugated to antibodies and enzymes. In the ABC method, secondary antibodies function as connectors between primary antibodies, which bind to tissue, and an avidin-biotin-peroxidase complex. Afterwards, a colorless substrate, carbazol solution, which contains 3-Amino-9-ethylcarbazole (Sigma, Steinheim, Germany) and N, N Dimethylformamide (Sigma, Steinheim, Germany) is added, which is transformed to a red endproduct by the peroxidase enzyme.

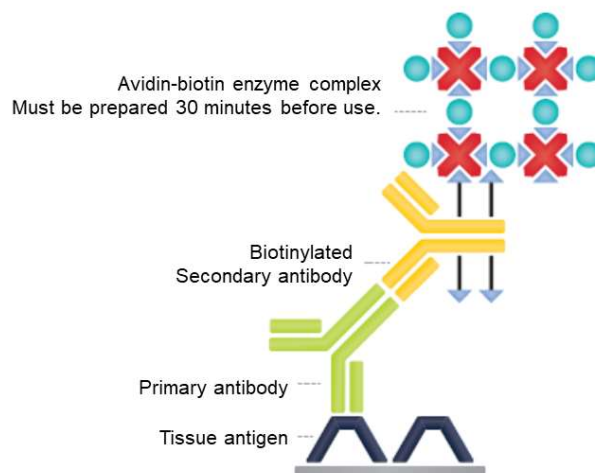


**Figure 3.14. Principle of the Avidin-Biotin Complex (Dako guide 6<sup>th</sup> ed.).**

This method was used for the detection of CD4<sup>+</sup>, CD8<sup>+</sup> and CD68<sup>+</sup> cells.

Hereto, slides were positioned in 1x Tris buffered saline (TBS) for 5 min, followed by incubation with 0.075% H<sub>2</sub>O<sub>2</sub> for 7 min on a horizontal shaker to block the endogenous peroxidase. Afterwards, slides were washed once with 1xTBS for 5 min on a shaker. Subsequently, 75 µl of the primary antibody (1<sup>st</sup> AB), which was previously prepared using 10% goat serum, 1% BSA in 1x TBS, and 4 drops avidin/ml, were added to every staining field and slides were stored for 30 min in a moist chamber.

**Table 3.17. Antibodies and dilutions used with the ABC method.**

1st AB	Species	Dilution	2nd AB	Company	Dilution
Anti-CD4	Rat	1:50	Biotinylated Goat anti-rat	Dianova	1:250
Anti-CD68	Rat	1:600	Biotinylated Goat anti-rat	Dianova	1:250
Anti-CD8	Rat	1:50	Biotinylated Goat anti-rat	Dianova	1:250

### 3.2.7.3.2 The Envision™ method

Polymer-based IHC is a highly sensitive method, which was developed due to the limitations observed in the ABC method like low sensitivity and the presence of endogenous biotin in tissues. This method uses a polymer (dextran) backbone, which facilitates the conjugation of multiple antibodies and enzymes. It uses the combination of the secondary antibodies with anti-mouse Ig and anti-rabbit Ig specificity, and horseradish peroxidase (HRP) or alkaline phosphatase (AP) as detection system (**Figure 3.15.**). This ‘universal’ mixture can be used to detect any tissue-bound primary antibody of mouse or rabbit source.

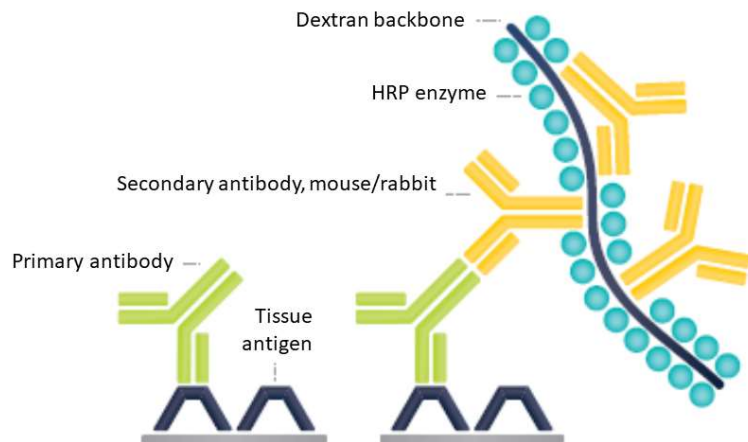


**Figure 3.15. The Envision™ polymer-based method (Dako guide 6<sup>th</sup> ed.).**

This method was used in this manuscript to investigate cardiac collagen I and collagen III.

Hereto, Slides were positioned in 1x PBS for 5 min, followed by incubation with 0.075% H<sub>2</sub>O<sub>2</sub> for 7 min on a horizontal shaker to block the endogenous peroxidase. Subsequently, slides were washed once with 1x PBS on a shaker. Afterwards, 75 µl of the 1<sup>st</sup> AB, which was previously prepared using 10% FBS in 1x PBS, were added to every staining field and slides were stored for one hour in a moist chamber. Slides were washed twice again with 1x PBS, followed by addition of 75 µl of the secondary antibody (2<sup>nd</sup> AB) per staining field and stored for 30 min in a moist chamber. As described above, additional washing was performed, and

slides were incubated for 12 min in the dark with substrate (Carbazol) solution. Prior Hemalum staining of cells nuclei, slides were again washed with 1x PBS for 5 min, and after 30 sec, slides were rinsed for 5 times in cold tap water. Next, the slides were washed with warm tap water for 10 min, followed by adding 200 µl of Kaiser's glycerol gelatine per slide before putting the mounting glass.

**Table 3.18. Antibodies and dilutions used with the Envision™ method.**

1. AB	Species	Dilution	2.AB	Dilution
Anti-Col I	Rabbit	1:350	EnVision Dako #K4003 anti-rabbit	undiluted
Anti-Col III	Rabbit	1:200	EnVision Dako #K4003 anti-rabbit	undiluted

Analysis of stained sections was performed in a blinded fashion manner by digital image analysis on a Leica DM2000 LED microscope (Leica Microsystems, Wetzlar, Germany) at 100x magnification.

### 3.2.8 Statistical analysis

Statistical analysis was performed using GraphPad Prism 7.0 (GraphPad Software, Inc., La Jolla, USA). Assumption of Gaussian distribution was consistently tested by the method of Shapiro-Wilk normality test. For normal distributed data, an ordinary one-way ANOVA with Fisher's LSD post hoc test was performed. When Gaussian distribution was not reached, Kruskal-Wallis test with the Dunn's post-hoc test was used. Data are presented as mean ± SEM. Differences were significant when the two-sided p-value was lower than 0.05. For the assessment of the chronic CVB3 model, by which the CVB3 was compared to the control group, an unpaired Student's t test was used with Welch's correction. A student t test was also performed for the *in vitro* viability assay comparing control versus CVB3 per timepoint. When Gaussian distribution was not reached, the Mann-Whitney test was used.

## 4. Results

### 4.1. Comparison of EMB-CardAPs versus EMB-cardiac fibroblasts in acute Coxsackievirus B3-induced myocarditis mice

#### 4.1.1. EMB-CardAPs and EMB-Cardiac fibroblasts improve the systolic and diastolic function in acute Coxsackievirus B3-induced myocarditis mice

Six days after i.v. application of EMB-CardAPs and EMB-CF in CVB3-induced myocarditis mice, LV function was assessed using conductance catheter. CVB3 impaired the cardiac function as indicated by a 15% ( $p < 0.01$ ) lower EF vs control mice (**Figure 4.1.1. A**). However, there was no significant difference in the EF, neither between CVB3+EMB-CardAPs nor CVB3+EMB-CF vs untreated CVB3-infected mice. CVB3 infection reduced the systolic function markedly as displayed by a 24% ( $p < 0.05$ ) and 39% ( $p < 0.001$ ) decline in  $P_{\max}$  and  $dP/dt_{\max}$ , respectively (**Figure 4.1.1. C-D**). EMB-CardAPs and EMB-CF did not alter  $P_{\max}$ , but improved  $dP/dt_{\max}$  by 65% and 47%, respectively, in comparison with CVB3-untreated mice. Diastolic function was impaired in the CVB3 mice as indicated by the 54% ( $p < 0.0001$ ) decline of  $dP/dt_{\min}$  and 130% ( $p < 0.0001$ ) increase of Tau in CVB3 versus control mice (**Figure 4.1.1. E-F**). Application of EMB-CardAPs and EMB-CF improved the diastolic function, which follows from the 120% and 87% increase of  $dP/dt_{\min}$ , and the 55% and 39% decrease of Tau, respectively, when compared with CVB3-infected mice.

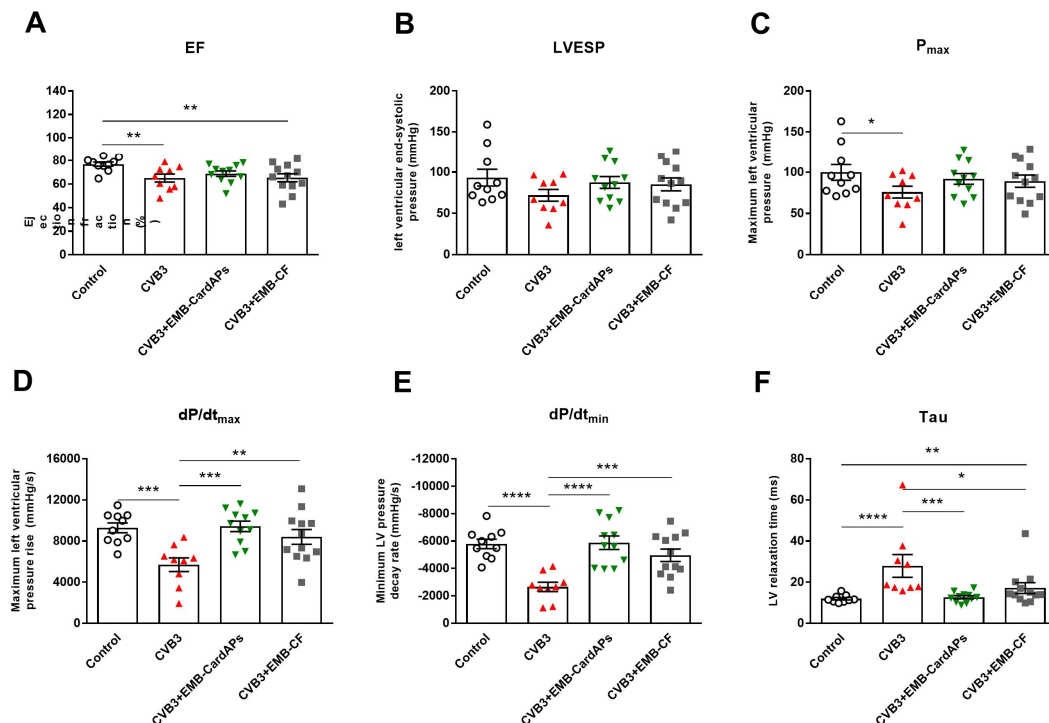


**Figure 4.1.1. Impact of intravenous injection of EMB-CardAPs and EMB-CF on the left ventricular function in acute Coxsackievirus B3-induced myocarditis mice.** Indices for the left ventricle (LV) were obtained by conductance catheter. Bar graphs represent the mean  $\pm$  SEM of **A.** Ejection fraction (EF; %), **B.** End systolic pressure (LVESP; mmHg), **C.** LV Maximum pressure ( $P_{\max}$ ; mmHg), **D.** LV contractility ( $dP/dt_{\max}$ ; mmHg/s), **E.** LV relaxation ( $dP/dt_{\min}$ ; mmHg/s) and **F.** Relaxation time (Tau; ms).

Statistical differences were assessed using One-way ANOVA (\* $p < 0.05$ , \*\* $p < 0.01$ , \*\*\* $p < 0.001$ , and \*\*\*\* $p < 0.0001$ ,  $n = 10-12$  / group).

#### **4.1.2. EMB-CardAPs but not EMB-cardiac fibroblasts reduce left ventricular fibrosis in acute Coxsackievirus B3-induced myocarditis mice**

Given the importance of cardiac fibrosis in the pathology of CVB3, immunohistochemistry analysis was performed on the main extracellular matrix proteins, collagen I and III. CVB3 mice displayed 1.8-fold ( $p < 0.001$ ) and 1.3-fold ( $p < 0.001$ ) higher LV collagen I and collagen III expression, respectively, vs control mice (**Figure 4.1.2. A-B**). In addition, the ratio of collagen I to collagen III elevated in CVB3-infected mice compared to control mice ( $p = 0.0885$ ). EMB-CardAPs application in CVB3-infected mice decreased LV collagen I by 1.3-fold ( $p < 0.05$ ), which was associated with a non-significant, but lower ratio of collagen I to collagen III in EMB-CardAPs treated CVB3-infected mice versus CVB3 mice (**Figure 4.1.2. C**). In contrast, treatment of CVB3-infected mice with EMB-CF, did not change the LV collagen I, significantly. Moreover, CF application displayed an elevation in the ratio of collagen I to collagen III ( $p = 0.0526$ ). However, EMB-CF reduced collagen III in CVB3 mice, as indicated by a 1.2-fold ( $p < 0.01$ ) decrease in collagen III, in comparison with CVB3 untreated mice.

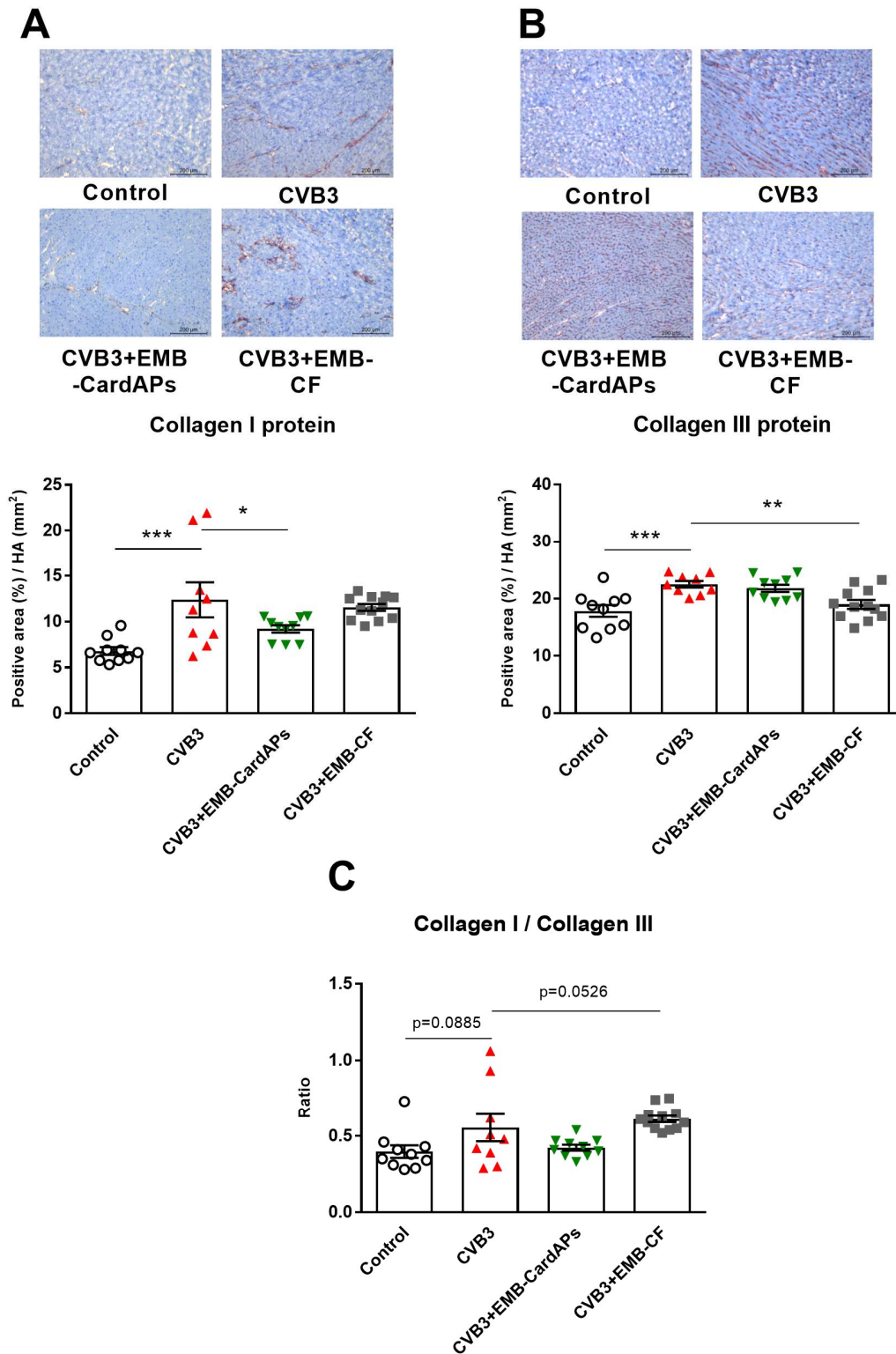


**Figure 4.1.2. Impact of intravenous injection of EMB-CardAPs and EMB-CF on left ventricular collagen expression in acute Coxsackievirus B3-induced myocarditis mice.** **A.** Upper panel: Representative left ventricular (LV) cryosections of Collagen I at a magnification of 100x, lower panel: bar graphs represent the mean±SEM of LV collagen I depicted as positive area (%) / heart area (HA) (mm<sup>2</sup>). **B.** Upper panel: Representative LV cryosections of Collagen III at a magnification of 100x, lower panel: bar graphs represent the mean±SEM of LV collagen III depicted as positive area (%) / heart area (HA) (mm<sup>2</sup>) and **C.** Ratio of Collagen I to III. Statistical differences were assessed using One-way ANOVA (\*p<0.05, \*\*p<0.01 and \*\*\*p<0.001, n=10-12 / group).

#### 4.1.3. EMB-CardAPs but not EMB-cardiac fibroblasts modulate left ventricular chemokine mRNA expression in acute Coxsackievirus B3-induced myocarditis mice

LV mRNA expression of the chemokines CCL2, CCL7, known to attract pro-inflammatory monocytes, and of CX3CL1, known to attract anti-inflammatory monocytes, was measured. CVB3-infected mice exhibited 22-fold ( $p<0.01$ ) and 31-fold ( $p<0.01$ ) higher LV mRNA levels of the chemokines CCL2 and CCL7 compared to control mice, respectively (**Figure 4.1.3. A-B**). CVB3 infection did not affect the LV CX3CL1 mRNA expression (**Figure 4.1.3. C**). However, CVB3-infected mice displayed 27-fold ( $p<0.01$ ) and 32-fold ( $p<0.001$ ) higher CCL2/CX3CL1 and CCL7/CX3CL1 ratios, respectively, in comparison with uninfected mice (**Figure 4.1.3. D-E**). EMB-CardAPs application reduced LV CCL2 and CCL7 chemokine expression by 11-fold ( $p<0.05$ ) and 23-fold ( $p<0.01$ ), respectively, when compared to untreated CVB3-infected mice, whereas EMB-CF did not change the mRNA levels of CCL2 and CCL7 versus CVB3 untreated mice.

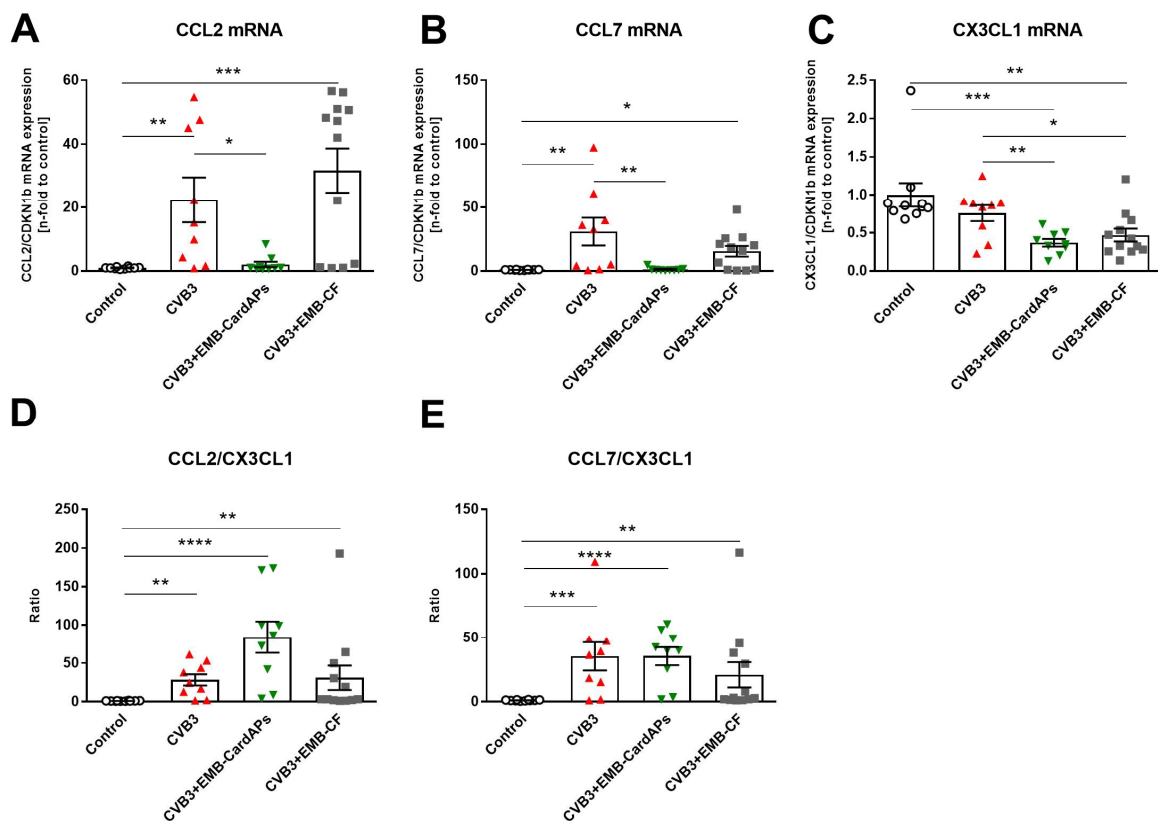


**Figure 4.1.3. Impact of intravenous injection of EMB-CardAPs and EMB-CF on left ventricular chemokine mRNA expression in acute Coxsackievirus B3-induced myocarditis mice.** Bar graphs represent the mean $\pm$ SEM of left ventricular (LV) of **A.** CCL2, **B.** CCL7, **C.** CX3CL1 mRNA expression, **D.** CCL2/CX3CL1, and **E.** CCL7/CX3CL1. Statistical differences were assessed using One-way ANOVA (\* $p<0.05$ , \*\* $p<0.01$ , \*\*\* $p<0.001$ , and \*\*\*\* $p<0.0001$ ,  $n=10-12$  / group).

#### 4.1.4. EMB-CardAPs but not EMB-cardiac fibroblasts reduce left ventricular mRNA levels of chemokine receptors in acute Coxsackievirus B3-induced myocarditis mice

CVB3 infection upregulated LV CCR2 mRNA expression by 12-fold ( $p < 0.01$ ) when compared to control mice, whereas LV CX3CR1 mRNA level did not change due to CVB3 infection (**Figure 4.1.4. A-B**). EMB-CardAPs application led to 11-fold ( $p < 0.01$ ) lower CCR2 LV mRNA level versus untreated CVB3-infected mice. EMB-CF application did not reduce LV CCR2, nor CX3CR1 mRNA expression in CVB3-infected mice.

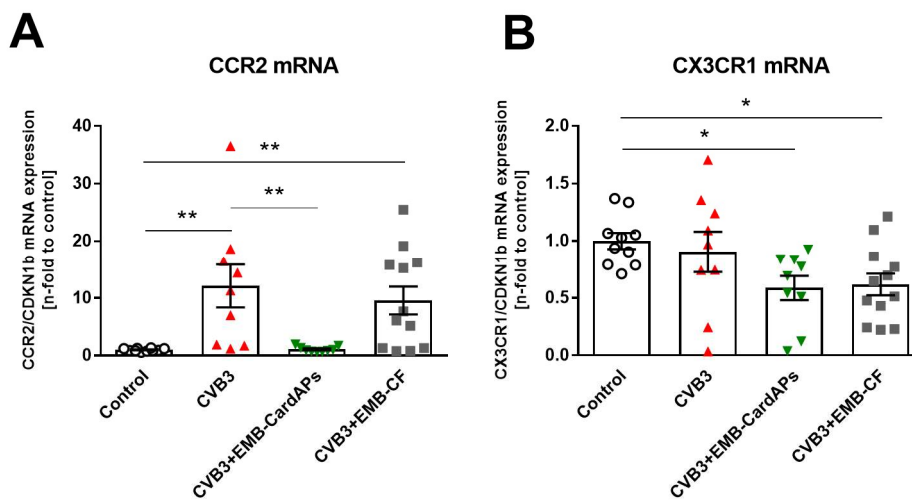


**Figure 4.1.4. Impact of intravenous injection of EMB-CardAPs and EMB-CF on left ventricular chemokine receptor mRNA expression in acute Coxsackievirus B3-induced myocarditis mice.** Bar graphs represent the mean $\pm$ SEM of left ventricular (LV) **A**. CCR2 and **B**. CX3CR1 mRNA expression. Statistical differences were assessed using One-way ANOVA (\* $p < 0.05$  and \*\* $p < 0.01$ ,  $n = 10-12$  / group).

#### 4.1.5. EMB-CardAPs but not EMB-cardiac fibroblasts reduce left ventricular monocyte and pro-inflammatory cell presence in acute Coxsackievirus B3-induced myocarditis mice

Immunohistochemistry analysis showed a high presence of inflammatory cells in the LV of CVB3-infected mice, as indicated by an 1.7-fold ( $p < 0.05$ ), 2.7-fold ( $p < 0.05$ ) and 3.2-fold ( $p < 0.0001$ ) increase in CD4<sup>+</sup>, CD8<sup>+</sup> and CD68<sup>+</sup> cells, respectively, in comparison with control mice (**Figure 4.1.5. A-B-C**). Moreover, CVB3 infection upregulated the LV Ly6c mRNA level by 2.1-fold ( $p < 0.05$ ) when compared to uninfected mice (**Figure 4.1.5. D**). EMB-CardAPs application alleviated monocyte and pro-inflammatory cell presence, as indicated by 2.0-fold ( $p < 0.01$ ) lower CD68<sup>+</sup> cells and 1.6-fold ( $p < 0.01$ ) lower LV Ly6c mRNA expression, when compared to untreated CVB3-infected mice.

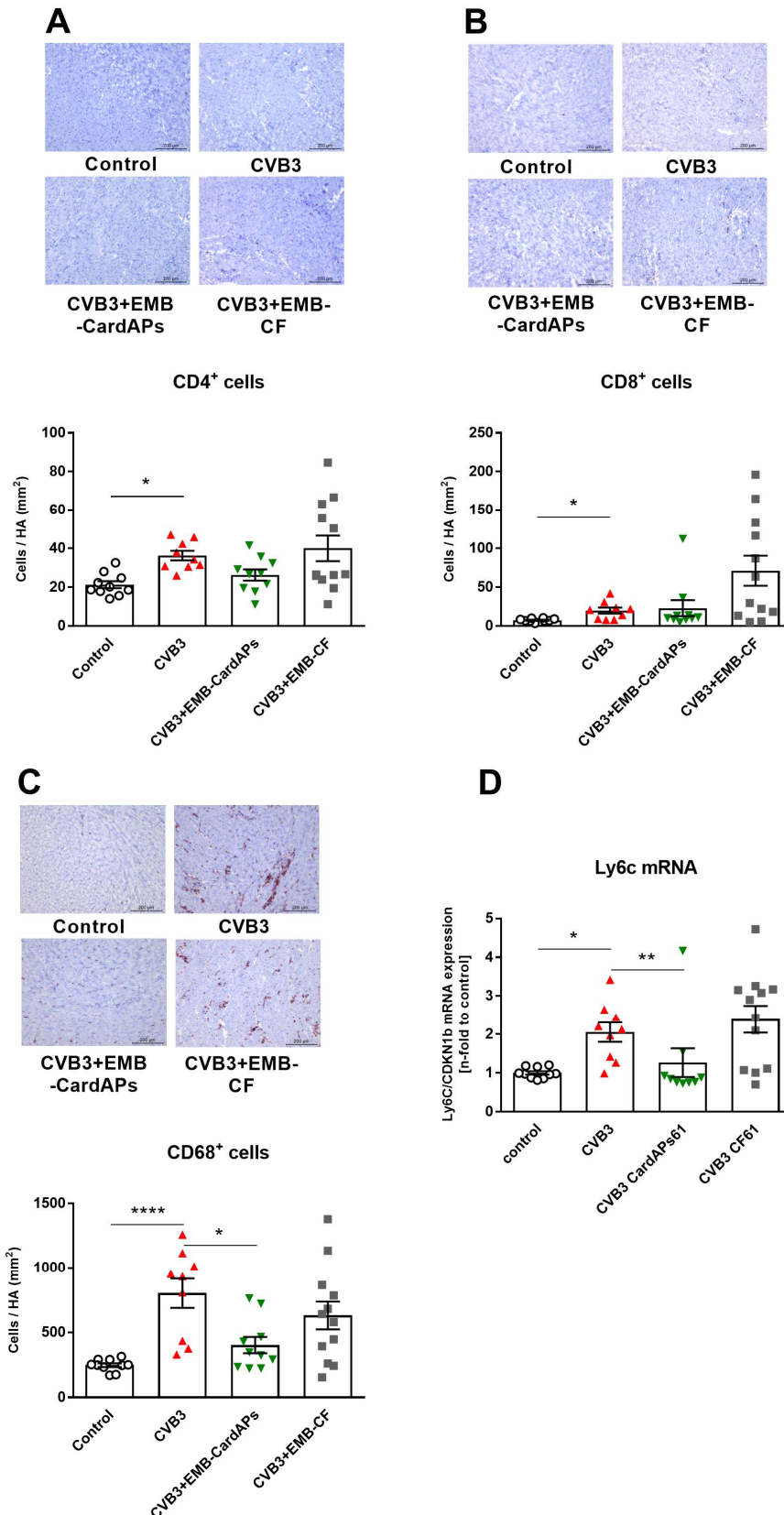


**Figure 4.1.5. Impact of intravenous injection of EMB-CardAPs and EMB-CF on left ventricular immune cell presence in acute Coxsackievirus B3-induced myocarditis mice.** Upper and lower panels of **A.-C.** depict representative left ventricular (LV) cryosections at a magnification of 100x, and bar graphs representing the mean $\pm$ SEM of **A.** CD4<sup>+</sup>cells, **B.** CD8<sup>+</sup>cells, and **C.** CD68<sup>+</sup>cells, respectively. **D.** bar graphs represent the mean $\pm$ SEM of LV Ly6c mRNA level normalized to GAPDH. Statistical differences were assessed using One-way ANOVA (\* $p$ <0.05, \*\* $p$ <0.01, and \*\*\*\* $p$ <0.0001,  $n$ =10-12 / group).

#### 4.1.6. EMB-CardAPs but not EMB-Cardiac fibroblasts reduce left ventricular mRNA levels of inflammatory cytokines in acute Coxsackievirus B3-induced myocarditis mice

CVB3 infection led to upregulation of inflammatory cytokines, as indicated by 6.6-fold ( $p < 0.0001$ ) and 11-fold ( $p < 0.01$ ) higher LV TNF- $\alpha$  and IL-6 mRNA expression compared to control mice, respectively (**Figure 4.1.6. A-C**). Moreover, CVB3-infected mice displayed 18-fold ( $p < 0.0001$ ), 48-fold ( $p < 0.001$ ) and 20-fold ( $p < 0.01$ ) higher mRNA expression of IL-10, IFN- $\gamma$  and IFN- $\beta$ , respectively, in comparison with uninfected mice (**Figure 4.1.6. D-F**). EMB-CardAPs application diminished the mRNA levels of pro-inflammatory cytokines, as indicated by 4.2-fold ( $p < 0.01$ ) and 13-fold ( $p < 0.01$ ) lower mRNA levels of TNF- $\alpha$  and IL-6, respectively, when compared to untreated CVB3-infected mice. Unlikely, EMB-CardAPs application led to downregulation of anti-inflammatory cytokines, as indicated by a 10.3-fold ( $p < 0.01$ ), 14.6-fold ( $p < 0.05$ ) and 10.8-fold ( $p < 0.01$ ) decrease in the mRNA levels of IL-10, IFN- $\gamma$  and IFN- $\beta$ , respectively, compared to CVB3 untreated mice. In contrast, EMB-CF application did not change the mRNA levels of inflammatory cytokines significantly, in comparison with untreated CVB3-infected mice.

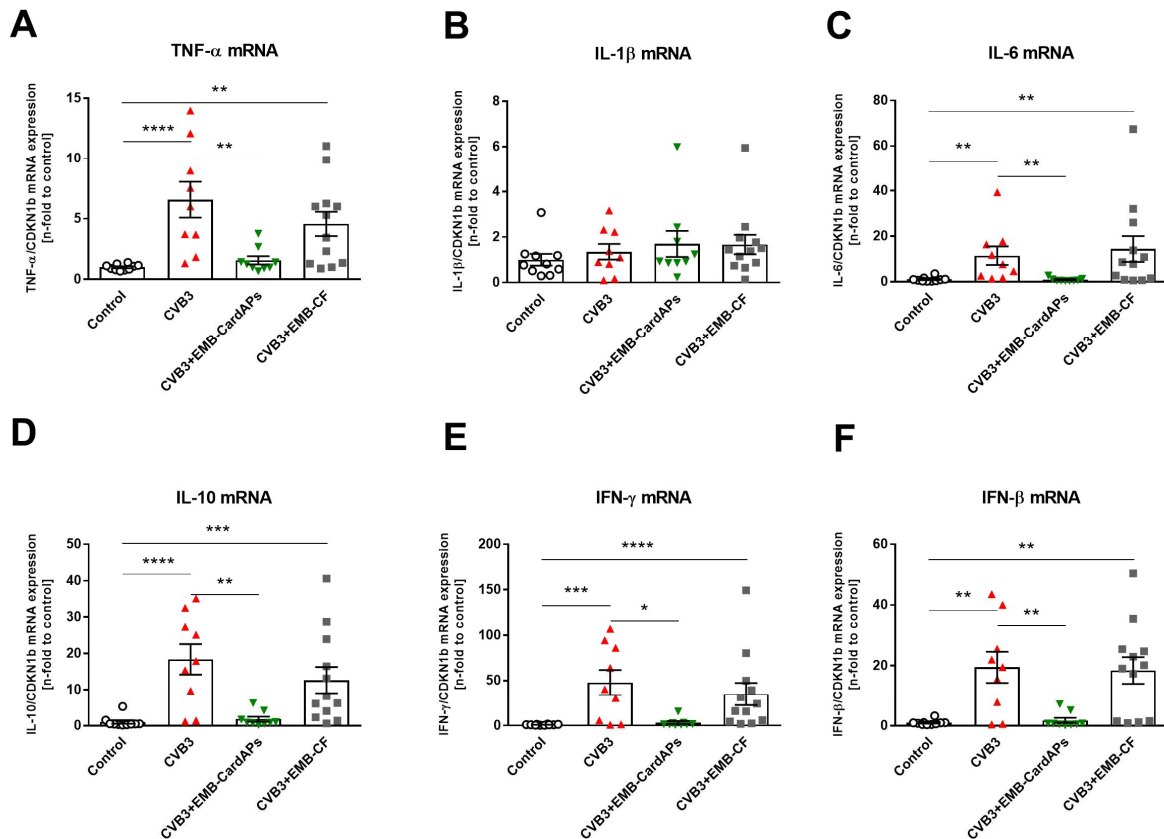


**Figure 4.1.6. Impact of intravenous injection of EMB-CardAPs and EMB-CF on left ventricular cytokine mRNA expression in acute Coxsackievirus B3-induced myocarditis mice.** Bar graphs represent the mean $\pm$ SEM of left ventricular (LV) of **A.** TNF- $\alpha$ , **B.** IL-1 $\beta$ , **C.** IL-6, **D.** IL-10, **E.** IFN- $\gamma$ , and

**F.** IFN- $\beta$  mRNA expression. Statistical differences were assessed using One-way ANOVA (\* $p < 0.05$ , \*\* $p < 0.01$ , \*\*\* $p < 0.001$ , and \*\*\*\* $p < 0.0001$ ,  $n = 10-12$  / group).

#### 4.1.7. EMB-CardAPs but not EMB-cardiac fibroblasts modulate markers of left ventricular apoptosis in acute Coxsackievirus B3-induced myocarditis mice

Infection with CVB3 increased the LV mRNA expression of the anti-apoptotic (Bcl-2) and pro-apoptotic (BAX) by 1.3-fold ( $p < 0.01$ ) and 1.6-fold ( $p < 0.05$ ), respectively, when compared to control mice (**Figure 4.1.7. A-B**). EMB-CardAPs application led to 1.3-fold ( $p < 0.01$ ) and 2.7-fold ( $p < 0.0001$ ) lower mRNA levels of Bcl-2 and BAX, respectively, in comparison with CVB3 untreated mice. Moreover, EMB-CardAPs application showed an increase in the ratio of Bcl-2 to BAX, as indicated by a 2.2-fold ( $p < 0.01$ ) higher ratio of Bcl-2/BAX, when compared to untreated CVB3-infected mice (**Figure 4.1.7. C**).

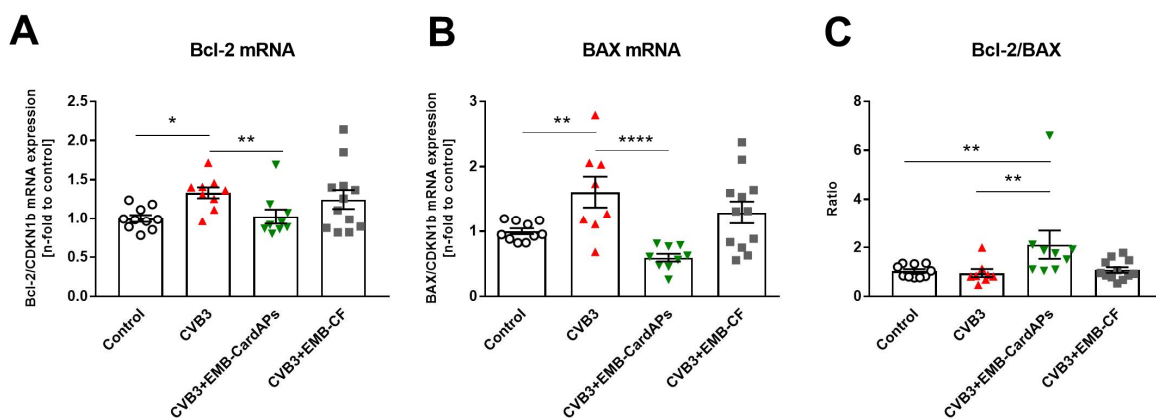


**Figure 4.1.7.** Impact of intravenous injection of EMB-CardAPs and EMB-CF on left ventricular mRNA expression of apoptotic markers in acute Coxsackievirus B3-induced myocarditis mice. Bar graphs represent the mean  $\pm$  SEM of left ventricular (LV) **A.** Bcl-2 and **B.** BAX mRNA levels, and **C.** Bcl-2/BAX ratio. Statistical differences were assessed using One-way ANOVA (\* $p < 0.05$ , \*\* $p < 0.01$ , and \*\*\*\* $p < 0.0001$ ,  $n = 10-12$  / group).

#### 4.1.8. EMB-CardAPs but not EMB-cardiac fibroblasts reduce left ventricular Coxsackievirus B3 mRNA expression in acute Coxsackievirus B3-induced myocarditis mice

EMB-CardAPs application decreased LV CVB3 mRNA expression by 34-fold ( $p < 0.05$ ) in comparison with non-treated CVB3-infected mice, whereas EMB-CF did not affect CVB3 mRNA expression in CVB3-infected mice (**Figure 4.1.8.**).

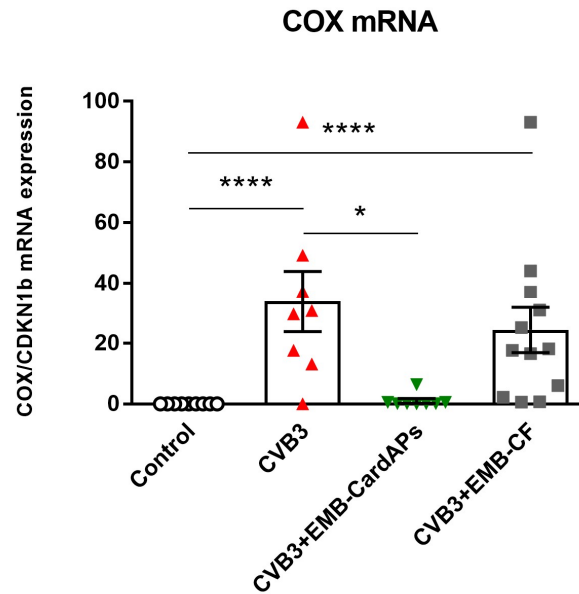


**Figure 4.1.8. Impact of intravenous injection of EMB-CardAPs and EMB-CF on left ventricular Coxsackievirus B3 mRNA expression in acute Coxsackievirus B3-induced myocarditis mice.** Bar graphs represent the mean±SEM of left ventricular (LV) **Coxsackievirus B3 (COX)** mRNA levels. Statistical differences were assessed using One-way ANOVA (\* $p < 0.05$  and \*\*\*\* $p < 0.0001$ ,  $n = 10-12$  / group).

## 4.2. *In vitro* evaluation of RAA-CardAPs

### 4.2.1. Impact of Coxsackievirus B3 infection on the viability of RAA-CardAPs

To evaluate whether RAA-CardAPs are resistant to CVB3 infection, RAA-CardAPs were infected with CVB3 or serum starved. Four h, 12h, 24h, and 48h post infection/serum starvation, respectively, the viability of RAA-CardAPs was evaluated via a MTT viability assay. Four h, and 24h post infection, the absorbance of CVB3-infected RAA-CardAPs was 1.2-fold ( $p < 0.0001$ ) and 1.1-fold ( $p < 0.0001$ ) higher compared to the respective controls (**Figure 4.2.1.**). At 48h after infection, there was no difference between the control and CVB3-infected cells. Furthermore, CVB3-infected and uninfected RAA-CardAPs exhibited a similar increase in absorbance between 4h versus 48h post infection.

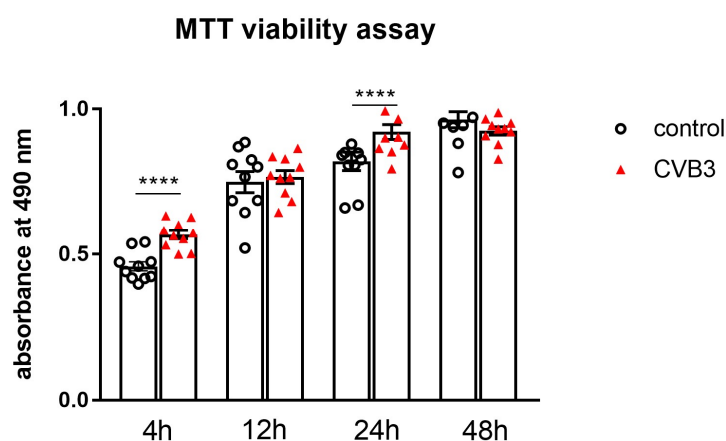


**Figure 4.2.1. Coxsackievirus B3 infection does not hamper the viability of RAA-CardAPs.** Bar graph represent the mean $\pm$ SEM of the absorbance at 490 nm of uninfected (open circle) and CVB3-infected (red triangle) RAA-CardAPs, 4h, 12h, 24h and 48h post serum starvation or infection, respectively. Statistical differences were assessed using Student t test (\*\*\*\* $p < 0.0001$ ,  $n = 10$  / group).

### 4.2.2. Impact of RAA-CardAPs on apoptosis of Coxsackievirus B3-infected HL-1 cardiomyocytes

Given the importance of apoptosis in viral progeny release, we next evaluated the impact of RAA-CardAPs on CVB3-infected DiO-labeled HL-1 cardiomyocytes. Therefore, RAA-CardAPs were added to HL-1 cells at a ratio of 1 RAA-CardAP to 10 DiO-labeled HL-1 cells, 1h post CVB3 infection or serum starvation. CVB3 infection increased the % of Annexin V+/7AAD- (% DiO gated cells) by 2.5-fold ( $p < 0.0001$ ), whereas RAA-CardAPs reduced the CVB3-induced apoptosis by 1.3-fold ( $p < 0.0001$ ) (**Figure 4.2.2.**).

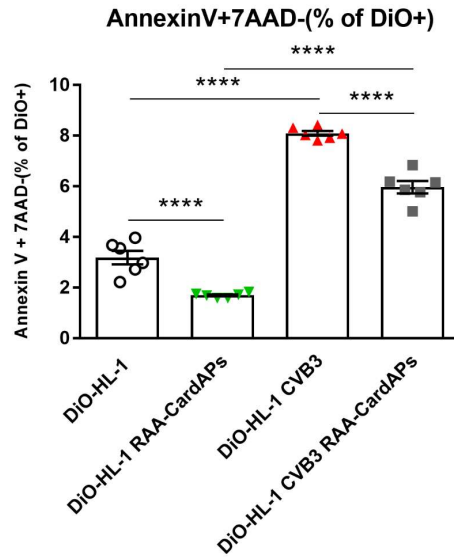


**Figure 4.2.2. RAA-CardAPs reduce Coxsackievirus B3-induced apoptosis of DiO-labeled HL-1 cardiomyocytes.** Bar graph represent the mean±SEM of Annexin V+/AAD- (% DiO+) 24h post serum starvation or infection. Statistical differences were assessed using One-way ANOVA (\*\*\*\*p<0.0001, n=6 / group).

#### 4.2.3. Impact of RAA-CardAPs on CVB3 mRNA expression in HL-1-RAA-CardAPs co-culture

We next evaluated whether the decrease in RAA-CardAPs CVB3-induced HL-1 apoptosis was associated with a reduction in CVB3 mRNA expression. Instead, co-culture of HL-1 with RAA-CardAPs was associated with a 1.2-fold (p<0.0001) increase in CVB3 mRNA expression compared to solo cultured CVB3-infected HL-1 cells (**Figure 4.2.3.**).

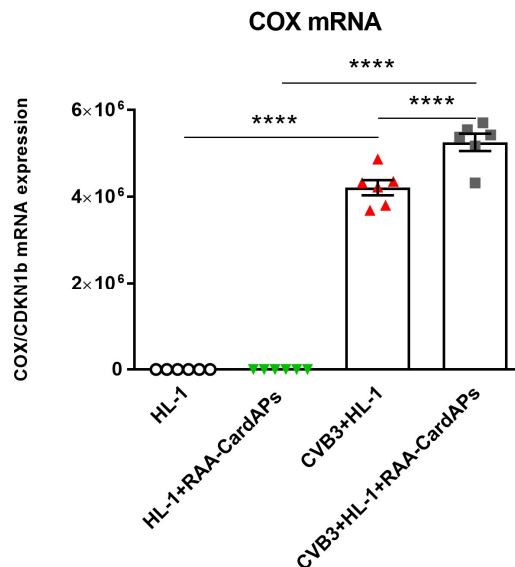


**Figure 4.2.3. RAA-CardAPs do not decrease Coxsackievirus B3 mRNA expression in a co-culture of DiO-labeled HL-1 cardiomyocytes with RAA-CardAPs.** Bar graph represent the mean±SEM of CVB3 (COX) mRNA expression. Statistical differences were assessed using One-way ANOVA (\*\*\*\*p<0.0001, n=6 / group).

### 4.3. Allogenic CardAPs in acute Coxsackievirus B3-induced myocarditis mice

#### 4.3.1. RAA-CardAPs improve left ventricular function in acute Coxsackievirus B3-induced myocarditis mice

Six days after i.v. application of RAA-CardAPs in CVB3-induced myocarditis mice, cardiac function was assessed using conductance catheter. CVB3 impaired the cardiac function as indicated by a 10% ( $p < 0.01$ ) reduction of the EF vs control mice (**Figure 4.3.1. A**). However, there was no significant difference in the EF between CVB3+RAA-CardAPs vs untreated CVB3-infected mice. Systolic function was deteriorated due to CVB3 infection, as indicated by a 27% ( $p < 0.0001$ ), 23% ( $p < 0.0001$ ), and 28% ( $p < 0.0001$ ) decline in LVESP,  $P_{\max}$  and  $dP/dt_{\max}$ , respectively (**Figure 4.3.1. B-C-D**). RAA-CardAPs improved systolic function, which follows from the 23% ( $p < 0.001$ ), 19% ( $p < 0.001$ ), and 29% ( $p < 0.001$ ) increase in LVESP,  $P_{\max}$  and  $dP/dt_{\max}$  in RAA-CardAPs+CVB3 compared to CVB3-infected mice, respectively. Diastolic function was impaired in the CVB3 mice as indicated by the 37% ( $p < 0.0001$ ) decline of  $dP/dt_{\min}$  and 18% ( $p = 0.055$ ) increase of Tau in CVB3 versus control mice (**Figure 4.3.1. E-F**). RAA-CardAPs application improved  $dP/dt_{\min}$  by 39% ( $p < 0.01$ ), but did not reduce Tau in comparison to untreated CVB3 mice.

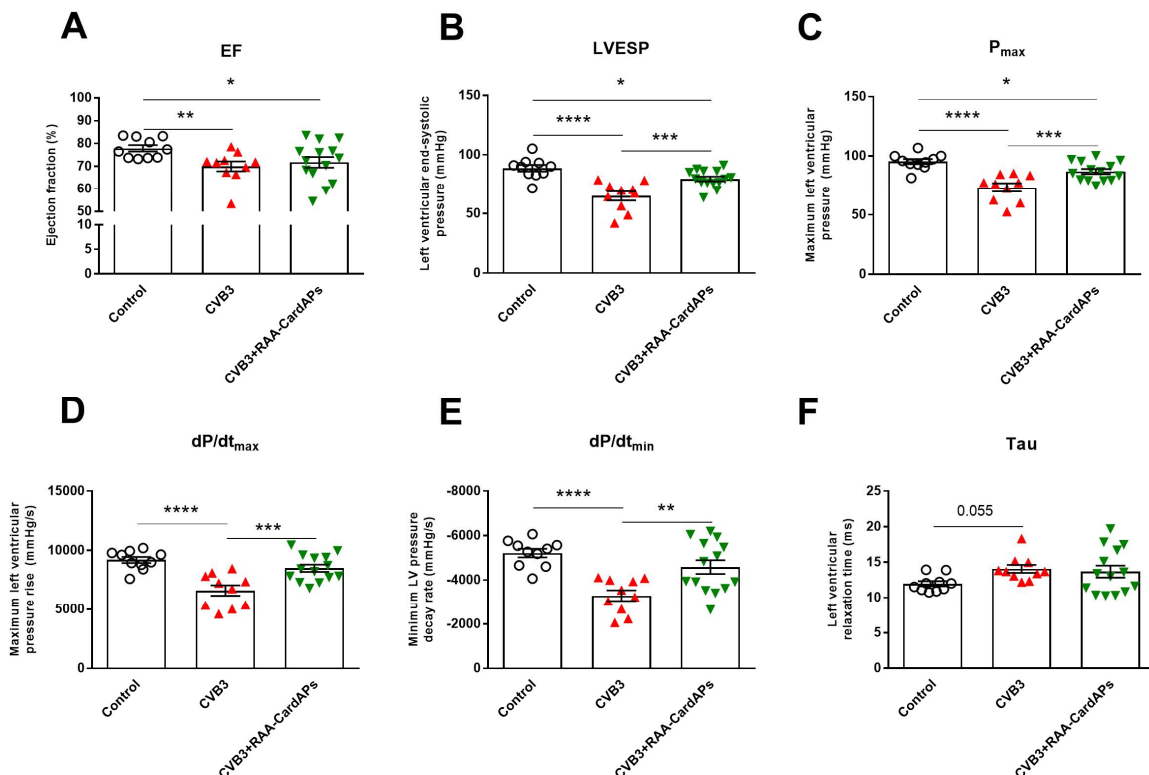


**Figure 4.3.1. Impact of intravenous injection of RAA-derived CardAPs on the left ventricular function in acute Coxsackievirus B3-induced myocarditis mice.** Indices for the left ventricle (LV) were obtained by conductance catheter. Bar graphs represent the mean  $\pm$  SEM of **A**. Ejection fraction (EF; %), **B**. End systolic pressure (LVESP; mmHg), **C**. LV Maximum pressure ( $P_{\max}$ ; mmHg), **D**. LV contractility ( $dP/dt_{\max}$ ; mmHg/s), **E**. LV relaxation ( $dP/dt_{\min}$ ; mmHg/s) and **F**. Relaxation time (Tau; ms).

Statistical differences were assessed using One-way ANOVA (\* $p < 0.05$ , \*\* $p < 0.01$ , \*\*\* $p < 0.001$ , and \*\*\*\* $p < 0.0001$ ,  $n = 10-14$  / group).

#### 4.3.2. RAA-CardAPs reduce left ventricular fibrosis in acute Coxsackievirus B3-induced myocarditis mice

To evaluate the impact of RAA-CardAPs on cardiac fibrosis in acute CVB3-induced myocarditis, immunohistochemistry of the main extracellular matrix proteins, collagen I and III was performed. CVB3 mice displayed 1.8-fold ( $p < 0.01$ ) higher LV collagen I vs control mice, which was reflected in a 1.5-fold ( $p < 0.05$ ) increased ratio of collagen I to collagen III compared to control mice (Figure 4.3.2. A-C). RAA-CardAPs application in CVB3 mice decreased LV collagen I by 1.9-fold ( $p < 0.01$ ), which was associated with a 1.6-fold ( $p < 0.01$ ) lower ratio of collagen I to collagen III in RAA-CardAPs CVB3 versus CVB3 mice.

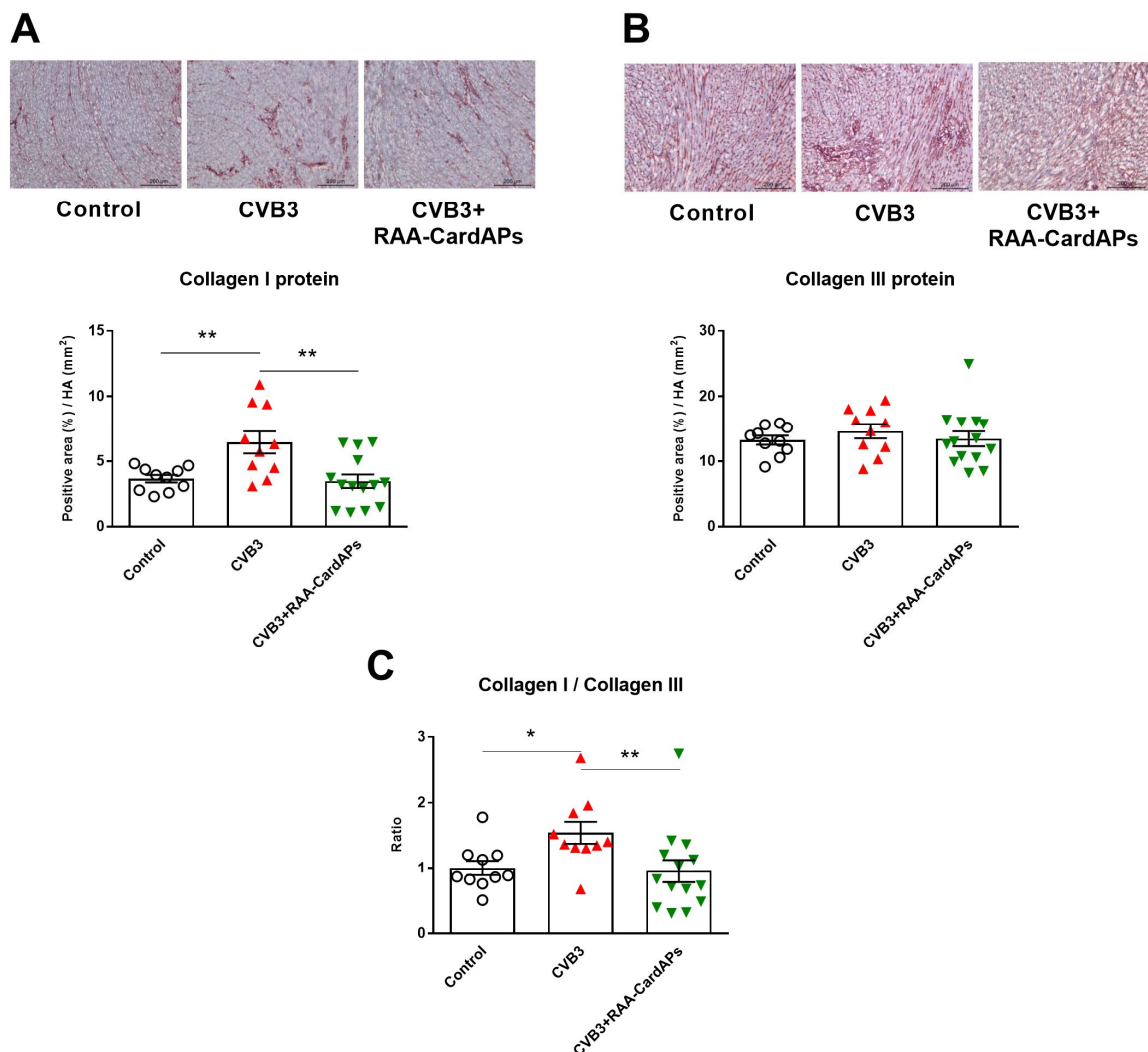


**Figure 4.3.2. Impact of intravenous injection of RAA-derived CardAPs on left ventricular collagen expression in acute Coxsackievirus B3-induced myocarditis mice. A.** Upper panel: Representative left ventricular (LV) cryosections of Collagen I at a magnification of 100x, lower panel: bar graphs represent the mean $\pm$ SEM of LV collagen I depicted as positive area (%) / heart area (HA) (mm<sup>2</sup>), **B.**

Upper panel: Representative LV cryosections of Collagen III at a magnification of 100x, lower panel: bar graphs represent the mean±SEM of LV collagen III depicted as positive area (%)/HA (mm<sup>2</sup>) and **C**. Ratio of Collagen I to III. Statistical differences were assessed using One-way ANOVA (\*p<0.05 and \*\*p<0.01, n=10-14 / group).

#### 4.3.3. RAA-CardAPs did not change the left ventricular chemokine mRNA expression in acute Coxsackievirus B3-induced myocarditis mice

Infection with CVB3 led to a 30-fold (p<0.01) and 32-fold (p<0.01) upregulation in LV mRNA expression of the chemokines CCL2 and CCL7 mRNA, respectively, in comparison with control mice (**Figure 4.3.3. A-B**). Fractalkine/CX3CL1, which has been shown to play a role in CVB3-induced myocarditis<sup>107</sup>, was not increased due to CVB3 infection (**Figure 4.3.3. C**). Furthermore, CVB3 mice displayed a 20-fold (p<0.001) and 21-fold (p<0.001) higher CCL2/CX3CL1 and CCL7/CX3CL1 ratio, vs control mice, respectively (**Figure 4.3.3. D-E**). RAA-CardAPs did not affect the expression of none of the evaluated chemokines.

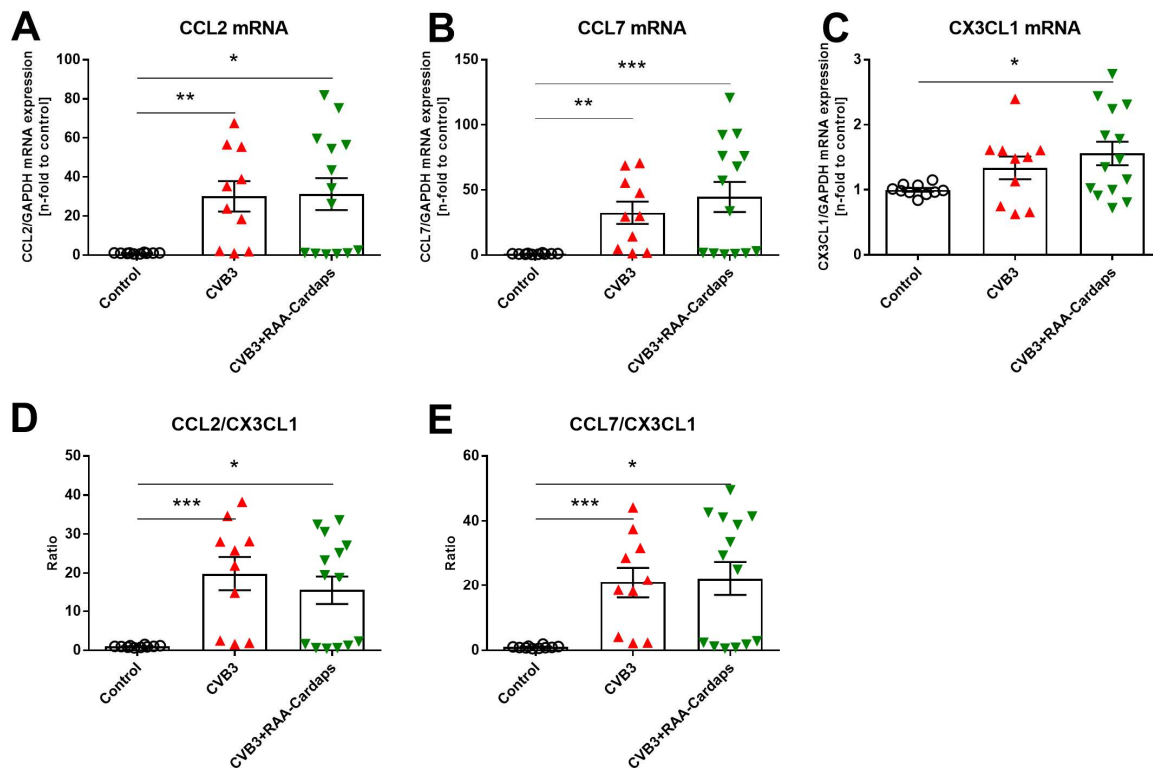


**Figure 4.3.3. Impact of intravenous injection of RAA-derived CardAPs on left ventricular chemokine mRNA expression in acute Coxsackievirus B3-induced myocarditis mice.** Bar graphs represent the mean±SEM of left ventricular (LV) **A**. CCL2, **B**. CCL7, and **C**. CX3CL1 mRNA expression, **D**. CCL2/CX3CL1, and **E**. CCL7/CX3CL1. Statistical differences were assessed using One-way ANOVA (\*p<0.05, \*\*p<0.01, and \*\*\*p<0.001, n=10-14 / group).

#### 4.3.4. RAA-CardAPs have no effect on the expression of left ventricular chemokine receptors in acute Coxsackievirus B3-induced myocarditis mice

The chemokine receptor CCR2, which is expressed on inflammatory monocytes, and binds to CCL2 and CCL7, plays an important role in CVB3-induced myocarditis<sup>108</sup>. CVB3 mice displayed 11-fold ( $p<0.01$ ) higher LV CCR2 mRNA expression compared to control mice (**Figure 4.3.4. A**). However, LV mRNA expression of the fractalkine receptor (CX3CR1) did not change due to the infection with CVB3 (**Figure 4.3.4. B**). RAA-CardAPs did not alter the CCR2 and CX3CR1 mRNA expression compared with CVB3 non-treated mice.

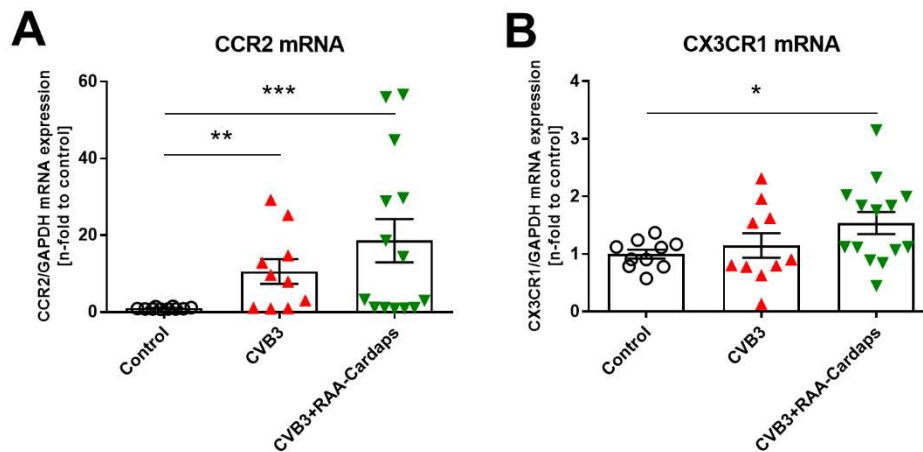


**Figure 4.3.4. Impact of intravenous injection of RAA-derived CardAPs on left ventricular chemokine receptors mRNA expression in acute Coxsackievirus B3-induced myocarditis mice.** Bar graphs represent the mean $\pm$ SEM of left ventricular (LV) **A**. CCR2, and **B**. CX3CR1 mRNA expression. Statistical differences were assessed using One-way ANOVA (\* $p<0.05$ , \*\* $p<0.01$ , and \*\*\* $p<0.001$ ,  $n=10-14$  / group).

#### 4.3.5. RAA-CardAPs had no effect on the left ventricular immune cell presence- in acute Coxsackievirus B3-induced myocarditis mice

Given the importance of immune cell infiltration in CVB3-induced myocarditis<sup>107</sup>, we next evaluated whether intravenous application of RAA-CardAPs could reduce the presence of immune cells in CVB3-infected mice. CVB3 infection displayed no significant increase in CD4<sup>+</sup> cells in comparison with control mice (**Figure 4.3.5. A**). However, CVB3-infected mice exhibited 6.7-fold ( $p<0.01$ ) and 2.8-fold ( $p<0.001$ ) higher LV CD8<sup>+</sup> cells and CD68<sup>+</sup> cells, respectively, compared to uninfected mice (**Figure 4.3.5. B-C**). RAA-CardAPs application did not reduce LV presence of CD4<sup>+</sup>, CD8<sup>+</sup> and CD68<sup>+</sup> cells, nor of LV mRNA expression of the monocyte marker Ly6c in CVB3-infected mice (**Figure 4.3.5. D**). Consequently, LV presence of CD4<sup>+</sup>, CD8<sup>+</sup> and CD68<sup>+</sup> cells and Ly6c mRNA expression in CVB3+RAA-CardAPs mice was 3.7-fold ( $p<0.05$ ), 63-fold ( $p<0.0001$ ), 5.0-fold ( $p<0.001$ ) and 3.0-fold ( $p<0.05$ ) higher compared to control mice, respectively.

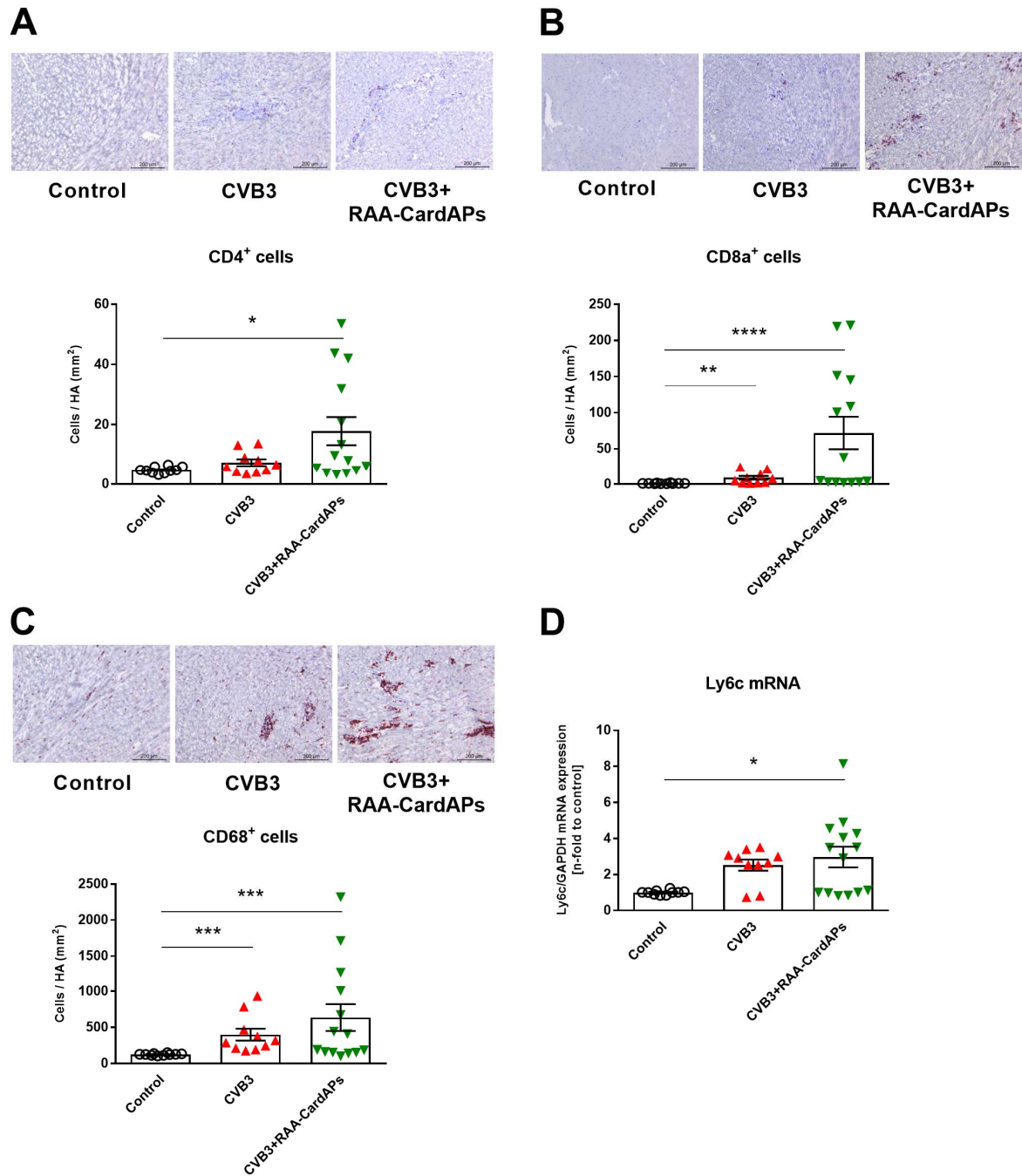


**Figure 4.3.5. Impact of intravenous injection of RAA-derived CardAPs on left ventricular immune cell presence in acute Coxsackievirus B3-induced myocarditis mice. A.-C.** Upper and lower panels depict representative left ventricular (LV) cryosections at a magnification of 100x, and bar graphs representing the mean $\pm$ SEM, respectively, of **A.** CD4<sup>+</sup>cells, **B.** CD8<sup>+</sup>cells, and **C.** CD68<sup>+</sup>cells. **D.** bar graphs represent the mean $\pm$ SEM of LV Ly6c mRNA level normalized to GAPDH. Statistical differences were assessed using One-way ANOVA (\*p<0.05, \*\*p<0.01, \*\*\*p<0.001, and \*\*\*\*p<0.0001, n=10-14 / group).

#### 4.3.6. RAA-CardAPs did not modulate left ventricular mRNA levels of pro- and anti-inflammatory and anti-viral cytokines in acute Coxsackievirus B3-induced myocarditis mice

mRNA expression of pro-inflammatory cytokines increased due to CVB3 infection, as indicated by a 6.7-fold ( $p < 0.01$ ), 2.6-fold ( $p < 0.05$ ), and 28-fold ( $p < 0.01$ ) elevation of LV TNF- $\alpha$ , IL-1 $\beta$ , and IL-6 mRNA levels compared to control mice, respectively (**Figure 4.3.6. A-B-C**). However, there was no significant difference in the mRNA expression of pro-inflammatory cytokines between CVB3+RAA-CardAPs vs untreated CVB3 mice. In parallel, LV mRNA expression of anti-inflammatory and anti-viral cytokines was upregulated in CVB3-infected vs control mice, as shown by a 20-fold ( $p < 0.01$ ), 63-fold ( $p < 0.01$ ), and 90-fold ( $p < 0.01$ ) increase in IL-10, IFN- $\gamma$ , and IFN- $\beta$ , respectively, compared to control mice (**Figure 4.3.6. D-E-F**). However, RAA-CardAPs did not change the mRNA levels of IL-10, IFN- $\gamma$ , and IFN- $\beta$ , significantly, in comparison with the untreated CVB3 group.

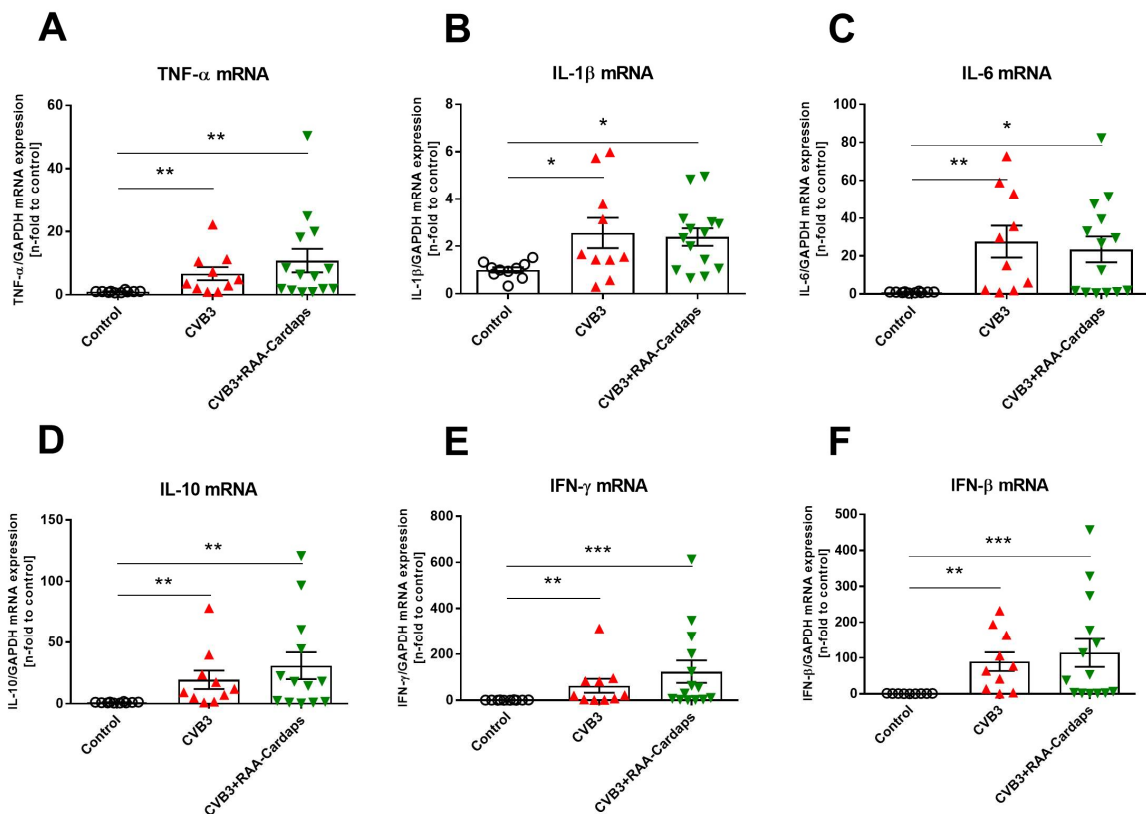


**Figure 4.3.6. Impact of intravenous injection of RAA-derived CardAPs on left ventricular cytokine mRNA expression in acute Coxsackievirus B3-infected mice.** Bar graphs represent the mean $\pm$ SEM of left ventricular (LV) of **A.** TNF- $\alpha$ , **B.** IL-1 $\beta$ , **C.** IL-6, **D.** IL-10, **E.** IFN- $\gamma$ , and **F.** IFN- $\beta$  mRNA expression. Statistical differences were assessed using One-way ANOVA (\* $p < 0.05$ , \*\* $p < 0.01$ , and \*\*\* $p < 0.001$ ,  $n = 10-14$  / group).

#### 4.3.7. RAA-CardAPs did not change the left ventricular mRNA expression of markers of cardiac apoptosis in acute Coxsackievirus B3-induced myocarditis mice

Given the importance of apoptosis in the pathogenesis of CVB3-induced myocarditis<sup>63</sup>, and the recognition of the Bcl-2/BAX ratio as an indicator for cardiac apoptosis<sup>107</sup>, we next evaluated the impact of RAA-CardAPs application on LV mRNA expression of Bcl-2, BAX, and their ratio, in acute CVB3-induced myocarditis mice (**Figure 4.3.7. A-B-C**). No significant differences among the groups were observed.

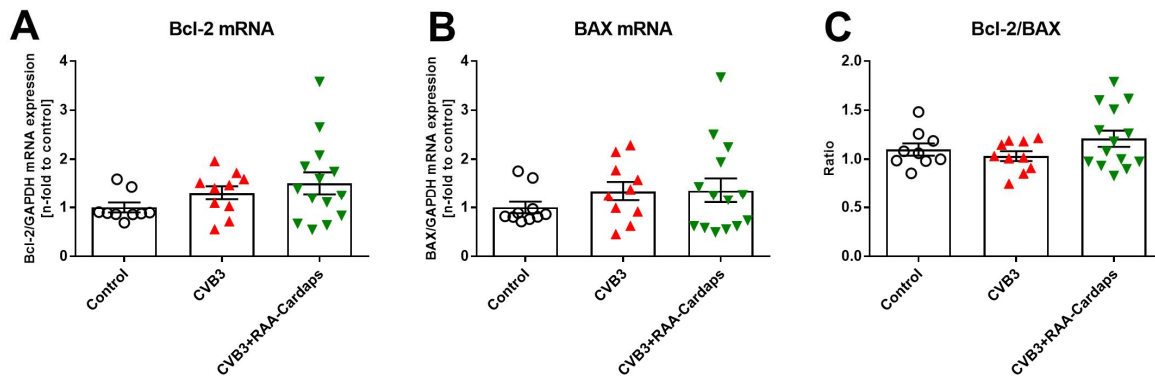


**Figure 4.3.7.** Impact of intravenous injection of RAA-derived CardAPs on left ventricular mRNA expression of apoptotic markers in acute Coxsackievirus B3-induced myocarditis mice. Bar graphs represent the mean±SEM of left ventricular (LV) **A.** Bcl-2 and **B.** BAX mRNA expression, and **C.** Bcl-2/BAX ratio. Statistical differences were assessed using One-way ANOVA (n=10-14 / group).

#### 4.3.8. RAA-CardAPs did not change the left ventricular Coxsackievirus B3 mRNA expression in acute Coxsackievirus B3-induced myocarditis mice

RAA-CardAPs application did not attenuate LV CVB3 mRNA expression in CVB3-infected mice (**Figure 4.3.8.**).

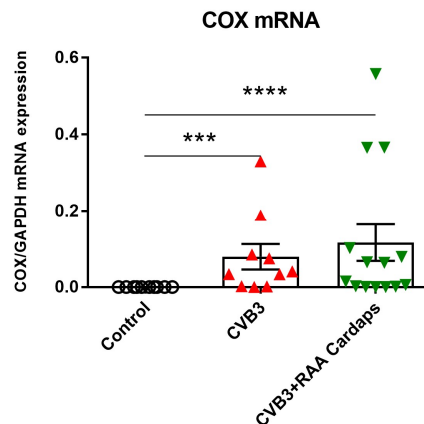


**Figure 4.3.8.** Impact of intravenous injection of RAA-derived CardAPs on left ventricular Coxsackievirus B3 mRNA expression in acute Coxsackievirus B3-induced myocarditis mice. Bar graphs represent the mean±SEM of left ventricular (LV) Coxsackievirus B3 (COX) mRNA levels.

Statistical differences were assessed using One-way ANOVA (\*\* $p < 0.001$  and \*\*\*\* $p < 0.0001$ ,  $n = 10-12$  / group).

#### 4.4. Assessment of the chronic Coxsackievirus B3-induced myocarditis model

##### 4.4.1. Coxsackievirus B3 infection of NMRI mice impairs left ventricular function at day 28 post infection

Twenty-eight days after i.p. injection of CVB3 in NMRI mice, LV function was assessed using conductance catheter. CVB3 deteriorated the LV function as indicated by a 12% ( $p < 0.01$ ) lower EF vs control mice (**Figure 4.4.1. A**). CVB3 infection reduced the systolic function significantly, as displayed by a 22% ( $p < 0.01$ ), 20% ( $p < 0.01$ ) and 27% ( $p < 0.05$ ) decline in LVESP,  $P_{\max}$  and  $dP/dt_{\max}$ , respectively (**Figure 4.4.1. B-C-D**). Diastolic function was impaired in the CVB3 mice as indicated by the 27% ( $p < 0.05$ ) reduction of  $dP/dt_{\min}$  (**Figure 4.4.1. E**). However, CVB3 infection did not change Tau significantly when compared to control mice (**Figure 4.4.1. F**).

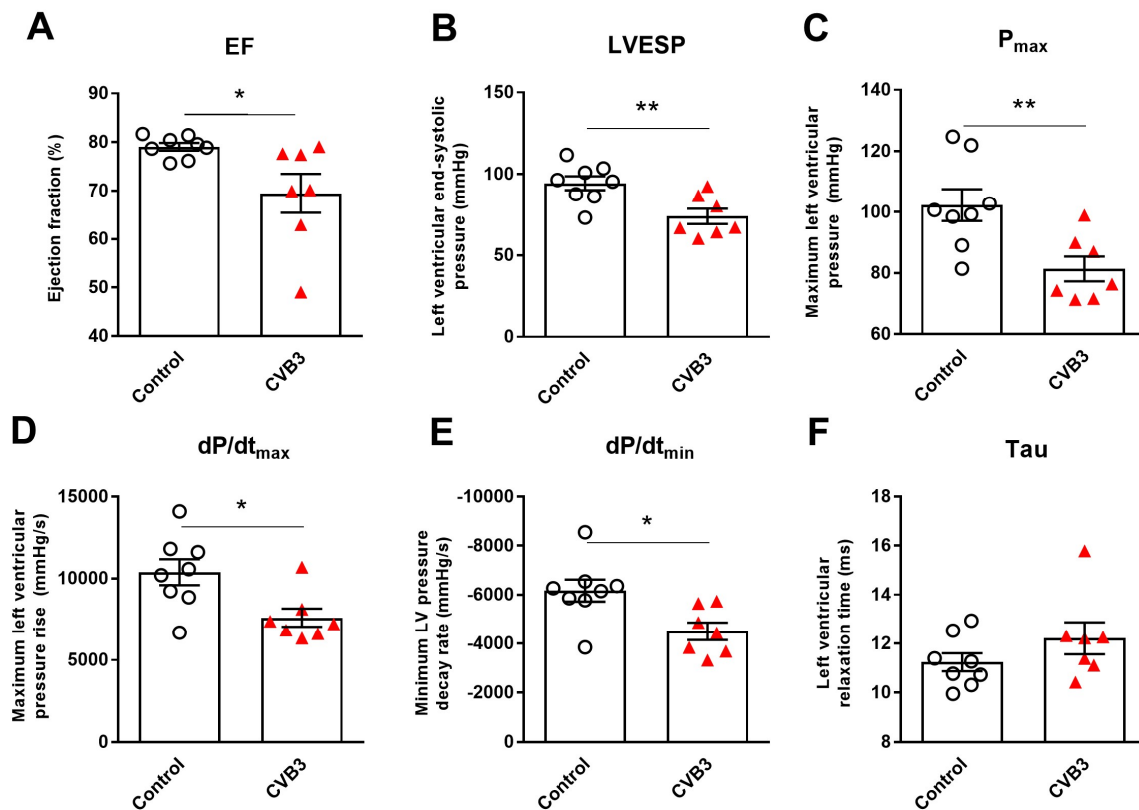


**Figure 4.4.1. Impact of Coxsackievirus B3 infection on the left ventricular function of NMRI mice at day 28 post infection.** Indices for the left ventricle (LV) were obtained by conductance catheter. Bar graphs represent the mean ± SEM of **A**. Ejection fraction (EF; %), **B**. End systolic pressure (LVESP; mmHg), **C**. LV Maximum pressure ( $P_{\max}$ ; mmHg), **D**. LV contractility ( $dP/dt_{\max}$ ; mmHg/s), **E**. LV relaxation ( $dP/dt_{\min}$ ; mmHg/s) and **F**. Relaxation time (Tau; ms). Statistical differences were assessed using Students t-test (\* $p < 0.05$  and \*\* $p < 0.01$ ,  $n = 7-8$  / group).

##### 4.4.2. Coxsackievirus B3 infection of NMRI mice leads to left ventricular fibrosis at day 28 post infection

Immunohistochemistry analysis of collagen I and collagen III was performed. Chronic CVB3 NMRI mice displayed 3.1-fold ( $p < 0.05$ ) higher LV collagen I vs control mice, whereas collagen III expression was not increased in CVB3 NMRI versus control mice (**Figure 4.4.2. A-B**). Moreover, the ratio of collagen I to collagen III increased by a 3.1-fold ( $p < 0.05$ ) in CVB3-infected NMRI mice versus control mice (**Figure 4.4.2. C**).

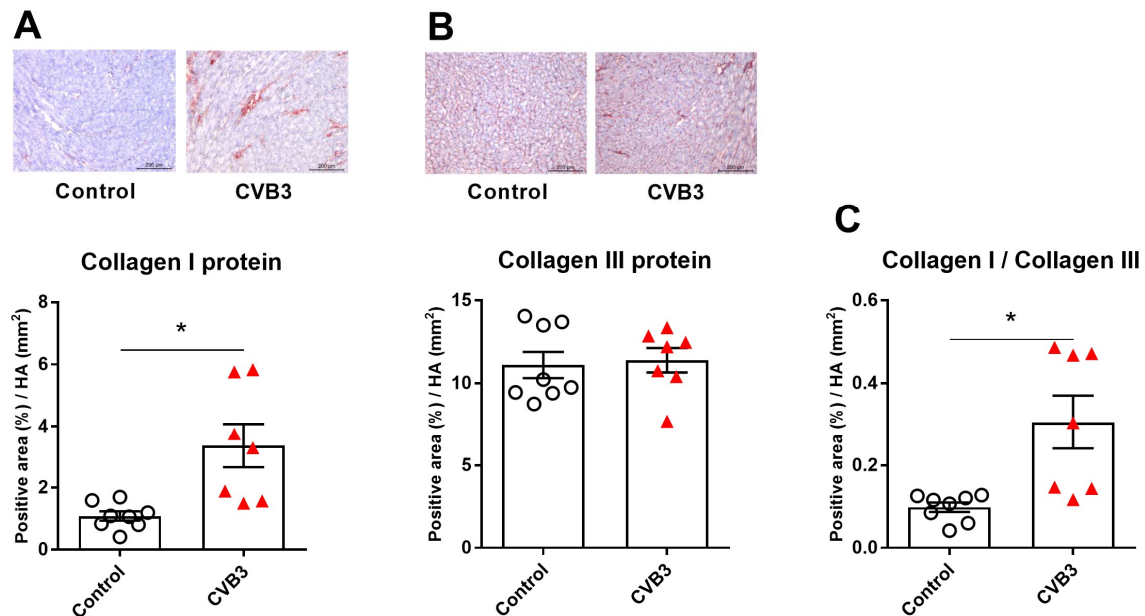


**Figure 4.4.2. Impact of Coxsackievirus B3 infection on the left ventricular collagen expression in NMRI mice at day 28 post infection.** **A.** Upper panel: representative left ventricular (LV) cryosections of Collagen I at a magnification of 100x, lower panel: bar graphs represent the mean $\pm$ SEM of LV collagen I, **B.** Upper panel: representative LV cryosections of Collagen III at a magnification of 100x, lower panel: bar graphs represent the mean $\pm$ SEM of LV collagen III, and **C.** bar graphs represent the ratio of Collagen I to III. Statistical differences were assessed using the Students t-test ( $*p < 0.05$ ,  $n = 7-8$  / group).

#### 4.4.3. Coxsackievirus B3 infection of NMRI mice does not change the left ventricular chemokine mRNA expression at day 28 post infection

CVB3-infected NMRI mice did not show any change in the mRNA levels of CCL2, CCL7 and CX3CL1 compared to non-infected NMRI control mice (**Figure 4.4.3. A-B-C**), which was reflected in no change in the ratio of CCL2 and CCL7 to CX3CL1 between control and CVB3-infected NMRI mice (**Figure 4.4.3. D-E**).

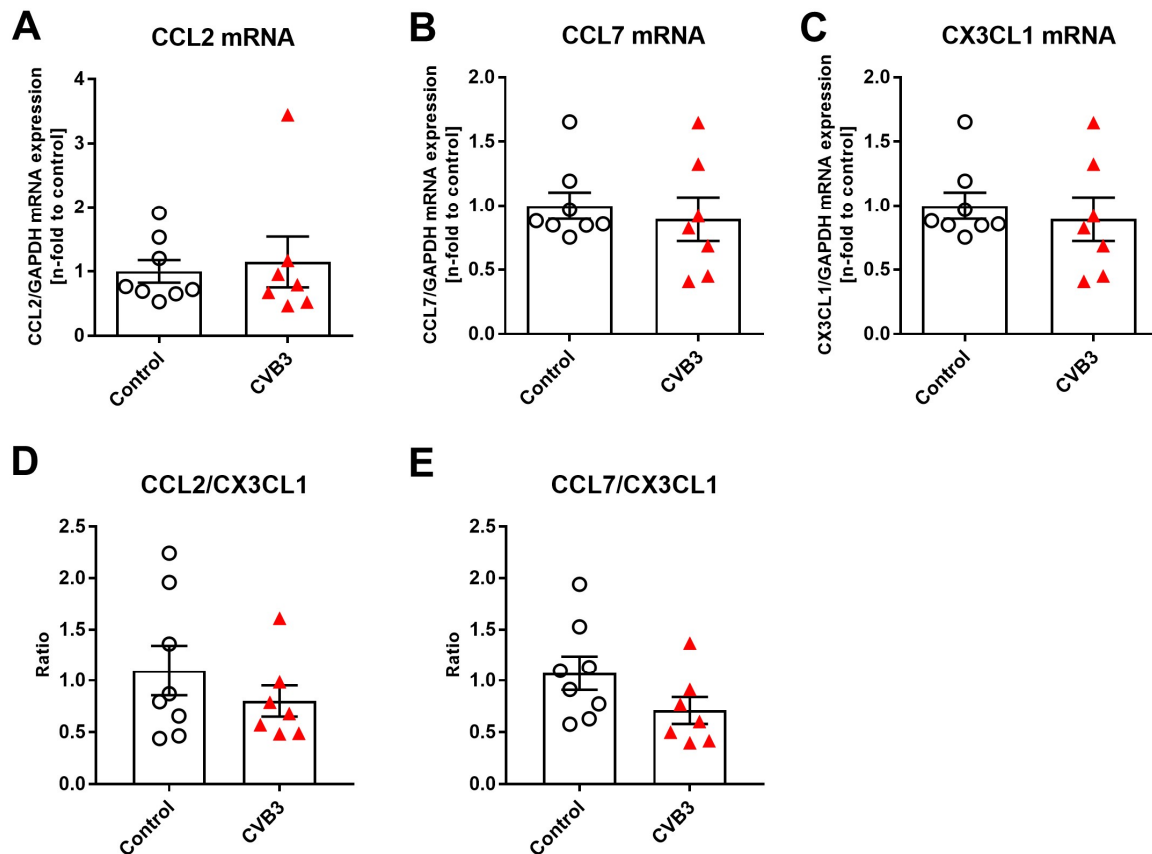


**Figure 4.4.3. Impact of Coxsackievirus B3 infection on the left ventricular chemokine mRNA expression in NMRI mice at day 28 post infection.** Bar graphs represent the mean $\pm$ SEM of LV **A.** CCL2, **B.** CCL7, and **C.** CX3CL1 mRNA expression, **D.** CCL2/CX3CL1, and **E.** CCL7/CX3CL1. Statistical differences were assessed using Student's t-test (n=7-8 / group).

#### 4.4.4. Coxsackievirus B3 infection of NMRI mice modulates left ventricular mRNA expression of chemokine receptors at day 28 post

CVB3 infection upregulated LV mRNA expression of CCR2 by 6.3-fold ( $p < 0.001$ ), but did not alter LV CX3CR1 mRNA expression compared to uninfected NMRI mice (**Figure 4.4.4. A-B**).

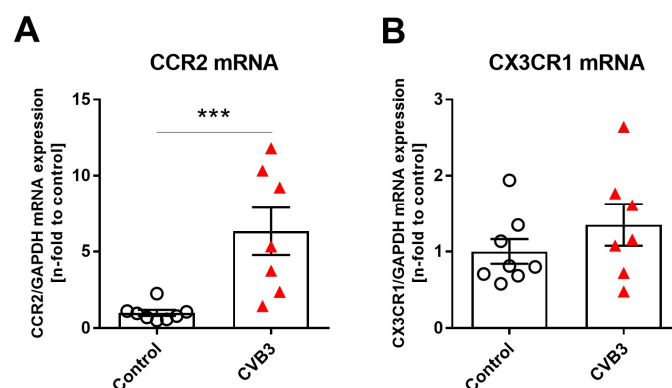


**Figure 4.4.4. Impact of Coxsackievirus B3 infection on the left ventricular mRNA expression of chemokine receptors in NMRI mice at day 28 post infection.** Bar graphs represent the mean $\pm$ SEM

of left ventricular (LV) **A.** CCR2, and **B.** CX3CR1 mRNA expression. Statistical differences were assessed using the Students t-test (\*\* $p < 0.001$ ,  $n = 7-8$  / group).

#### 4.4.5. Coxsackievirus B3 infection of NMRI mice increases left ventricular monocyte and pro-inflammatory cell presence at day 28 post infection

CVB3 infection of NMRI mice led to a high infiltration of inflammatory cells in the LV at day 28 post infection, as indicated by a 9.9-fold ( $p < 0.001$ ), 3.7-fold ( $p < 0.01$ ) and 1.8-fold ( $p = 0.0784$ ) increase in  $CD4^+$ ,  $CD8^+$  and  $CD68^+$  cells, respectively, in comparison with control NMRI mice (**Figure 4.4.5. A-B-C**). Interestingly, CVB3 infection resulted in a 1.2-fold ( $p < 0.05$ ) downregulation of LV Ly6c mRNA expression versus uninfected NMRI control mice (**Figure 4.4.5. D**).

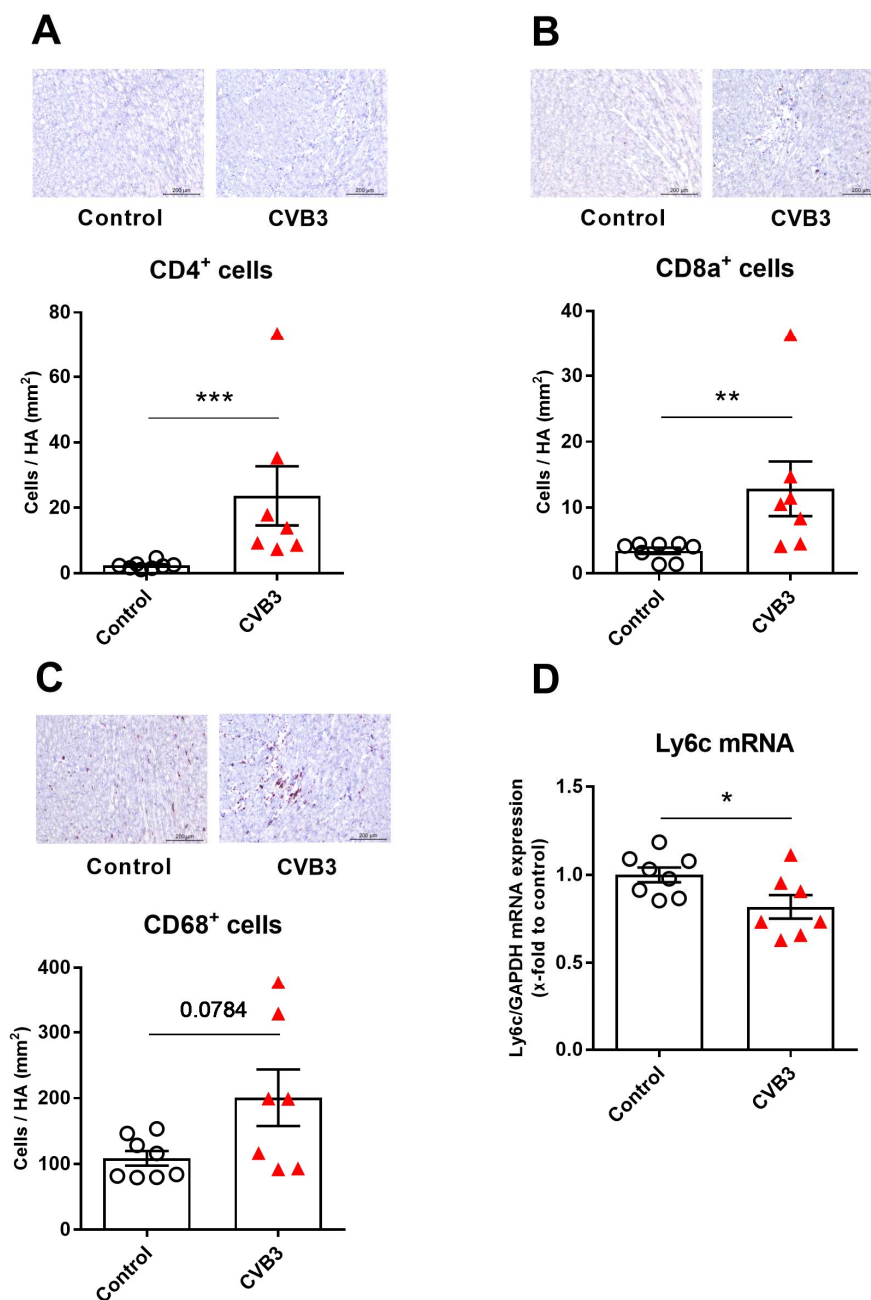


**Figure 4.4.5. Impact of Coxsackievirus B3 infection on left ventricular immune cell presence in NMRI mice at day 28 post infection.** A-C. Upper and lower panels depict representative left ventricular (LV) cryosections at a magnification of 100x, and bar graphs representing the mean±SEM of **A.** CD4<sup>+</sup>cells, **B.** CD8a<sup>+</sup>cells, and **C.** CD68<sup>+</sup>cells. **D.** Bar graphs represent the mean±SEM of LV Ly6c mRNA level normalized to GAPDH. Statistical differences were assessed using Students t-test (\*p<0.05, \*\*p<0.01, and \*\*\*p<0.001, n=7-8 / group).

#### 4.4.6. Coxsackievirus B3 infection of NMRI mice induces left ventricular inflammation at day 28 post infection

LV mRNA expression of the pro-inflammatory cytokines, TNF- $\alpha$ , IL-1 $\beta$  and IL-6, showed no significant regulation due to CVB3 infection 28 days post infection in NMRI mice (**Figure 4.4.6. A-B-C**). However, CVB3-infected mice displayed 23-fold (p<0.001) higher LV IFN- $\gamma$  mRNA expression, in comparison with control mice (**Figure 4.4.6. D**). Interestingly, LV mRNA expression of the anti-inflammatory cytokines IL-10 and IFN- $\beta$ , did not change at day 28 post infection (**Figure 4.4.6. E-F**).

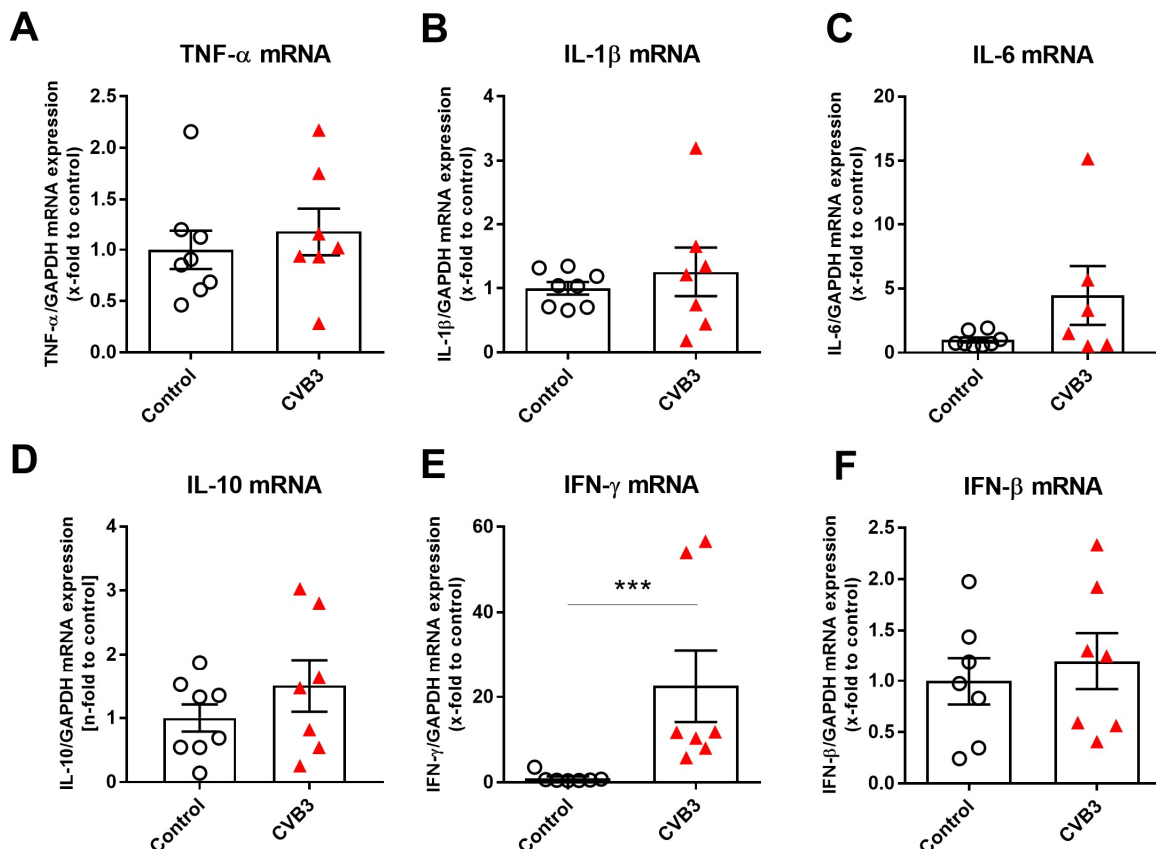


**Figure 4.4.6. Impact of Coxsackievirus B3 infection on left ventricular cytokine mRNA expression in NMRI mice at day 28 post infection.** Bar graphs represent the mean±SEM of left ventricular (LV) **A.** TNF- $\alpha$ , **B.** IL-1 $\beta$ , **C.** IL-6, **D.** IL-10, **E.** IFN- $\gamma$ , and **F.** IFN- $\beta$  mRNA expression. Statistical differences were assessed using the Students t-test (\*\*\*p<0.001, n=7-8 / group).

#### 4.4.7. Coxsackievirus B3 infection of NMRI mice does not change left ventricular mRNA expression of factors indicative for cardiac apoptosis at day 28 post infection

Infection of NMRI mice with CVB3 did not change the LV mRNA expression of pro-apoptotic BAX and anti-apoptotic Bcl-2 and their ratio at day 28 post infection compared to non-infected NMRI control mice (**Figure 4.4.7. A-B-C**).

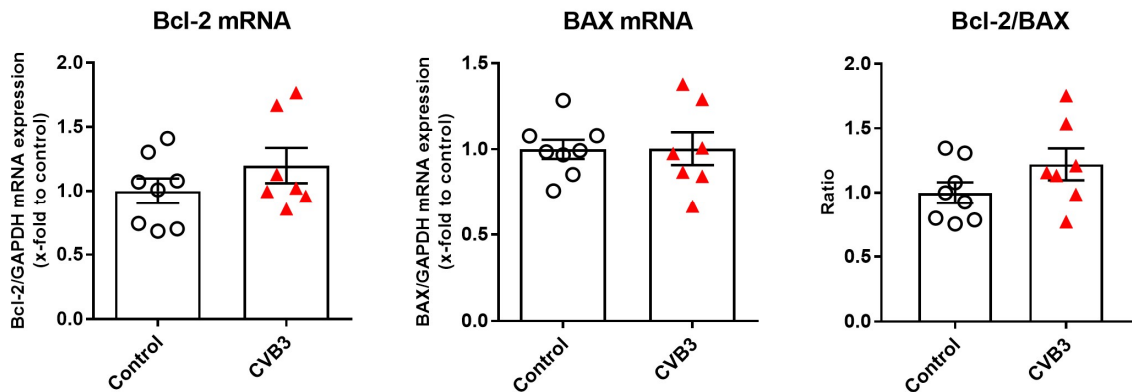


**Figure 4.4.7. Impact of Coxsackievirus B3 infection on left ventricular mRNA expression of apoptotic markers in NMRI mice at day 28 post infection.** Bar graphs represent the mean±SEM of left ventricular (LV) **A.** Bcl-2 and **B.** BAX mRNA expression, and **C.** Bcl-2/BAX ratio. Statistical differences were assessed using Students t-test (n=7-8 / group).

#### 4.4.8. Coxsackievirus B3 infection of NMRI mice is associated with low Coxsackievirus B3 mRNA expression at day 28 post infection

CVB3-infected NMRI mice displayed low persistence of CVB3 mRNA expression at day 28 post-infection (**Figure 4.4.8.**).

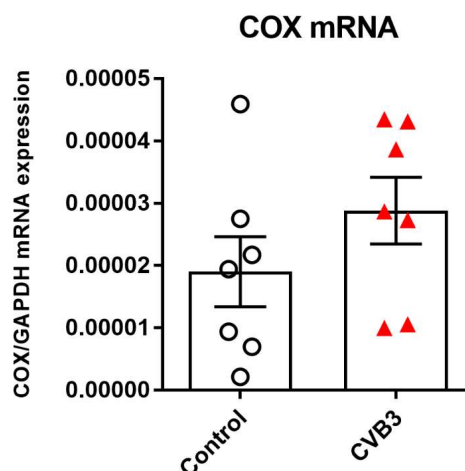


**Figure 4.3.8. Impact of Coxsackievirus B3 infection on left ventricular Coxsackievirus B3 mRNA expression in NMRI mice at day 28 post infection.** Bar graphs represent the mean±SEM of left

ventricular (LV) Coxsackievirus B3 (COX) mRNA expression. Statistical differences were assessed using Students t-test (n=7-8 / group).

## 4.5. Allogenic CardAPs in chronic Coxsackievirus B3-induced myocarditis mice

### 4.5.1. RAA-CardAPs moderately improve left ventricular function in chronic Coxsackievirus B3-induced myocarditis mice

Eighteen days after i.v. application of RAA-CardAPs in CVB3-induced chronic myocarditis NMRI mice, LV function was assessed using conductance catheter. CVB3-infected mice showed a 14% ( $p < 0.01$ ) lower EF, when compared to control mice (**Figure 4.5.1. A**). RAA-CardAPs improved the EF as indicated by a 11% ( $p < 0.01$ ) increase in EF, in comparison with untreated CVB3 infected mice. LV contractility was impaired due to CVB3 infection, as indicated by 37% ( $p < 0.0001$ ), 32% ( $p < 0.0001$ ), and 40% ( $p < 0.0001$ ) reduction in LVESP,  $P_{\max}$  and  $dP/dt_{\max}$ , respectively (**Figure 4.5.1. B-C-D**). RAA-CardAPs improved the LV contractility, which follows from the 21% ( $p < 0.05$ ) increase in  $dP/dt_{\max}$  in RAA-CardAPs+CVB3 compared to CVB3-infected mice. Diastolic function was deteriorated in the CVB3-infected mice as indicated by the 41% ( $p < 0.0001$ ) decline of  $dP/dt_{\min}$  in CVB3 versus control NMRI mice (**Figure 4.5.1. E**). RAA-CardAPs application did not change  $dP/dt_{\min}$  nor in Tau in CVB3-infected mice, when compared to untreated CVB3-infected NMRI mice (**Figure 4.5.1. E-F**).

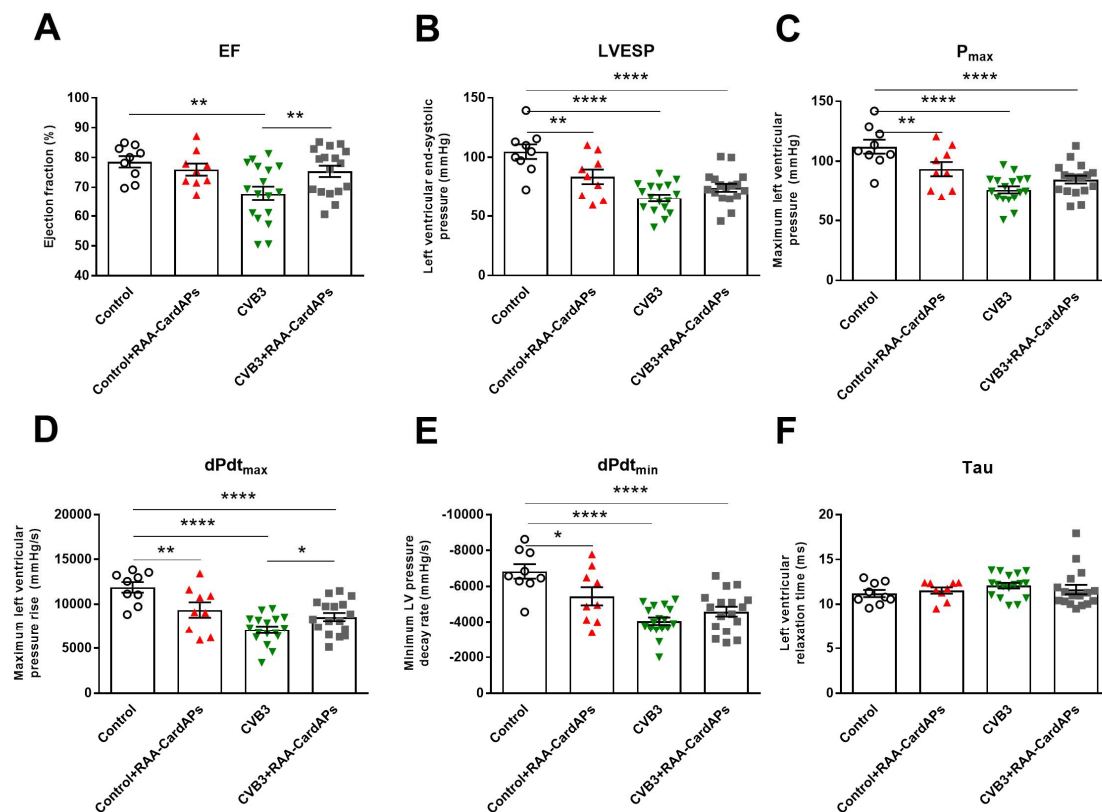


**Figure 4.5.1. Impact of intravenous injection of RAA-CardAPs on the left ventricular function in Coxsackievirus B3-infected NMRI mice.** Indices for the left ventricle (LV) were obtained by conductance catheter. Bar graphs represent the mean $\pm$ SEM of **A**. Ejection fraction (EF; %), **B**. End systolic pressure (LVESP; mmHg), **C**. LV Maximum pressure ( $P_{\max}$ ; mmHg), **D**. LV contractility ( $dP/dt_{\max}$ ;

mmHg/s), **E.** LV relaxation ( $dP/dt_{min}$ ; mmHg/s) and **F.** Relaxation time (Tau; ms). Statistical differences were assessed using One-way ANOVA (\* $p < 0.05$ , \*\* $p < 0.01$  and \*\*\*\* $p < 0.0001$ ,  $n = 9-10$ /control and control+RAA-CardAPs groups,  $n = 19$ /CVB3 and CVB3+RAA-CardAPs groups).

#### 4.5.2. RAA-CardAPs reduced left ventricular fibrosis in chronic Coxsackievirus B3-induced myocarditis mice

CVB3 infection upregulated collagen I protein expression by 1.4-fold ( $p < 0.05$ ) in NMRI mice (**Figure 4.5.2.**). RAA-CardAPs application decreased cardiac fibrosis as shown by the 1.5-fold ( $p < 0.01$ ) lower collagen I expression in CVB3+RAA-CardAPs compared to untreated CVB3-infected mice.

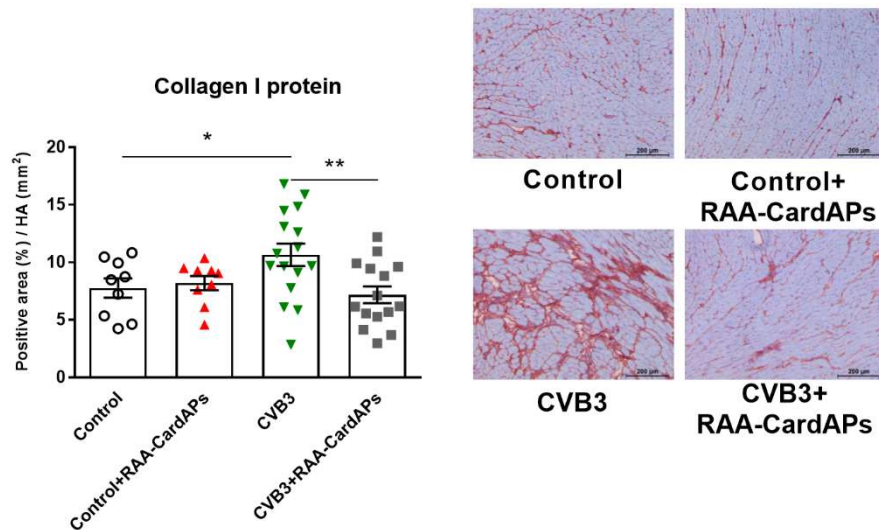


**Figure 4.5.2. Impact of intravenous injection of RAA-derived CardAPs on left ventricular collagen I expression in chronic Coxsackievirus B3-infected NMRI mice.** Left panel: bar graphs represent the mean $\pm$ SEM of Collagen I depicted as positive area (%/heart area (HA)) ( $mm^2$ ); right panel: representative Collagen I-stained left ventricular (LV) cryosections at a magnification of 100x. Statistical differences were assessed using One-way ANOVA (\* $p < 0.05$  and \*\* $p < 0.01$ ,  $n = 9-10$ /control and control+RAA-CardAPs groups,  $n = 19$ /CVB3 and CVB3+RAA-CardAPs groups).

#### 4.5.3. RAA-CardAPs did not change the left ventricular chemokine mRNA expression in chronic Coxsackievirus B3-induced myocarditis mice

Infection of NMRI mice with CVB3 led to no significant differences in the mRNA levels of the chemokines CCL2, CCL7, nor CX3CL1 in CVB3-infected compared to control NMRI mice at day 28 post infection (**Figure 4.5.3. A-B-C**), which was reflected in no changes in the CCL2 to CX3CL1, nor CCL7 to CX3CL1 ratio in CVB3 versus control NMRI mice (**Figure 4.5.3. D-E**). RAA-CardAPs application did not alter LV mRNA levels of CCL2, CCL7 nor CX3CL1, but reduced the CCL2/CX3CL1 ratio by 1.1-fold ( $p < 0.05$ ) in comparison with untreated CVB3-infected mice.

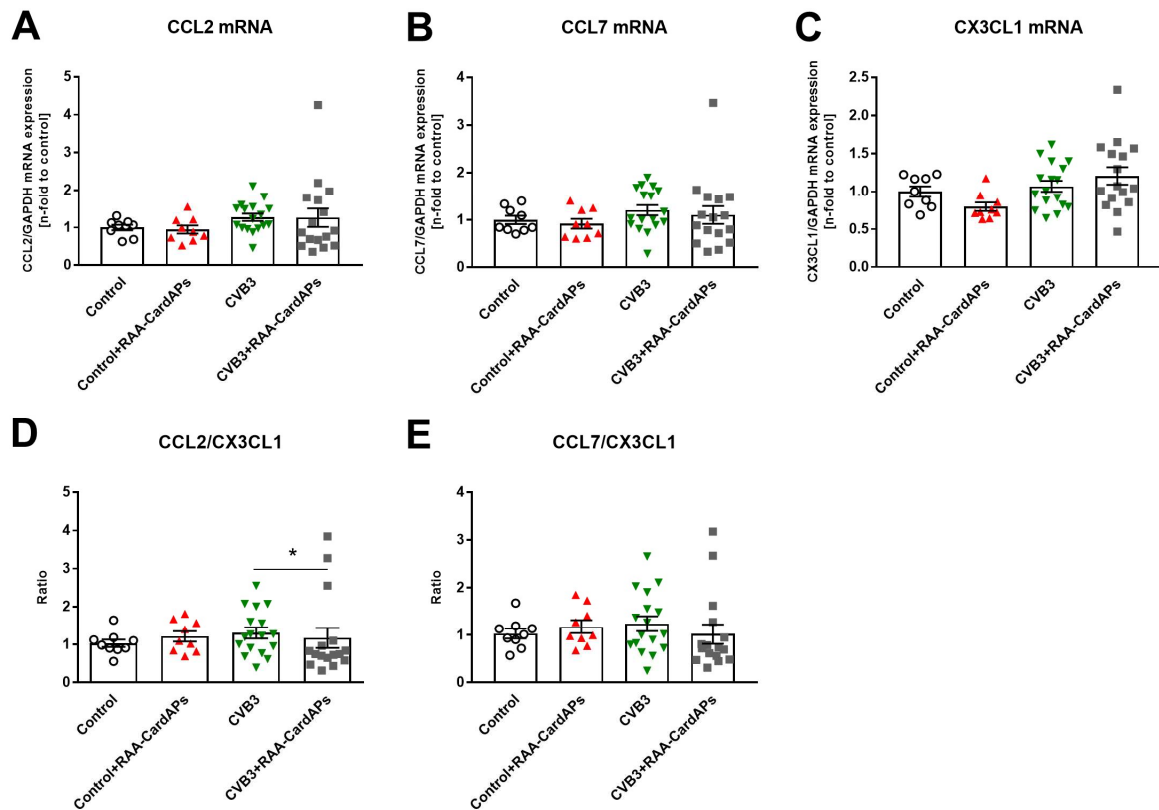


**Figure 4.5.3. Impact of intravenous injection of RAA-derived CardAPs on left ventricular chemokine mRNA expression in Coxsackievirus B3-infected NMRI mice.** Bar graphs represent the mean $\pm$ SEM of left ventricular (LV) **A.** CCL2, **B.** CCL7, and **C.** CX3CL1 mRNA expression, **D.** CCL2/CX3CL1 and **E.** CCL7/CX3CL1. Statistical differences were assessed using One-way ANOVA (\* $p < 0.05$ ,  $n = 9-10$ /control and control+RAA-CardAPs groups,  $n = 19$ /CVB3 and CVB3+RAA-CardAPs groups).

#### 4.5.4. RAA-CardAPs have no effect on the left ventricular mRNA expression of chemokine receptors in chronic Coxsackievirus B3-induced myocarditis mice

CVB3 infection of NMRI mice led to upregulation of CCR2 mRNA level as indicated by a 7.7-fold ( $p < 0.0001$ ) elevation of CCR2 mRNA expression in CVB3 infected mice, when compared to control mice (**Figure 4.5.4. A**). However, no significant change was observed in CX3CR1 mRNA expression in CVB3-infected mice, in comparison with control mice (**Figure 4.5.4. B**). Application of RAA-CardAPs did not change the mRNA levels of CCR2 and CX3CR1 compared to untreated CVB3-infected mice.

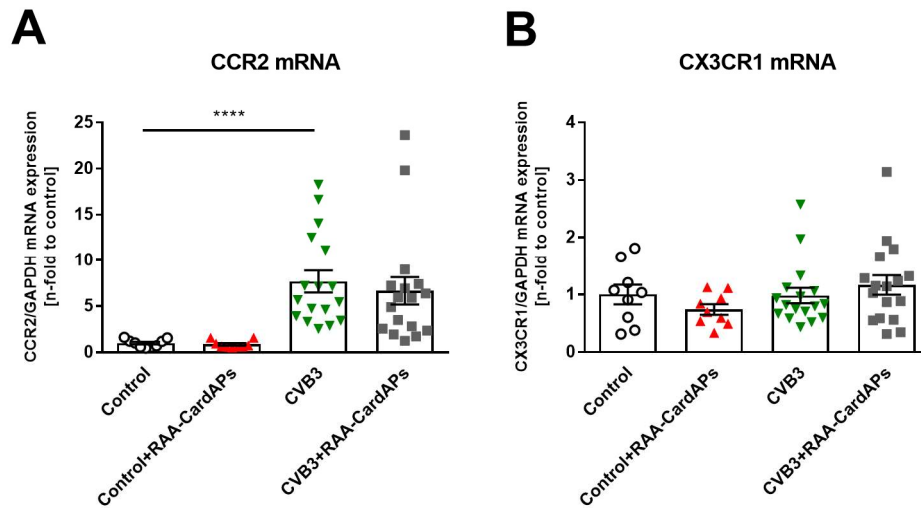


**Figure 4.5.4. Impact of intravenous injection of RAA-derived CardAPs on left ventricular chemokine-receptors mRNA expression in Coxsackievirus B3-infected NMRI mice.** Bar graphs represent the mean±SEM of left ventricular (LV) of **A.** CCR2, and **B.** CX3CR1 mRNA expression. Statistical differences were assessed using One-way ANOVA (\*\*\*\* $p < 0.0001$ ,  $n = 9-10$ /control and control+RAA-CardAPs groups,  $n = 19$ /CVB3 and CVB3+RAA-CardAPs groups).

#### 4.5.5. RAA-CardAPs reduce the left ventricular presence of monocytes in chronic Coxsackievirus B3-induced myocarditis mice

CVB3 infection increased LV monocytes/macrophages as indicated by 2.2-fold ( $p < 0.001$ ) higher CD68<sup>+</sup> cells in CVB3-infected mice compared to control mice. RAA-CardAPs application slightly decreased the LV presence of CD68<sup>+</sup> cells as shown by 1.5-fold ( $p = 0.0596$ ) lower CD68<sup>+</sup> cells in CVB3+RAA-CardAPs in comparison with untreated CVB3-infected mice (**Figure 4.5.5.A**). However, LV mRNA expression of Ly6c was not different between the groups (**Figure 4.5.5.B**).

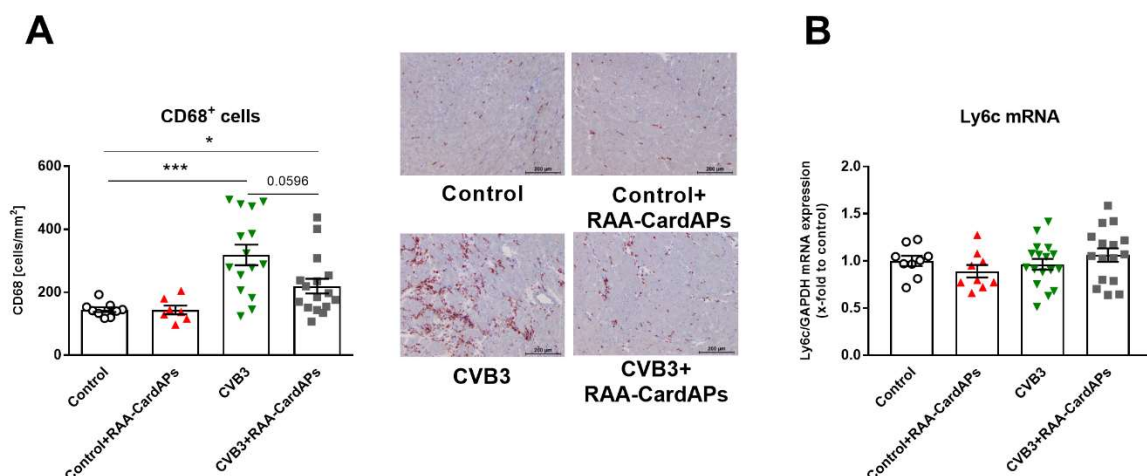


**Figure 4.5.5. Impact of intravenous injection of RAA-derived CardAPs on left ventricular immune cell presence in chronic Coxsackievirus B3-infected NMRI mice.** **A.** Left panel: bar graphs represent the mean±SEM of CD68<sup>+</sup> cells depicted as cells/mm<sup>2</sup>; right panel: representative CD68-stained left ventricular (LV) cryosections at a magnification of 100x. **B.** Bar graphs represent the mean±SEM of LV Ly6c mRNA level normalized to GAPDH. Statistical differences were assessed using One-way ANOVA

(\*p<0.05 and \*\*\*p<0.001, n=9-10/control and control+RAA-CardAPs groups, n=19/CVB3 and CVB3+RAA-CardAPs groups).

#### 4.5.6. RAA-CardAPs modulate the left ventricular mRNA levels of cytokines in chronic Coxsackievirus B3-induced myocarditis mice

CVB3 infection led to upregulation of pro-inflammatory cytokines, as indicated by a 3.0-fold ( $p<0.05$ ) increase in IL-6 mRNA expression in CVB3 infected mice, compared to control mice (**Figure 4.5.6. C**). However, RAA-CardAPs application in CVB3 infected mice did not change the mRNA levels of the pro-inflammatory cytokines, in comparison with untreated CVB3 infected mice (**Figure 4.5.6. A-B-C**). Anti-inflammatory and anti-viral cytokines upregulated in CVB3 infected mice, which indicated by a 3.4-fold ( $p<0.001$ ), 62.2-fold ( $p<0.0001$ ), and 2.6-fold ( $p<0.0001$ ) increase in IL-10, IFN- $\gamma$ , and IFN- $\beta$ , respectively, compared to control mice (**Figure 4.5.6. D-E-F**). Intravenous application of RAA-CardAPs in CVB3 infected mice led to downregulation of IL-10, as indicated by a 1.7-fold ( $p<0.05$ ) reduction in IL-10 mRNA expression, in comparison with untreated CVB3 infected mice. However, the mRNA levels of IFN- $\gamma$  and IFN- $\beta$ , did not change after RAA-CardAPs intravenous injection in CVB3 infected mice, when compared to CVB3 mice .

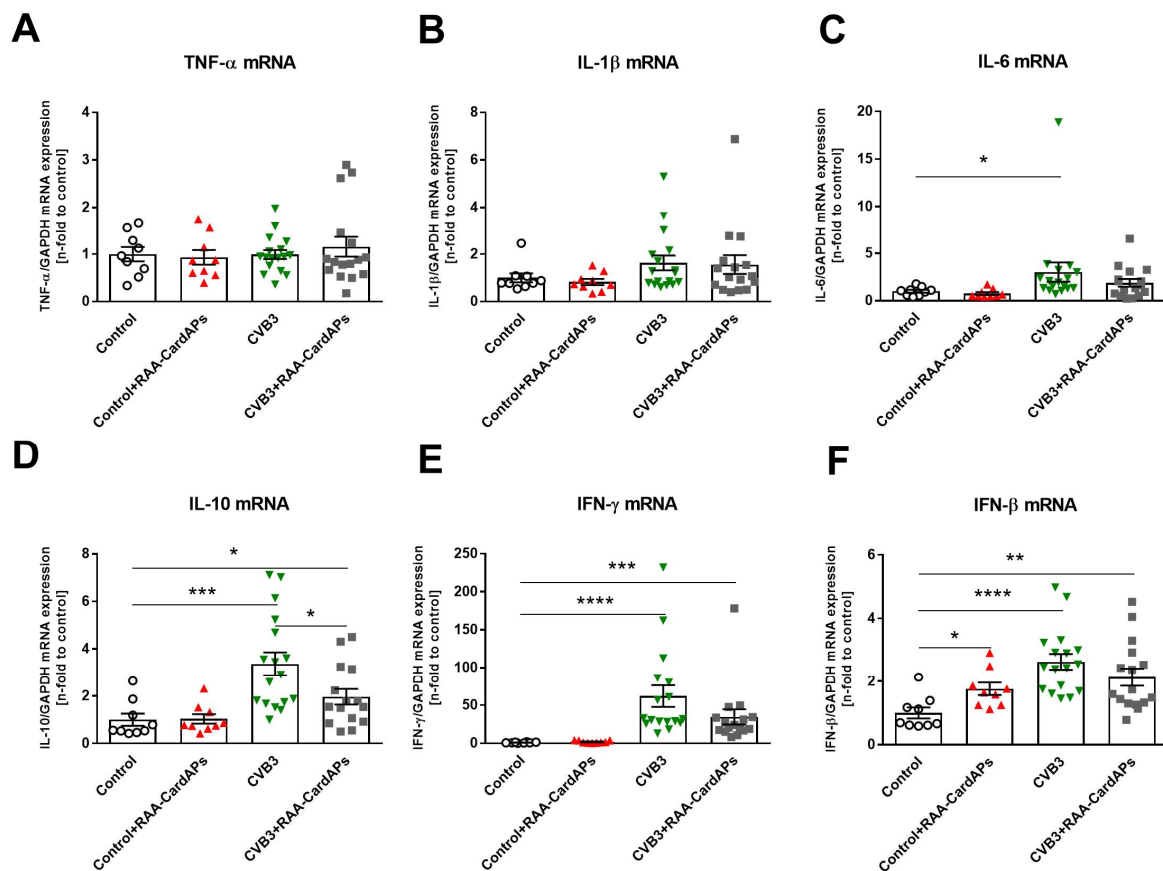


**Figure 4.5.6. Impact of intravenous injection of RAA-derived CardAPs on left ventricular mRNA expression of cytokines in Coxsackievirus B3-infected NMRI mice.** Bar graphs represent the mean  $\pm$  SEM of left ventricular (LV) of **A.** TNF- $\alpha$ , **B.** IL-1 $\beta$ , **C.** IL-6, **D.** IL-10, **E.** IFN- $\gamma$ , and **F.** IFN- $\beta$  mRNA

expression. Statistical differences were assessed using One-way ANOVA (\* $p < 0.05$ , \*\* $p < 0.01$ , \*\*\* $p < 0.001$ , and \*\*\*\* $p < 0.0001$ ,  $n = 9-10$ /control and control+RAA-CardAPs groups,  $n = 19$ /CVB3 and CVB3+RAA-CardAPs groups).

#### 4.5.7. RAA-CardAPs did not change left ventricular mRNA expression of factors indicative for cardiac apoptosis in chronic Coxsackievirus B3-induced myocarditis mice

Infection of NMRI mice with CVB3 led to upregulation of Bcl-2, as indicated by a 1.7-fold ( $p < 0.01$ ) increase in Bcl-2 mRNA expression in CVB3 infected mice, when compared to control mice (**Figure 4.5.7. A**). Whereas, CVB3 infection showed no significant difference in the mRNA expression of BAX, in comparison with control mice (**Figure 4.5.7. B**). Bcl-2/BAX ratio was increased due to CVB3 infection as indicated by a 1.8-fold ( $p < 0.001$ ) elevation in Bcl-2/BAX ratio in CVB3 infected mice vs control mice (**Figure 4.5.7. C**). RAA-CardAPs application did not change the mRNA levels of Bcl-2 and BAX as well as the Bcl-2/BAX ratio in CVB3 infected, when compared to untreated CVB3 infected mice.

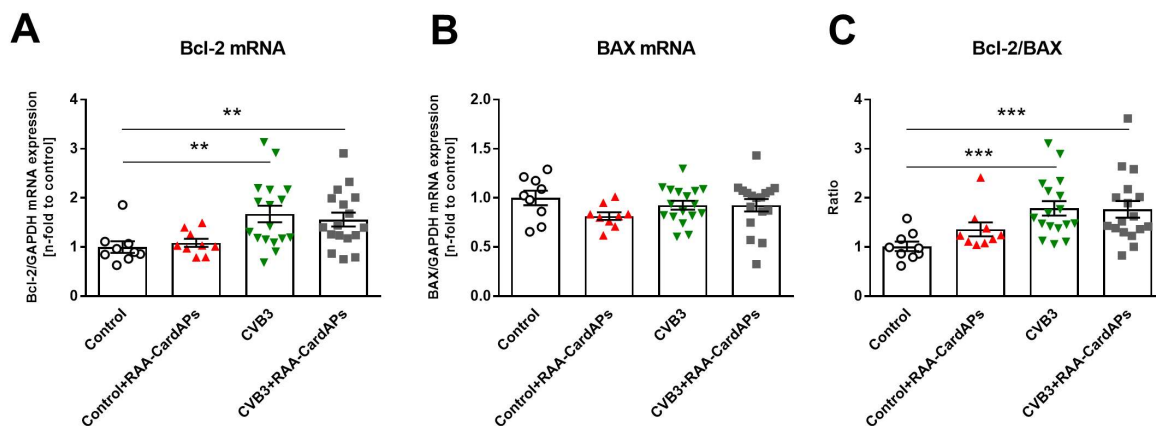


**Figure 4.5.7. Impact of intravenous injection of RAA-derived CardAPs on left ventricular mRNA expression of apoptotic markers in Coxsackievirus B3-infected NMRI mice.** Bar graphs represent the mean $\pm$ SEM of left ventricular (LV) **A**. Bcl-2 and **B**. BAX mRNA levels, and **C**. Bcl-2/BAX. Statistical differences were assessed using One-way ANOVA (\*\* $p < 0.01$  and \*\*\* $p < 0.001$ ,  $n = 9-10$ /control and control+RAA-CardAPs groups,  $n = 19$ /CVB3 and CVB3+RAA-CardAPs groups).

#### 4.5.8. RAA-CardAPs did not affect left ventricular Coxsackievirus B3 mRNA expression in chronic Coxsackievirus B3-induced myocarditis mice

I.v. RAA-CardAPs application did not affect LV CVB3 mRNA expression at day 28 post infection in NMRI mice (**Figure 4.5.8.**).

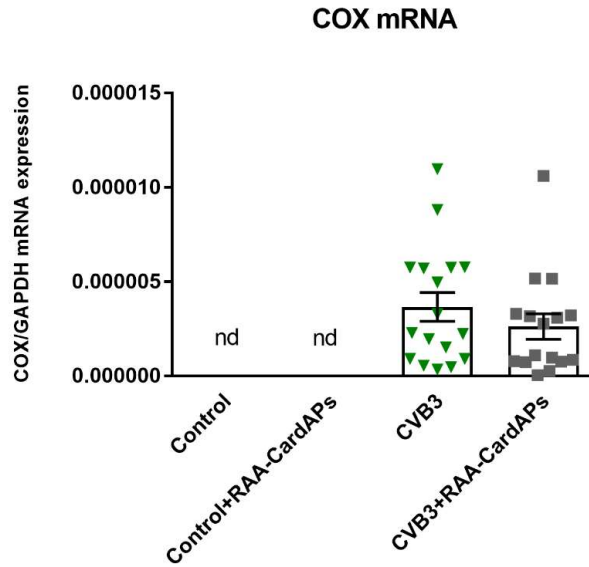


**Figure 4.5.8. Impact of intravenous injection of RAA-derived CardAPs on left ventricular Coxsackievirus B3 mRNA expression in Coxsackievirus B3-infected NMRI mice.** Bar graphs represent the mean±SEM of left ventricular (LV) Coxsackievirus B3 (COX) mRNA expression. Statistical differences were assessed using One-way ANOVA (\*\* $p < 0.01$  and \*\*\* $p < 0.001$ ,  $n = 9-10$ /control and control+RAA-CardAPs groups,  $n = 16-17$ /CVB3 and CVB3+RAA-CardAPs groups).

## 5. Discussion

The present study aimed to evaluate the impact of i.v. injection of cardiac stromal cells on acute and chronic CVB3-induced myocarditis. Briefly, EMB-CardAPs and EMB-CF improved LV function in mice. However, EMB-CardAPs, but not EMB-CF reduced LV fibrosis, immune cell infiltration, inflammation and CVB3 mRNA expression in acute CVB3-induced myocarditis. Beyond EMB-CardAPs, also RAA-CardAPs improved systolic and diastolic function in acute CVB3-induced myocarditis, illustrating the potential of RAA as an alternative source for CardAPs. To assess the cardioprotective potential of RAA-CardAPs in a chronic setting of CVB3 myocarditis, myocarditis was induced with the 31-1-93 CVB3 virus strain in NMRI mice. RAA-CardAPs could minimally improve LV function in CVB3-induced chronic myocarditis, which was associated with a decrease in LV collagen I expression and a reduction in CD68<sup>+</sup> cell presence.

### 5.1. EMB-CardAPs versus EMB-CF in acute Coxsackievirus B3-induced myocarditis mice

The first experiment demonstrated that EMB-CardAPs and EMB-CF improved LV systolic and diastolic function in acute CVB3-induced myocarditis. However, EMB-CardAPs but not EMB-CF reduced LV fibrosis, the presence of monocytes, inflammation, CVB3 mRNA expression and the expression of parameters indicative for cardiac apoptosis in acute CVB3-induced myocarditis mice. EMB-CardAPs and EMB-CF have been isolated from the same patient by outgrowth culture in two different culture media. Since both EMB-CardAPs and EMB-CF were derived from EMB from the same patient, patient-specific differences can be excluded. In agreement with our previous data illustrating variations in proteoforms between EMB-CardAPs and EMB-CF (see paragraph 2), both cells exerted different effects upon i.v. application in acute CVB3-induced myocarditis mice. Conform to previous studies in different murine models of cardiac disease<sup>66, 98</sup> EMB-CardAPs exerted cardioprotective effects in acute CVB3-induced myocarditis mice, whereas EMB-CF did not reduce cardiac fibrosis, inflammation and CVB3 mRNA expression. These findings are on their turn in frame with Savvatis-Van Linthout *et al.*<sup>67</sup> who demonstrated that MSCs, but not CF decreased LV fibrosis and modulated the inflammatory response. Importantly, MSCs and CF from that study were not derived from the same patient, neither were the CF obtained via outgrowth from EMB.

The current study showed that CVB3 infection decreased the EF,  $P_{\max}$ ,  $dP/dt_{\max}$  and  $dP/dt_{\min}$ , which is in agreement with previous studies demonstrating that CVB3 reduced  $P_{\max}$ ,  $dP/dt_{\max}$  and  $dP/dt_{\min}$  parameters in acute CVB3-induced myocarditis mice<sup>63, 66, 67, 70</sup>. Both EMB-CardAPs and EMB-CF improved LV function following i.v. injection in CVB3-induced

myocarditis mice. However, only i.v. application of EMB-CardAPs and not of EMB-CF reduced collagen I expression.

Inflammation is a key player in the pathogenesis of CVB3-induced myocarditis, which is associated with high levels of chemokines<sup>107</sup>. MSCs application has been shown to modulate the cardiac chemokine pattern by decreasing CCL2 and CCL7, chemokines, known to attract pro-inflammatory monocytes, as well as CCR2 mRNA expression in CVB3-infected mice. This was translated in the reduction of infiltrated pro-inflammatory monocytes<sup>63, 68</sup>. Equivalently, in the present study, EMB-CardAPs application reduced LV CCL2 and CCL7 mRNA expression in acute CVB3-induced myocarditis mice. Furthermore, EMB-CardAPs decreased LV mRNA expression of CX3CL1, known to attract anti-inflammatory monocytes<sup>68, 109</sup>, whereas EMB-CF only reduced CX3CL1 mRNA levels. The decline of CCL2 and CCL7 by EMB-CardAPs application in CVB3-infected mice was further associated with the reduction of CCR2, which is the main ligand for CCL2 and CCL7.

Homing of leukocytes to the sites of injury in viral myocarditis is important for the elimination of pathogens<sup>14</sup>. The chemokine system is the main regulator of monocytes recruitment<sup>68</sup>. High levels of CCL2, CCL7 and CX3CL1 are followed by high monocyte infiltration<sup>110</sup>. Modulation of the chemokine system has been associated with reduced levels of immune cells infiltration in the heart<sup>67</sup>. Application of EMB-CardAPs has been shown to reduce mononuclear cell activation and to increase the % of Treg, known for their cardioprotective effects in CVB3-induced myocarditis<sup>111, 112</sup>. In agreement with our observations with EMB-CardAPs in acute CVB3-induced myocarditis mice, intravenous application of Treg has been shown to reduce the mRNA as well as the protein levels of CCL2, CCL7 and CX3CL1 in the LV, the LV mRNA levels of CCR2 and Ly6c, as well as the number of pro-inflammatory Ly6C<sup>high</sup>CCR2<sup>high</sup>CX3CR1<sup>low</sup> monocytes<sup>70</sup>.

Upregulated chemokines attract immune cells such as monocytes to the site of injury<sup>68</sup>. CVB3-induced myocarditis is characterized by infiltration of inflammatory cells, especially T cells<sup>63</sup>, which can cause direct myocardial damage by CD8<sup>+</sup> cytotoxic T cells, or indirect by upregulation of pro-inflammatory cytokines<sup>113</sup>. Treatment of CVB3-infected mice with a monoclonal antibody against total T cells markedly reduced the myocardial damage<sup>114</sup>. EMB-CardAPs diminished the presence of CD68<sup>+</sup> cells as well as the mRNA expression of Ly6c pro-inflammatory cells.

In line with the attenuated inflammatory cell infiltration, a reduced LV mRNA expression of pro-inflammatory cytokines such as TNF- $\alpha$  and IL-6 was observed in EMB-CardAPs-treated CVB3-infected mice, which is conform to previous observations following MSCs application in CVB3-

induced myocarditis mice<sup>63, 67, 68</sup>. In this regard, increased myocardial inflammation has been shown to impair outcome of patients with viral cardiomyopathy<sup>22</sup>. Treatment with an anti-IL-6 receptor antibody has been demonstrated to downregulate the cardiac expression of TNF- $\alpha$ , as well as to attenuate the infiltration of CD68<sup>+</sup> monocytes in CVB3-induced acute myocarditis<sup>115</sup>. In contrast, treatment with EMB-CF could not modulate the inflammatory cytokine pattern.

There is growing evidence from *in vitro* and *in vivo* studies showing that the anti-inflammatory cytokine IL-10 as well as the anti-viral cytokines IFN- $\gamma$  and IFN- $\beta$  increase due to viral myocarditis<sup>17, 22, 67, 116</sup>. Those cytokines play a crucial role to govern cardiac inflammation induced by CVB3 infection<sup>67, 115</sup>. The immunomodulatory actions of MSCs have been shown to be associated with IL-10<sup>97</sup>. Other researchers reported that i.v. application of MSCs induces prominent cardioprotective effects involving the upregulation of IL-10 and the activation of IL-10-producing T regulatory cells<sup>63, 67, 68</sup> and the increase of IFN- $\gamma$  mRNA as well as the systemic levels of IFN- $\gamma$  and IFN- $\gamma$ -producing CD4<sup>+</sup> and CD8<sup>+</sup> cells<sup>67</sup>. IFN- $\gamma$  is a pro-inflammatory cytokine, which has anti-viral<sup>66</sup> and anti-fibrotic<sup>117</sup> functions, and plays a crucial role in the priming of MSCs needed to exert their immunomodulatory effects<sup>63, 97</sup>. Beyond MSCs, also EMB-CardAPs require IFN- $\gamma$  for their cardioprotective effects<sup>66</sup>. IFN- $\gamma$  has been proven to increase nitric oxide (NO) production in MSCs *in vitro*<sup>63</sup>, whereas EMB-CardAPs supplemented with IFN- $\gamma$  have been shown to increase IL-10 release<sup>66</sup>. Analogue to MSCs, EMB-CardAPs have been shown to exert immunomodulatory effects in CVB3-infected mice involving the release of IL-10<sup>66</sup>. Interestingly, in the present study, EMB-CardAPs as well as EMB-CF downregulated the CVB3-induced LV mRNA expression of IL-10, IFN- $\gamma$  and IFN- $\beta$  to levels of uninfected control mice. These differences in EMB-CardAPs-mediated IL-10, IFN- $\gamma$  and IFN- $\beta$  regulation might be due to the differences in severity of the CVB3 myocarditis model, and herewith-associated cardiac inflammatory microenvironment. In the present study, myocarditis was induced via i.p. 10<sup>5</sup> p.f.u. CVB3 injection, whereas in the reported study, 5x10<sup>5</sup> p.f.u. CVB3 was i.p. injected to induce myocarditis.

Despite the downregulated LV mRNA expression of the antiviral cytokines IL-10, IFN- $\gamma$  and IFN- $\beta$ , CVB3 mRNA expression was decreased in the LV of EMB-CardAPs injected CVB3 versus untreated CVB3 mice. The reduction in LV CVB3 mRNA expression might be due to an EMB-CardAPs-mediated decrease in cardiomyocyte apoptosis, which is important for viral progeny release<sup>63</sup>, and suggested by the increase in Bcl-2 to BAX ratio<sup>118</sup>. Since the spleen is a target organ of CVB3<sup>27</sup> and cardiac monocyte infiltration was less pronounced in CVB3+EMB-CardAPs versus CVB3 mice, the reduced cardiac CVB3 copy number found after EMB-CardAPs treatment in CVB3 mice can partly be explained via modulation of the cardiosplenic axis.

In summary, the present results report the beneficial cardioprotective effects of EMB-CardAPs for the treatment of acute CVB3-induced myocarditis, as indicated by the reduced cardiac fibrosis, lower LV mRNA expression of inflammatory cytokines and chemokines, the decrease of infiltrated monocytes and LV CVB3 mRNA expression, which were reflected in an improved LV systolic and diastolic function in CVB3+EMB-CardAPs versus untreated CVB3 mice. The abovementioned cardioprotective effects were not observed following i.v. EMB-CF injection in acute CVB3-induced myocarditis mice, documenting differences between EMB-CardAPs and EMB-CF. Nevertheless, EMB-CF application improved LV function, a finding, which needs further investigation.

## **5.2. RAA-CardAPs in acute Coxsackievirus B3-induced myocarditis mice**

From translational point of view, EMB-CardAPs have been isolated for autologous administration<sup>100</sup>. Whereas autologous cells are considered to be safe, due to the absence of a potential graft versus host immune rejection<sup>92</sup>, they are difficult in application because of the time consuming preparation, disabling off-the-shelf use, and the limited reachable cell numbers<sup>119</sup>. To overcome these limitations, RAA-CardAPs have been generated from RAA by outgrowth culture under standard cell culture conditions, followed by negative CD90 immunomagnetic sorting. RAA-CardAPs have been isolated and expanded as a promising candidate for off-the-shelf allogeneic use allowing sufficient cells for the treatment of more than 250 patients.<sup>100</sup> Allogeneic cell-based approach has several advantages over an autologous one. It can: 1) reduce the exposure of the injected cells to the patients risk factors<sup>101</sup>, 2) provide immediate care at the time of tissue injury<sup>101</sup> and 3) be expanded *in vitro* to clinically relevant dosages<sup>101</sup>. Allogeneic cells, however, have some limitations, which are mainly addressed to the alloreactivity to T lymphocytes<sup>120</sup>. Preclinical<sup>121</sup> and clinical studies<sup>76, 88</sup> have demonstrated the favorable use of allogeneic MSCs for the treatment of cardiac dysfunction, providing supportive evidence to use allogeneic MSCs for the treatment of inflammatory cardiomyopathy. Beyond MSCs<sup>122</sup>, also EMB-CardAPs<sup>92</sup> are hypo-immunogenic, as shown by low expression levels of HLA, which addresses the safety of using them clinically. Recent evidence from *in vitro* experiments by immune cell co-cultures (performed at the BCRT, AG Seifert) illustrate that RAA- and EMB-CardAPs have similar immunogenic and immunomodulatory properties,<sup>123</sup> enabling the potential therapeutic use of RAA-CardAPs in an allogeneic setting<sup>100</sup>.

Similar to EMB-CardAPs<sup>90</sup>, also RAA-CardAPs display an expression profile different from that of MSCs or cardiac resident cells<sup>90</sup>. In contrast to EMB-CardAPs, of which the mechanisms of action of are well described, involving pro-angiogenic<sup>94</sup>, anti-apoptotic<sup>66</sup>, anti-fibrotic<sup>98</sup> as well as immunomodulatory<sup>92</sup> effects, including their ability to modulate various immune cell types of both the innate and adapted immune response<sup>124</sup>, the cardioprotective effects of RAA-

CardAPs have not been explored so far. Therefore, the aim of this study was to investigate whether RAA-CardAPs can exert the same beneficial effects as EMB-CardAPs in acute CVB3-infected myocarditis mice.

Before investigating the cardioprotective potential of RAA-CardAPs in acute CVB3 myocarditis mice, it was evaluated whether the viability of RAA-CardAPs would be hampered following CVB3 infection. *In vitro* evaluation of RAA-CardAPs' viability 4h, 12h, 24h, and 48h post infection showed an increased absorbance at 4h and 24h post infection compared to respective serum starvation conditions. This increase may be a virus-induced increase in cell metabolism. Though, CVB3-infected and uninfected RAA-CardAPs exhibited a similar increase in absorbance between 4h versus 48h post infection, indicating that the viability of RAA-CardAPs was not hampered following CVB3 infection. Based on the relevance of cardiomyocyte apoptosis for viral progeny release<sup>63</sup> and the described anti-apoptotic potential of EMB-CardAPs<sup>66</sup>, we next evaluated whether RAA-CardAPs could decrease CVB3-induced apoptosis in HL-1 cells. Therefore, RAA-CardAPs were co-cultured with DiO-labeled HL-1 cells, allowing specific analysis of cardiomyocyte apoptosis via flow cytometry. Similar to EMB-CardAPs, RAA-CardAPs were able to reduce CVB3-induced apoptosis in HL-1 cells. Though, this effect was not associated with a decrease in CVB3 mRNA expression in the HL-1+RAA-CardAPs co-culture. A limitation of this experiment is that the CVB3 mRNA level reflects the CVB3 mRNA expression of the co-culture and not of the sole HL-1 cardiomyocytes. Therefore, the CVB3 mRNA expression data should be interpreted with caution.

Following the promising *in vitro* experiments, the cardioprotective potential of RAA-CardAPs was evaluated in acute CVB3-induced myocarditis mice. Intravenous application of RAA-CardAPs improved LV systolic function, as manifested by an increased LVESP,  $P_{\max}$  and  $dP/dt_{\max}$  versus untreated acute CVB3-infected myocarditis mice. Moreover, LV diastolic function improved following RAA-CardAPs administration in CVB3-infected mice, as indicated by the elevation of  $dP/dt_{\min}$  in CVB3+RAA-CardAPs compared to untreated CVB3 myocarditis mice. In parallel, intravenous administration of RAA-CardAPs attenuated collagen deposition, as indicated by the decreased LV collagen I protein level and collagen I/collagen III ratio in CVB3-induced myocarditis. These findings are in agreement with the previously shown anti-fibrotic potential of EMB-CardAPs<sup>98</sup>. The ratio of collagen I/ collagen III within the heart is an important parameter, since it reflects the proportion of both collagen fibers, which have different mechanical characteristics<sup>125</sup>: collagen I is the stiff fiber, whereas collagen III is the compliant form. Myocardial tissues of DCM patients have been found to have a marked increase in the ratio of collagen I / collagen III at both mRNA and protein level<sup>126</sup>. The RAA-CardAPs mediated decrease in LV collagen I / collagen III ratio hereby reflects a reduction of "stiff" collagen fibers in acute CVB3 myocarditis mice, which is reflected in the improvement in diastolic function.

Intravenous application of RAA-CardAPs was further not associated with any reduction in LV mRNA expression neither of chemokine nor of chemokine receptors. Chemokines are a family of low-molecular-weight proteins, which have been found to control the migration and infiltration of immune cells into the heart<sup>14, 97</sup>. Whereas MSCs exhibit immunosuppressive properties<sup>16</sup>, MSCs also have immunostimulatory properties, in certain settings<sup>127</sup>. In fact, MSCs adapt their function depending on the inflammatory microenvironment<sup>97, 128</sup>. Zhou *et al.* reported the immunostimulatory effect of MSCs, which was indicated by the MSC-mediated induction of CD4<sup>+</sup> and CD8<sup>+</sup> T cells proliferation through CCL2<sup>128</sup>. RAA-CardAPs application in CVB3-infected mice did not modulate LV CCL2 mRNA expression, neither the number of CD4<sup>+</sup> and CD8<sup>+</sup> T cells. It should be mentioned that Savvatis-Van Linthout<sup>67</sup> previously demonstrated an increase in CD4<sup>+</sup> and CD8<sup>+</sup> lymphocytes in acute CVB3 myocarditis mice following i.v. MSCs application, despite lower expression of pro-inflammatory cytokines. Since MSCs application decreased the proliferation/activation of cardiac mononuclear cells, it was suggested that the activity of the retrieved CD4<sup>+</sup> and CD8<sup>+</sup> T cells in the heart was suppressed. These data indicate that not solely the amount of CD4<sup>+</sup> and CD8<sup>+</sup> T cells in the heart is of importance, but also their activity, which can be analyzed via evaluation of their proliferation and is reflected in the expression of cytokines.

A grown body of evidence has demonstrated that viral infection leads to a severe immune response, which is characterized by the release of pro-inflammatory cytokines, including TNF- $\alpha$ , IL-1 $\beta$  and IL-6<sup>6, 70, 107, 115</sup>. In agreement, mRNA expression of TNF- $\alpha$ , IL-1 $\beta$  and IL-6 increased in the LV of CVB3-infected mice. In line with the unchangeable LV mRNA expression of chemokines, chemokine receptors and immune cell presence, RAA-CardAPs did not reduce the LV mRNA expression of the abovementioned pro-inflammatory cytokines.

Interestingly, RAA-CardAPs application did also not modulate the LV mRNA levels of the anti-viral cytokines IFN- $\gamma$ , IFN- $\beta$ , and IL-10. IFN- $\gamma$  has been shown to play a crucial role in priming MSCs<sup>63</sup> and EMB-CardAPs<sup>66</sup> to exert their immunoregulatory effects. Miteva *et al.*<sup>66</sup> reported that EMB-CardAPs attenuated CVB3-induced cardiomyocyte apoptosis and the proliferation/activity of CD4<sup>+</sup> and CD8<sup>+</sup> T cells in an IL-10- and IFN- $\gamma$ -dependent manner. Furthermore, they showed that IFN- $\gamma$  supplementation increased IL-10 production by EMB-CardAPs, further supporting that EMB-CardAPs require IFN- $\gamma$  for their priming<sup>66</sup>. In contrast to the findings with RAA-CardAPs, Miteva *et al.* observed higher LV IL-10 and IFN- $\gamma$  mRNA expression in EMB-CardAPs-treated versus untreated CVB3-infected myocarditis mice<sup>66</sup>. This discrepancy might be due to 1) differences in CVB3 myocarditis model, since in the present myocarditis model, myocarditis was induced by only 10<sup>5</sup> p.f.u. CVB3, whereas by Miteva *et al.*<sup>66</sup> 5x10<sup>5</sup> p.f.u. CVB3 was used; and 2) differences between EMB-CardAPs and RAA-CardAPs. The unaltered LV mRNA expression of antiviral IFN- $\gamma$  and IFN- $\beta$  upon RAA-CardAPs

application was associated with no changes in LV CVB3 mRNA expression in CVB3+RAA-CardAPs versus untreated CVB3 mice.

In summary, RAA-CardAPs improved LV function in acute CVB3-induced myocarditis, which was paralleled by a decrease in cardiac fibrosis, in the absence of any modulation of cardiac inflammation and CVB3 mRNA expression.

### **5.3. Assessment of the chronic Coxsackievirus B3-induced myocarditis model**

The third experiment was performed to assess chronic CVB3-induced myocarditis in NMRI mice. NMRI mice have been used for the induction of chronic myocarditis by encephalomyocarditis-virus<sup>129</sup> and CVB3<sup>130, 131</sup>. Since CVB3 infection has different effects in human<sup>132, 133</sup>, some patients with CVB3 infection may spontaneously eliminate the virus and recover, whereas those with virus persistence deteriorate and progress to heart failure<sup>134</sup>, the NMRI outbred mouse model depicts better the variability of the human population<sup>130</sup>. Indeed, inbred mice are genetically homogeneous<sup>135</sup>, leading to no pronounced differences among the mice. Inbred mouse models are studied for both acute<sup>114, 136</sup> and chronic<sup>137, 138</sup> myocarditis, by which some inbred mouse strains only develop acute myocarditis after CVB3 infection, but not chronic myocarditis<sup>136</sup>. In a previous study exploring the long-term outcome of CVB3-induced myocarditis in C57BL/6j mice, Becher and co-workers demonstrated reversible cardiac inflammation and fibrosis with impaired cardiac function 28 days after infection<sup>17</sup>.

In the present study, CVB3 of the 31-1-93<sup>131</sup>/SAP batch was used to induce chronic myocarditis followed until to 28 days<sup>130, 131</sup> post infection in NMRI mice. CVB3-induced chronic myocarditis in NMRI mice has been characterized by fibrosis and virus persistence in cardiac tissue up to day 98 post infection<sup>130</sup>. Based on this finding, we re-established the chronic myocarditis mouse model with CVB3 in NMRI mice to further investigate the effect of CVB3 on cardiac function and to explore the therapeutic effect of RAA-CardAPs in a chronic myocarditis model. In previous experimental chronic CVB3-induced myocarditis models<sup>42, 48, 130</sup>, the cardiac phenotype was characterized by evaluation of the triggered immune response and tissue lesions, without evaluation of hemodynamic parameters. Therefore, we characterized the cardiac function in this model via hemodynamic measurements. CVB3-infected NMRI mice displayed LV dysfunction, as indicated by the reduction of systolic and diastolic parameters. In parallel, chronic CVB3-induced myocarditis NMRI mice displayed increased LV collagen I protein level, which was reflected in an upregulated ratio of collagen I/collagen III. This finding is in line with a previous report<sup>131</sup>, which showed that CVB3-infected NMRI mice exhibited increased cardiac fibrosis at late stages, and is conform to DCM patients, which have an increased collagen I/collagen III ratio<sup>126, 139</sup>.

Chemokine patterns and their respective receptors have been intensively studied in CVB3-induced acute myocarditis<sup>68, 107, 113</sup>. However, there is little evidence about chemokine and chemokine receptor regulation in experimental chronic CVB3-induced myocarditis. The present study demonstrated no alteration in LV mRNA expression of CCL2, CCL7 and CX3CL1, 28 days post-CVB3 infection. Moreover, the ratio of CCL2/CX3CL1 and CCL7/CX3CL1 was not changed. Interestingly, CVB3-infected mice displayed an increase in the LV mRNA level of CCR2, which has been described as an important receptor on inflammatory monocytes and known to bind to CCL2 and CCL7<sup>140</sup>.

Infiltration of inflammatory cells is a main characteristic of acute myocarditis<sup>38</sup>, whereas a lower percent of immune cell infiltration is found in chronic myocarditis and DCM<sup>38</sup>. In the present study, CVB3-infected NMRI mice displayed an increase in infiltrated CD4<sup>+</sup> and CD8<sup>+</sup> T cells, whereas LV CD68<sup>+</sup> monocytes/macrophages were only slightly elevated compared to non-infected mice. Consistent with the increase of infiltrated T lymphocytes, CVB3-infected mice displayed an elevation in the mRNA expression of IFN- $\gamma$ , which is mainly secreted by T cells<sup>141</sup>. However, LV mRNA expression of the pro-inflammatory cytokines TNF- $\alpha$ , IL-1 $\beta$  and IL-6 was not increased at this chronic stage. In agreement with these findings, Glück *et al.*<sup>131</sup> reported the persistence of IFN- $\gamma$  in chronic myocarditis at day 28 post infection. Along with the increased expression of anti-viral IFN- $\gamma$  at day 28 post CVB3 infection in NMRI mice, LV CVB3 mRNA expression was minimal at this chronic stage.

In summary, the results of the present study demonstrate that CVB3 of the 31-1-93/SAP batch induces chronic myocarditis in NMRI mice at day 28 post infection. The chronic stage was characterized by LV dysfunction, paralleled by increased collagen I protein and collagen I/collagen III ratio, upregulated mRNA levels of CCR2 and IFN- $\gamma$ , elevated presence of CD4<sup>+</sup> and CD8<sup>+</sup> T cells, in the absence of pronounced CVB3 mRNA expression.

#### **5.4. RAA-CardAPs in chronic Coxsackievirus B3-induced myocarditis mice**

RAA-CardAPs 1) are low immunogenic similar to EMB-CardAPs<sup>123</sup> and 2) can easily be expanded to high cell numbers<sup>100</sup> and herewith fulfill two prerequisites for an allogenic off-the-shelf cell product. Following first evaluations of RAA-CardAPs in acute CVB3-induced myocarditis mice, the fourth experiment was designed to evaluate the cardioprotective potential of RAA-CardAPs in chronic CVB3-induced myocarditis mice. Whereas in the acute CVB3-induced myocarditis model, the cells were injected 1 day after CVB3 injection, i.e. in the viral phase, RAA-CardAPs were injected in NMRI mice at day 10 post CVB3 injection, i.e. in the inflammatory phase.

Chronic CVB3-induced myocarditis NMRI mice displayed an impaired LV function, as indicated by the reduction of EF and LV systolic and diastolic functions due to viral infection. Furthermore, LV mRNA levels of CCR2, the pro-inflammatory cytokine IL-6, the anti-viral cytokines IFN- $\beta$  and IFN- $\gamma$ , and the anti-inflammatory cytokine IL-10 were upregulated in NMRI mice at day 28 post infection, whereas the LV mRNA expression of the chemokines CCL2, CCL7 and CX3CL1 were not increased versus control mice. LV CVB3 mRNA expression was minimal.

I.v. application of RAA-CardAPs improved the cardiac function as indicated by the increase of EF and  $dP/dt_{max}$  in RAA-CardAPs-treated versus untreated CVB3-infected mice. Conform to the findings in acute CVB3-induced myocarditis, RAA-CardAPs reduced LV collagen I expression compared to untreated chronic CVB3 myocarditis NMRI mice. Furthermore, RAA-CardAPs slightly decreased the LV presence of CD68<sup>+</sup> cells in chronic CVB3-induced myocarditis NMRI mice, an observation, which was not found in the acute CVB3 setting. Conform to the findings in acute CVB3 myocarditis mice, RAA-CardAPs did not downregulate LV mRNA expression of anti-viral IFN- $\beta$  and IFN- $\gamma$ . In contrast, RAA-CardAPs decreased LV mRNA IL-10 expression in chronic but not in acute myocarditis mice. These findings indicate that, similar to MSCs<sup>97, 128</sup> and EMB-CardAPs<sup>66</sup>, RAA-CardAPs differ in their properties/cardioprotective effects depending on the microenvironment. To further confirm this hypothesis, experiments still need to be performed in which RAA-CardAPs are injected during the viral phase of CVB3-infected NMRI mice, allowing a comparison in the same mouse background.

In summary, RAA-CardAPs improved LV function in chronic myocarditis NMRI mice following i.v. injection at day 10. This was paralleled by a decrease in cardiac fibrosis and a slight reduction in CD68<sup>+</sup> cells in the LV.

In general, the cardioprotective effects of RAA-CardAPs are modest in both acute and chronic CVB3-induced myocarditis mice. Further evaluation is required to understand the differences in the cardioprotective potential of RAA-CardAPs and EMB-CardAPs.

## 6. References

1. Stewart J, Manmathan G and Wilkinson P. Primary prevention of cardiovascular disease: A review of contemporary guidance and literature. *JRSM Cardiovasc Dis.* 2017;6:1-9.
2. Roth GA, Johnson C, Abajobir A, Abd-Allah F, Abera SF, Abyu G, Ahmed M, Aksut B, Alam T, Alam K, Alla F, Alvis-Guzman N, Amrock S, Ansari H, Ärnlöv J, Asayesh H, Atey TM, Avila-Burgos L, Awasthi A, Banerjee A, Barac A, Bärnighausen T, Barregard L, Bedi N, Belay Ketema E, Bennett D, Berhe G, Bhutta Z, Bitew S, Carapetis J, Carrero JJ, Malta DC, Castaneda-Orjuela CA, Castillo-Rivas J, Catala-Lopez F, Choi JY, Christensen H, Cirillo M, Cooper L, Jr., Criqui M, Cundiff D, Damasceno A, Dandona L, Dandona R, Davletov K, Dharmaratne S, Dorairaj P, Dubey M, Ehrenkranz R, El Sayed Zaki M, Faraon EJA, Esteghamati A, Farid T, Farvid M, Feigin V, Ding EL, Fowkes G, Gebrehiwot T, Gillum R, Gold A, Gona P, Gupta R, Habtewold TD, Hafezi-Nejad N, Hailu T, Hailu GB, Hankey G, Hassen HY, Abate KH, Havmoeller R, Hay SI, Horino M, Hotez PJ, Jacobsen K, James S, Javanbakht M, Jeemon P, John D, Jonas J, Kalkonde Y, Karimkhani C, Kasaeian A, Khader Y, Khan A, Khang YH, Khera S, Khoja AT, Khubchandani J, Kim D, Kolte D, Kosen S, Krohn KJ, Kumar GA, Kwan GF, Lal DK, Larsson A, Linn S, Lopez A, Lotufo PA, El Razek HMA, Malekzadeh R, Mazidi M, Meier T, Meles KG, Mensah G, Meretoja A, Mezgebe H, Miller T, Mirrakhimov E, Mohammed S, Moran AE, Musa KI, Narula J, Neal B, Ngalesoni F, Nguyen G, Obermeyer CM, Owolabi M, Patton G, Pedro J, Qato D, Qorbani M, Rahimi K, Rai RK, Rawaf S, Ribeiro A, Safiri S, Salomon JA, Santos I, Santric Milicevic M, Sartorius B, Schutte A, Sepanlou S, Shaikh MA, Shin MJ, Shishehbor M, Shore H, Silva DAS, Sobngwi E, Stranges S, Swaminathan S, Tabares-Seisdedos R, Tadele Atnafu N, Tesfay F, Thakur JS, Thrift A, Topor-Madry R, Truelsen T, Tyrovolas S, Ukwaja KN, Uthman O, Vasankari T, Vlassov V, Vollset SE, Wakayo T, Watkins D, Weintraub R, Werdecker A, Westerman R, Wiysonge CS, Wolfe C, Workicho A, Xu G, Yano Y, Yip P, Yonemoto N, Younis M, Yu C, Vos T, Naghavi M and Murray C. Global, Regional, and National Burden of Cardiovascular Diseases for 10 Causes, 1990 to 2015. *J Am Coll Cardiol.* 2017;70:1-25.
3. Celermajer DS, Chow CK, Marijon E, Anstey NM and Woo KS. Cardiovascular disease in the developing world: prevalences, patterns, and the potential of early disease detection. *J Am Coll Cardiol.* 2012;60:1207-1216.
4. (WHO) WHO. Cardiovascular diseases (CVDs) fact sheet. 2017.
5. Buggey J and ElAmm CA. Myocarditis and cardiomyopathy. *Curr Opin Cardiol.* 2018;33:341-346.
6. Van Linthout S and Tschöpe C. Viral myocarditis: a prime example for endomyocardial biopsy-guided diagnosis and therapy. *Curr Opin Cardiol.* 2018;33:325-333.
7. Lv S, Rong J, Ren S, Wu M, Li M, Zhu Y and Zhang J. Epidemiology and diagnosis of viral myocarditis. *Hellenic J Cardiol.* 2013;54:382-391.
8. Yajima T. Viral myocarditis: potential defense mechanisms within the cardiomyocyte against virus infection. *Future Microbiol.* 2011;6:551-566.
9. Valdes O, Acosta B, Pinon A, Savon C, Goyenechea A, Gonzalez G, Gonzalez G, Palerm L, Sarmiento L, Pedro ML, Martinez PA, Rosario D, Kouri V, Guzman MG, Llop A, Casas I and Perez Brena MP. First report on fatal myocarditis associated with adenovirus infection in Cuba. *J Med Virol.* 2008;80:1756-1761.
10. Verdonschot J, Hazebroek M, Merken J, Debing Y, Dennert R, Brunner-La Rocca HP and Heymans S. Relevance of cardiac parvovirus B19 in myocarditis and dilated cardiomyopathy: review of the literature. *Eur J Heart Fail.* 2016;18:1430-1441.
11. Hidron AI, Gilman RH, Justiniano J, Blackstock AJ, Lafuente C, Selum W, Calderon M, Verastegui M, Ferrufino L, Valencia E, Tornheim JA, O'Neal S, Comer R, Galdos-Cardenas G, Bern C, Chagas Disease Working Group in P and Bolivia. Chagas cardiomyopathy in the context of the chronic disease transition. *PLoS Negl Trop Dis.* 2010;4:e688.
12. Pergola G, Cascone A and Russo M. Acute pericarditis and myocarditis by *Toxoplasma gondii* in an immunocompetent young man: a case report. *Infez Med.* 2010;18:48-52.

13. Jin O, Sole MJ, Butany JW, Chia WK, McLaughlin PR, Liu P and Liew CC. Detection of enterovirus RNA in myocardial biopsies from patients with myocarditis and cardiomyopathy using gene amplification by polymerase chain reaction. *Circulation*. 1990;82:8-16.
14. Schultheiss H-P, Kühl U and Cooper LT. The management of myocarditis. *E heart J*. 2011;32:2616-2625.
15. Schultz JC, Hilliard AA, Cooper LT, Jr. and Rihal CS. Diagnosis and treatment of viral myocarditis. *Mayo Clin Proc*. 2009;84:1001-1009.
16. Van Linthout S, Stamm C, Schultheiss HP and Tschöpe C. Mesenchymal stem cells and inflammatory cardiomyopathy: cardiac homing and beyond. *Cardiol Res Pract*. 2011;2011:757154.
17. Becher PM, Gotzhein F, Klingel K, Escher F, Blankenberg S, Westermann D and Lindner D. Cardiac Function Remains Impaired Despite Reversible Cardiac Remodeling after Acute Experimental Viral Myocarditis. *J Immunol Res*. 2017;2017:6590609.
18. Brambatti M, Matassini MV, Adler ED, Klingel K, Camici PG and Ammirati E. Eosinophilic Myocarditis: Characteristics, Treatment, and Outcomes. *J Am Coll Cardiol*. 2017;70:2363-2375.
19. Cooper LT, Jr., Berry GJ and Shabetai R. Idiopathic giant-cell myocarditis--natural history and treatment. Multicenter Giant Cell Myocarditis Study Group Investigators. *N Engl J Med*. 1997;336:1860-1866.
20. Pollack A, Kontorovich AR, Fuster V and Dec GW. Viral myocarditis--diagnosis, treatment options, and current controversies. *Nat Rev Cardiol*. 2015;12:670-680.
21. Heymans S, Eriksson U, Lehtonen J and Cooper LT, Jr. The Quest for New Approaches in Myocarditis and Inflammatory Cardiomyopathy. *J Am Coll Cardiol*. 2016;68:2348-2364.
22. Jenke A, Holzhauser L, Löbel M, Savvatis K, Wilk S, Weithäuser A, Pinkert S, Tschöpe C, Klingel K, Poller W, Scheibenbogen C, Schultheiss HP and Skurk C. Adiponectin promotes coxsackievirus B3 myocarditis by suppression of acute anti-viral immune responses. *Basic Res Cardiol*. 2014;109:408.
23. Epelman S, Liu PP and Mann DL. Role of innate and adaptive immune mechanisms in cardiac injury and repair. *Nat Rev Immunol*. 2015;15:117-129.
24. D'Ambrosio A, Patti G, Manzoli A, Sinagra G, Di Lenarda A, Silvestri F and Di Sciascio G. The fate of acute myocarditis between spontaneous improvement and evolution to dilated cardiomyopathy: a review. *Heart*. 2001;85:499-504.
25. Sagar S, Liu PP and Cooper LT, Jr. Myocarditis. *Lancet*. 2012;379:738-747.
26. Fairweather D, Stafford KA and Sung YK. Update on coxsackievirus B3 myocarditis. *Curr Opin Rheumatol*. 2012;24:401-407.
27. Klingel K, Stephan S, Sauter M, Zell R, McManus BM, Bültmann B and Kandolf R. Pathogenesis of murine enterovirus myocarditis: virus dissemination and immune cell targets. *J Virol*. 1996;70:8888-8895.
28. Weithäuser A, Bobbert P, Antoniak S, Böhm A, Rauch BH, Klingel K, Savvatis K, Kroemer HK, Tschöpe C, Stroux A, Zeichhardt H, Poller W, Mackman N, Schultheiss HP and Rauch U. Protease-activated receptor-2 regulates the innate immune response to viral infection in a coxsackievirus B3-induced myocarditis. *J Am Coll Cardiol*. 2013;62:1737-1745.
29. Levine B, Kalman J, Mayer L, Fillit HM and Packer M. Elevated circulating levels of tumor necrosis factor in severe chronic heart failure. *N Engl J Med*. 1990;323:236-241.
30. Matsumori A. Cytokines in myocarditis and cardiomyopathies. *Curr Opin Cardiol*. 1996;11:302-309.
31. De Luca G, Cavalli G, Campochiaro C, Tresoldi M and Dagna L. Myocarditis: An Interleukin-1-Mediated Disease? *Front Immunol*. 2018;9:1335.
32. Satoh M, Tamura G, Segawa I, Tashiro A, Hiramori K and Satodate R. Expression of cytokine genes and presence of enteroviral genomic RNA in endomyocardial biopsy tissues of myocarditis and dilated cardiomyopathy. *Virchows Arch*. 1996;427:503-509.
33. Izumi T and Nishii M. Diagnostic and prognostic biomarkers in acute myocarditis. Interleukin-10. *Herz*. 2012;37:627-631.
34. Kania G, Blyszczuk P, Stein S, Valaperti A, Germano D, Dirnhofer S, Hunziker L, Matter CM and Eriksson U. Heart-infiltrating prominin-1+/CD133+ progenitor cells represent the

- cellular source of transforming growth factor beta-mediated cardiac fibrosis in experimental autoimmune myocarditis. *Circ Res*. 2009;105:462-470.
35. Bishop JE and Laurent GJ. Collagen turnover and its regulation in the normal and hypertrophying heart. *Eur Heart J*. 1995;16 Suppl C:38-44.
  36. Weber KT, Janicki JS, Shroff SG, Pick R, Chen RM and Bashey RI. Collagen remodeling of the pressure-overloaded, hypertrophied nonhuman primate myocardium. *Circ Res*. 1988;62:757-765.
  37. Fomovsky GM, Thomopoulos S and Holmes JW. Contribution of extracellular matrix to the mechanical properties of the heart. *J Mol Cell Cardiol*. 2010;48:490-496.
  38. Dominguez F, Kühl U, Pieske B, Garcia-Pavia P and Tschöpe C. Update on Myocarditis and Inflammatory Cardiomyopathy: Reemergence of Endomyocardial Biopsy. *Rev Esp Cardiol (Engl Ed)*. 2016;69:178-187.
  39. Aretz HT. Myocarditis: the Dallas criteria. *Hum Pathol*. 1987;18:619-624.
  40. Grun K, Markova B, Bohmer FD, Berndt A, Kosmehl H and Leipner C. Elevated expression of PDGF-C in coxsackievirus B3-induced chronic myocarditis. *Eur Heart J*. 2005;26:728-739.
  41. Klingel K, Schnorr JJ, Sauter M, Szalay G and Kandolf R. beta2-microglobulin-associated regulation of interferon-gamma and virus-specific immunoglobulin G confer resistance against the development of chronic coxsackievirus myocarditis. *Am J Pathol*. 2003;162:1709-1720.
  42. Andreoletti L, Hober D, Becquart P, Belaich S, Copin MC, Lambert V and Wattré P. Experimental CVB3-induced chronic myocarditis in two murine strains: evidence of interrelationships between virus replication and myocardial damage in persistent cardiac infection. *J Med Virol*. 1997;52:206-214.
  43. Leipner C, Grün K, Müller A, Buchdunger E, Borsi L, Kosmehl H, Berndt A, Janik T, Uecker A, Kiehntopf M and Böhmer FD. Imatinib mesylate attenuates fibrosis in coxsackievirus b3-induced chronic myocarditis. *Cardiovasc Res*. 2008;79:118-126.
  44. Abston ED, Coronado MJ, Bucek A, Bedja D, Shin J, Kim JB, Kim E, Gabrielson KL, Georgakopoulos D, Mitzner W and Fairweather D. Th2 regulation of viral myocarditis in mice: different roles for TLR3 versus TRIF in progression to chronic disease. *Clin Dev Immunol*. 2012;2012:129486.
  45. Coronado MJ, Brandt JE, Kim E, Bucek A, Bedja D, Abston ED, Shin J, Gabrielson KL, Mitzner W and Fairweather D. Testosterone and interleukin-1beta increase cardiac remodeling during coxsackievirus B3 myocarditis via serpin A 3n. *Am J Physiol Heart Circ Physiol*. 2012;302:H1726-1736.
  46. Cheung CT, Deisher TA, Luo H, Yanagawa B, Bonigut S, Samra A, Zhao H, Walker EK and McManus BM. Neutralizing anti-4-1BBL treatment improves cardiac function in viral myocarditis. *Lab Invest*. 2007;87:651-661.
  47. Reyes MP and Lerner AM. Coxsackievirus myocarditis--with special reference to acute and chronic effects. *Prog Cardiovasc Dis*. 1985;27:373-794.
  48. Lodge PA, Herzum M, Olszewski J and Huber SA. Coxsackievirus B-3 myocarditis. Acute and chronic forms of the disease caused by different immunopathogenic mechanisms. *Am J Pathol*. 1987;128:455-463.
  49. Andreoletti L, Hober D, Decoene C, Copin MC, Lobert PE, Dewilde A, Stankowiac C and Wattré P. Detection of enteroviral RNA by polymerase chain reaction in endomyocardial tissue of patients with chronic cardiac diseases. *J Med Virol*. 1996;48:53-59.
  50. Kandolf R, Klingel K, Zell R, Selinka HC, Raab U, Schneider-Brachert W and Bültmann B. Molecular pathogenesis of enterovirus-induced myocarditis: virus persistence and chronic inflammation. *Intervirology*. 1993;35:140-151.
  51. Abelmann WH. Myocarditis and dilated cardiomyopathy. *West J Med*. 1989;150:458-459.
  52. Manolio TA, Baughman KL, Rodeheffer R, Pearson TA, Bristow JD, Michels VV, Abelmann WH and Harlan WR. Prevalence and etiology of idiopathic dilated cardiomyopathy (summary of a National Heart, Lung, and Blood Institute workshop. *Am J Cardiol*. 1992;69:1458-1466.

53. Guglin M and Nallamshetty L. Myocarditis: diagnosis and treatment. *Curr Treat Options Cardiovasc Med.* 2012;14:637-651.
54. Caforio AL, Pankuweit S, Arbustini E, Basso C, Gimeno-Blanes J, Felix SB, Fu M, Heliö T, Heymans S, Jahns R, Klingel K, Linhart A, Maisch B, McKenna W, Mogensen J, Pinto YM, Ristic A, Schultheiss HP, Seggewiss H, Tavazzi L, Thiene G, Yilmaz A, Charron P, Elliott PM, European Society of Cardiology Working Group on M and Pericardial D. Current state of knowledge on aetiology, diagnosis, management, and therapy of myocarditis: a position statement of the European Society of Cardiology Working Group on Myocardial and Pericardial Diseases. *Eur Heart J.* 2013;34:2636-48, 2648a-2648d.
55. Frustaci A, Russo MA and Chimenti C. Randomized study on the efficacy of immunosuppressive therapy in patients with virus-negative inflammatory cardiomyopathy: the TIMIC study. *Eur Heart J.* 2009;30:1995-2002.
56. Eschenhagen T, Bolli R, Braun T, Field LJ, Fleischmann BK, Frisen J, Giacca M, Hare JM, Houser S, Lee RT, Marban E, Martin JF, Molkentin JD, Murry CE, Riley PR, Ruiz-Lozano P, Sadek HA, Sussman MA and Hill JA. Cardiomyocyte Regeneration: A Consensus Statement. *Circulation.* 2017;136:680-686.
57. Del Corso C and Campos de Carvalho AC. Cell therapy in dilated cardiomyopathy: from animal models to clinical trials. *Braz J Med Biol Res.* 2011;44:388-393.
58. Scorsin M, Hagege AA, Dolizy I, Marotte F, Mirochnik N, Copin H, Barnoux M, le Bert M, Samuel JL, Rappaport L and Menasche P. Can cellular transplantation improve function in doxorubicin-induced heart failure? *Circulation.* 1998;98:II151-5; discussion II155-6.
59. Yoo KJ, Li RK, Weisel RD, Mickle DA, Jia ZQ, Kim EJ, Tomita S and Yau TM. Heart cell transplantation improves heart function in dilated cardiomyopathic hamsters. *Circulation.* 2000;102:III204-209.
60. Tang GH, Fedak PW, Yau TM, Weisel RD, Kulik A, Mickle DA and Li RK. Cell transplantation to improve ventricular function in the failing heart. *Eur J Cardiothorac Surg.* 2003;23:907-916.
61. Tomita S. Cell-based therapy to regenerate myocardium: from bench to bedside. *Artif Organs.* 2004;28:40-44.
62. Tang YL, Wang YJ, Chen LJ, Pan YH, Zhang L and Weintraub NL. Cardiac-derived stem cell-based therapy for heart failure: progress and clinical applications. *Exp Biol Med (Maywood).* 2013;238:294-300.
63. Van Linthout S, Savvatis K, Miteva K, Peng J, Ringe J, Warstat K, Schmidt-Lucke C, Sittlinger M, Schultheiss HP and Tschöpe C. Mesenchymal stem cells improve murine acute coxsackievirus B3-induced myocarditis. *Eur Heart J.* 2011;32:2168-2178.
64. Carmona MD, Canadillas S, Romero M, Blanco A, Nogueras S and Herrera C. Intramyocardial bone marrow mononuclear cells versus bone marrow-derived and adipose mesenchymal cells in a rat model of dilated cardiomyopathy. *Cytotherapy.* 2017;19:947-961.
65. Mao C, Hou X, Wang B, Chi J, Jiang Y, Zhang C and Li Z. Intramuscular injection of human umbilical cord-derived mesenchymal stem cells improves cardiac function in dilated cardiomyopathy rats. *Stem Cell Res Ther.* 2017;8:18.
66. Miteva K, Haag M, Peng J, Savvatis K, Becher PM, Seifert M, Warstat K, Westermann D, Ringe J, Sittlinger M, Schultheiss HP, Tschöpe C and Van Linthout S. Human cardiac-derived adherent proliferating cells reduce murine acute Coxsackievirus B3-induced myocarditis. *PLoS One.* 2011;6:e28513.
67. Savvatis K, van Linthout S, Miteva K, Pappritz K, Westermann D, Schefold JC, Fusch G, Weithauser A, Rauch U, Becher PM, Klingel K, Ringe J, Kurtz A, Schultheiss HP and Tschöpe C. Mesenchymal stromal cells but not cardiac fibroblasts exert beneficial systemic immunomodulatory effects in experimental myocarditis. *PLoS One.* 2012;7:e41047.
68. Miteva K, Pappritz K, El-Shafeey M, Dong F, Ringe J, Tschöpe C and Van Linthout S. Mesenchymal Stromal Cells Modulate Monocytes Trafficking in Coxsackievirus B3-Induced Myocarditis. *Stem Cells Transl Med.* 2017;6:1249-1261.
69. Miteva K, Pappritz K, Sosnowski M, El-Shafeey M, Müller I, Dong F, Savvatis K, Ringe J, Tschöpe C and Van Linthout S. Mesenchymal stromal cells inhibit NLRP3 inflammasome activation in a model of Coxsackievirus B3-induced inflammatory cardiomyopathy. *Sci Rep.* 2018;8:2820.

70. Pappritz K, Savvatis K, Miteva K, Kerim B, Dong F, Fechner H, Müller I, Brandt C, Lopez B, Gonzalez A, Ravassa S, Klingel K, Diez J, Reinke P, Volk HD, Van Linthout S and Tschöpe C. Immunomodulation by adoptive regulatory T-cell transfer improves Coxsackievirus B3-induced myocarditis. *FASEB J*. 2018:fj201701408R.
71. Ohnishi S, Yanagawa B, Tanaka K, Miyahara Y, Obata H, Kataoka M, Kodama M, Ishibashi-Ueda H, Kangawa K, Kitamura S and Nagaya N. Transplantation of mesenchymal stem cells attenuates myocardial injury and dysfunction in a rat model of acute myocarditis. *J Mol Cell Cardiol*. 2007;42:88-97.
72. Maleki M, Ghanbarvand F, Reza Behvarz M, Ejtemaei M and Ghadirkhomi E. Comparison of mesenchymal stem cell markers in multiple human adult stem cells. *Int J Stem Cells*. 2014;7:118-126.
73. Van Linthout S, Hamdani N, Miteva K, Koschel A, Müller I, Pinzur L, Aberman Z, Pappritz K, Linke WA and Tschöpe C. Placenta-Derived Adherent Stromal Cells Improve Diabetes Mellitus-Associated Left Ventricular Diastolic Performance. *Stem Cells Transl Med*. 2017;6:2135-2145.
74. Pilato CA, Stadiotti I, Maione AS, Saverio V, Catto V, Tundo F, Russo AD, Tondo C, Pompilio G and Casella M. Isolation and Characterization of Cardiac Mesenchymal Stromal Cells from Endomyocardial Bioptic Samples of Arrhythmogenic Cardiomyopathy Patients. *J Vis Exp.: JoVE*. 2018.
75. Prockop DJ. Marrow stromal cells as stem cells for nonhematopoietic tissues. *Science*. 1997;276:71-74.
76. Psaltis PJ, Carbone A, Nelson AJ, Lau DH, Jantzen T, Manavis J, Williams K, Itescu S, Sanders P, Gronthos S, Zannettino AC and Worthley SG. Reparative effects of allogeneic mesenchymal precursor cells delivered transendocardially in experimental nonischemic cardiomyopathy. *JACC Cardiovasc Interv*. 2010;3:974-983.
77. Makino S, Fukuda K, Miyoshi S, Konishi F, Kodama H, Pan J, Sano M, Takahashi T, Hori S, Abe H, Hata J, Umezawa A and Ogawa S. Cardiomyocytes can be generated from marrow stromal cells in vitro. *J Clin Invest*. 1999;103:697-705.
78. Tomita S, Li RK, Weisel RD, Mickle DA, Kim EJ, Sakai T and Jia ZQ. Autologous transplantation of bone marrow cells improves damaged heart function. *Circulation*. 1999;100:II247-256.
79. Bittner RE, Schöfer C, Weipoltshammer K, Ivanova S, Streubel B, Hauser E, Freilinger M, Höger H, Elbe-Bürger A and Wachtler F. Recruitment of bone-marrow-derived cells by skeletal and cardiac muscle in adult dystrophic mdx mice. *Anat Embryol (Berl)*. 1999;199:391-396.
80. Ohnishi S and Nagaya N. Prepare cells to repair the heart: mesenchymal stem cells for the treatment of heart failure. *Am J Nephrol*. 2007;27:301-307.
81. Li J, Zhang N and Wang J. Improved anti-apoptotic and anti-remodeling potency of bone marrow mesenchymal stem cells by anoxic pre-conditioning in diabetic cardiomyopathy. *J Endocrinol Invest*. 2008;31:103-110.
82. Mias C, Lairez O, Trouche E, Roncalli J, Calise D, Seguelas MH, Ordener C, Piercecchi-Marti MD, Auge N, Salvayre AN, Bourin P, Parini A and Cussac D. Mesenchymal stem cells promote matrix metalloproteinase secretion by cardiac fibroblasts and reduce cardiac ventricular fibrosis after myocardial infarction. *Stem Cells*. 2009;27:2734-2743.
83. Sorrell JM, Baber MA and Caplan AI. Influence of adult mesenchymal stem cells on in vitro vascular formation. *Tissue Eng Part A*. 2009;15:1751-1761.
84. Cai M, Shen R, Song L, Lu M, Wang J, Zhao S, Tang Y, Meng X, Li Z and He ZX. Bone Marrow Mesenchymal Stem Cells (BM-MSCs) Improve Heart Function in Swine Myocardial Infarction Model through Paracrine Effects. *Sci Rep*. 2016;6:28250.
85. Wu T, Xie Y, Huang J, Li P, Wang X, Yan Y, Xia T, Li L, Zhu F, Li H and Wu R. The Optimal Intervention Time of Bone Marrow Mesenchymal Stem Cells in Ameliorating Cardiac Fibrosis Induced by Viral Myocarditis: A Randomized Controlled Trial in Mice. *Stem Cells Int*. 2017;2017:3258035.
86. Okada H, Suzuki J, Futamatsu H, Maejima Y, Hirao K and Isobe M. Attenuation of autoimmune myocarditis in rats by mesenchymal stem cell transplantation through enhanced expression of hepatocyte growth factor. *Int Heart J*. 2007;48:649-661.

87. Zhang N, Li J, Luo R, Jiang J and Wang JA. Bone marrow mesenchymal stem cells induce angiogenesis and attenuate the remodeling of diabetic cardiomyopathy. *Exp Clin Endocrinol Diabetes*. 2008;116:104-111.
88. Hare JM, DiFede DL, Rieger AC, Florea V, Landin AM, El-Khorazaty J, Khan A, Mushtaq M, Lowery MH, Byrnes JJ, Hendel RC, Cohen MG, Alfonso CE, Valasaki K, Pujol MV, Golpanian S, Ghersin E, Fishman JE, Pattany P, Gomes SA, Delgado C, Miki R, Abuzeid F, Vidro-Casiano M, Premer C, Medina A, Porras V, Hatzistergos KE, Anderson E, Mendizabal A, Mitrani R and Heldman AW. Randomized Comparison of Allogeneic Versus Autologous Mesenchymal Stem Cells for Nonischemic Dilated Cardiomyopathy: POSEIDON-DCM Trial. *J Am Coll Cardiol*. 2017;69:526-537.
89. Nagaya N, Kangawa K, Itoh T, Iwase T, Murakami S, Miyahara Y, Fujii T, Uematsu M, Ohgushi H, Yamagishi M, Tokudome T, Mori H, Miyatake K and Kitamura S. Transplantation of mesenchymal stem cells improves cardiac function in a rat model of dilated cardiomyopathy. *Circulation*. 2005;112:1128-1135.
90. Haag M, Van Linthout S, Schröder SE, Freymann U, Ringe J, Tschöpe C and Sittlinger M. Endomyocardial biopsy derived adherent proliferating cells - a potential cell source for cardiac tissue engineering. *J Cell Biochem*. 2010;109:564-575.
91. Jucaud V. The immunogenicity of HLA class II mismatches: the predicted presentation of nonself allo-HLA-derived peptide by the HLA-DR phenotype of the recipient is associated with the formation of DSA. *J Immunol Res*. 2017;2017:1-12.
92. Haag M, Stolk M, Ringe J, Linthout SV, Tschöpe C, Sittlinger M and Seifert M. Immune attributes of cardiac-derived adherent proliferating (CAP) cells in cardiac therapy. *J Tissue Eng Regen Med*. 2013;7:362-370.
93. Dehne T, Adam X, Materne E-M, Reimann MC, Krüger JP, Van Linthout S, Tschöpe C, Haag M, Sittlinger M and Ringe J. A P19 and P19CL6 cell-based complementary approach to determine paracrine effects in cardiac tissue engineering. *Cells Tissues Organs*. 2014;199:24-36.
94. Haag M, Ritterhoff J, Dimura A, Miteva K, Van Linthout S, Tschöpe C, Ringe J and Sittlinger M. Pro-Angiogenic Effect of Endomyocardial Biopsy-Derived Cells for Cardiac Regeneration. *Curr Tissue Eng*. 2013;2:154-159.
95. Szelid Z, Pokreisz P, Liu X, Vermeersch P, Marsboom G, Gillijns H, Pellens M, Verbeken E, Van de Werf F and Collen D. Cardiospecific nitric oxide synthase 3 gene transfer protects against myocardial reperfusion injury. *Basic Res Cardiol*. 2010;105:169-179.
96. Dhingra S, Sharma AK, Arora RC, Slezak J and Singal PK. IL-10 attenuates TNF- $\alpha$ -induced NF $\kappa$ B pathway activation and cardiomyocyte apoptosis. *Cardiovasc Res*. 2009;82:59-66.
97. Ren G, Zhang L, Zhao X, Xu G, Zhang Y, Roberts AI, Zhao RC and Shi Y. Mesenchymal stem cell-mediated immunosuppression occurs via concerted action of chemokines and nitric oxide. *Cell stem cell*. 2008;2:141-150.
98. Miteva K, Van Linthout S, Pappritz K, Müller I, Spillmann F, Haag M, Stachelscheid H, Ringe J, Sittlinger M and Tschöpe C. Human endomyocardial biopsy specimen-derived stromal cells modulate angiotensin II-induced cardiac remodeling. *Stem cells Transl Med*. 2016;5:1707-1718.
99. Jansen\_of\_Lorkeers SJ, Eding JE, Vesterinen HM, van der Spoel TI, Sena ES, Duckers HJ, Doevendans PA, Macleod MR and Chamuleau SA. Similar effect of autologous and allogeneic cell therapy for ischemic heart disease: systematic review and meta-analysis of large animal studies. *Circ Res*. 2015;116:80-86.
100. Detert S, Stamm C, Beez C, Diedrichs F, Ringe J, Van Linthout S, Seifert M, Tschöpe C, Sittlinger M and Haag M. The atrial appendage as a suitable source to generate cardiac-derived adherent proliferating cells for regenerative cell-based therapies. *J Tissue Eng Regen Med*. 2018;12:e1404-e1417.
101. Madonna R, Van Laake LW, Botker HE, Davidson SM, De Caterina R, Engel FB, Eschenhagen T, Fernandez-Aviles F, Hausenloy DJ, Hulot J-S, Lecour S, Leor J, Menasché P, Pesce M, Perrino C, Prunier F, Van Linthout S, Ytrehus K, Zimmermann W-H, Ferdinandy P and Sluijter JPG. ESC Working Group on Cellular Biology of the Heart: position paper for

- Cardiovascular Research: tissue engineering strategies combined with cell therapies for cardiac repair in ischaemic heart disease and heart failure. *Cardiovasc Res.* 2019;115:488-500.
102. Westermann D, Lindner D, Kasner M, Zietsch C, Savvatis K, Escher F, von Schlippenbach J, Skurk C, Steendijk P, Riad A, Poller W, Schultheiss HP and Tschöpe C. Cardiac inflammation contributes to changes in the extracellular matrix in patients with heart failure and normal ejection fraction. *Circ Heart Fail.* 2011;4:44-52.
103. Lindner D, Zietsch C, Becher PM, Schulze K, Schultheiss HP, Tschöpe C and Westermann D. Differential expression of matrix metalloproteases in human fibroblasts with different origins. *Biochem Res Int.* 2012;2012:875742.
104. Baan J, van der Velde ET, de Bruin HG, Smeenk GJ, Koops J, van Dijk AD, Temmerman D, Senden J and Buis B. Continuous measurement of left ventricular volume in animals and humans by conductance catheter. *Circulation.* 1984;70:812-823.
105. Steendijk P, Tulner SAF, Wiemer M, Bleasdale RA, Bax JJ, van der Wall EE, Vogt J and Schalij MJ. Pressure-volume measurements by conductance catheter during cardiac resynchronization therapy. *Eur Heart J Suppl.* 2004;6:D35-D42.
106. Pfaffl MW. Relative quantification *Real-time PCR*: Taylor & Francis; 2007: 89-108.
107. Müller I, Pappritz K, Savvatis K, Puhl K, Dong F, El-Shafeey M, Hamdani N, Hamann I, Noutsias M, Infante-Duarte C, Linke WA, Van Linthout S and Tschöpe C. CX3CR1 knockout aggravates Coxsackievirus B3-induced myocarditis. *PLoS one.* 2017;12:e0182643.
108. Leuschner F, Courties G, Dutta P, Mortensen LJ, Gorbатов R, Sena B, Novobrantseva TI, Borodovsky A, Fitzgerald K and Koteliensky V. Silencing of CCR2 in myocarditis. *Eur heart J.* 2014;36:1478-1488.
109. Pappritz K, Savvatis K, Koschel A, Miteva K, Tschöpe C and Van Linthout S. Cardiac (myo) fibroblasts modulate the migration of monocyte subsets. *Sci Rep.* 2018;8:5575.
110. Shi C and Pamer EG. Monocyte recruitment during infection and inflammation. *Nat Rev Immunol.* 2011;11:762.
111. Shi Y, Fukuoka M, Li G, Liu Y, Chen M, Konviser M, Chen X, Opavsky MA and Liu PP. Regulatory T cells protect mice against coxsackievirus-induced myocarditis through the transforming growth factor beta-coxsackie-adenovirus receptor pathway. *Circulation.* 2010;121:2624-2634.
112. Cao Y, Xu W and Xiong S. Adoptive transfer of regulatory T cells protects against Coxsackievirus B3-induced cardiac fibrosis. *PLoS one.* 2013;8:e74955.
113. Westermann D, Savvatis K, Lindner D, Zietsch C, Becher PM, Hammer E, Heimesaat MM, Bereswill S, Volker U, Escher F, Riad A, Plendl J, Klingel K, Poller W, Schultheiss HP and Tschöpe C. Reduced degradation of the chemokine MCP-3 by matrix metalloproteinase-2 exacerbates myocardial inflammation in experimental viral cardiomyopathy. *Circulation.* 2011;124:2082-2093.
114. Kishimoto C, Kuribayashi K, Masuda T, Tomioka N and Kawai C. Immunologic behavior of lymphocytes in experimental viral myocarditis: significance of T lymphocytes in the severity of myocarditis and silent myocarditis in BALB/c-nu/nu mice. *Circulation.* 1985;71:1247-1254.
115. Savvatis K, Müller I, Fröhlich M, Pappritz K, Zietsch C, Hamdani N, Grote K, Schieffer B, Klingel K and Van Linthout S. Interleukin-6 receptor inhibition modulates the immune reaction and restores titin phosphorylation in experimental myocarditis. *Basic Res Cardiol.* 2014;109:449.
116. Lindner D, Li J, Savvatis K, Klingel K, Blankenberg S, Tschöpe C and Westermann D. Cardiac fibroblasts aggravate viral myocarditis: cell specific coxsackievirus B3 replication. *Mediators Inflamm.* 2014;2014: 519528.
117. Fairweather D, Frisancho-Kiss S, Yusung SA, Barrett MA, Davis SE, Gatewood SJ, Njoku DB and Rose NR. Interferon- $\gamma$  protects against chronic viral myocarditis by reducing mast cell degranulation, fibrosis, and the profibrotic cytokines transforming growth factor- $\beta$ 1, interleukin-1 $\beta$ , and interleukin-4 in the heart. *Am J Pathol.* 2004;165:1883-1894.
118. Spillmann F, Graiani G, Van Linthout S, Meloni M, Campesi I, Lagrasta C, Westermann D, Tschöpe C, Quaini F, Emanuelli C and Madeddu P. Regional and global protective effects of tissue kallikrein gene delivery to the peri-infarct myocardium. *Regen Med.* 2006;1:235-254.

119. Zhang J, Huang X, Wang H, Liu X, Zhang T, Wang Y and Hu D. The challenges and promises of allogeneic mesenchymal stem cells for use as a cell-based therapy. *Stem Cell Res Ther.* 2015;6:234.
120. Consentius C, Reinke P and Volk HD. Immunogenicity of allogeneic mesenchymal stromal cells: what has been seen in vitro and in vivo? *Regen Med.* 2015;10:305-315.
121. Hiel A-L, Hermans D, Vercruyssen J, Gianello P, Poncelet AJ and Zech F. Intracardiac allogeneic mesenchymal stem cell transplantation elicits neo-angiogenesis in a fully immunocompetent ischaemic swine model. *Eur J Cardiothorac Surg.* 2010;38:781-787.
122. Nauta AJ and Fibbe WE. Immunomodulatory properties of mesenchymal stromal cells. *Blood.* 2007;110:3499-3506.
123. El-Shafeey M, Pappritz K, Diedrichs F, Seifert M, Stamm C, Haag M, Sittlinger M, Tschöpe C and Van Linthout S. Cardioprotective and immunomodulatory effects of endomyocardial biopsy- and atrial appendage-derived stromal cells in an acute model of Coxsackievirus B3-induced myocarditis. *Eur J Heart Fail.* 2018;20:517. P1982.
124. Griffin MD, Ryan AE, Alagesan S, Lohan P, Treacy O and Ritter T. Anti-donor immune responses elicited by allogeneic mesenchymal stem cells: what have we learned so far? *Immunol Cell Biol.* 2013;91:40-51.
125. Lapiere CM, Nusgens B and Pierard G. Interaction between collagen type I and type III in conditioning bundles organization. *Connect Tissue Res.* 1977;5:21-29.
126. Pauschinger M, Knopf D, Petschauer S, Doerner A, Poller W, Schwimmbeck PL, Kühl U and Schultheiss H-P. Dilated cardiomyopathy is associated with significant changes in collagen type I/III ratio. *Circulation.* 1999;99:2750-2756.
127. Glenn JD and Whartenby KA. Mesenchymal stem cells: emerging mechanisms of immunomodulation and therapy. *World J Stem Cells.* 2014;6:526.
128. Zhou Y, Day A, Haykal S, Keating A and Waddell TK. Mesenchymal stromal cells augment CD4<sup>+</sup> and CD8<sup>+</sup> T-cell proliferation through a CCL2 pathway. *Cytotherapy.* 2013;15:1195-1207.
129. Kruppenbacher JP, Arnold G, Mertens T, Fischer A, Zimmermann J and Eggers HJ. Outbred mice infected by an encephalomyocarditis virus variant: A model for studying chronic viral heart disease. *Virchows Archiv A.* 1993;422:405-413.
130. Merkle I, Tonew M, Glück B, Schmidtke M, Egerer R and Stelzner A. Coxsackievirus B3-induced chronic myocarditis in outbred NMRI mice. *J Hum Virol.* 1999;2:369-379.
131. Glück B, Schmidtke M, Merkle I, Stelzner A and Gemsa D. Persistent Expression of Cytokines in the Chronic Stage of CVB3-induced Myocarditis in NMRI Mice. *J Mol Cell Cardiol.* 2001;33:1615-1626.
132. Kühl U, Pauschinger M, Schwimmbeck PL, Seeberg B, Lober C, Noutsias M, Poller W and Schultheiss HP. Interferon-beta treatment eliminates cardiotropic viruses and improves left ventricular function in patients with myocardial persistence of viral genomes and left ventricular dysfunction. *Circulation.* 2003;107:2793-2798.
133. Kühl U, Lassner D, von Schlippenbach J, Poller W and Schultheiss HP. Interferon-Beta improves survival in enterovirus-associated cardiomyopathy. *J Am Coll Cardiol.* 2012;60:1295-1296.
134. Lassner D, Siegismund CS, Kühl U, Rohde M, Stroux A, Escher F and Schultheiss HP. CCR5del32 genotype in human enteroviral cardiomyopathy leads to spontaneous virus clearance and improved outcome compared to wildtype CCR5. *J Transl Med.* 2018;16:249.
135. Casellas J. Inbred mouse strains and genetic stability: a review. *Animal.* 2011;5:1-7.
136. Leipner C, Grün K, Schneider I, Glück B, Sigusch HH and Stelzner A. Coxsackievirus B3-induced myocarditis: differences in the immune response of C57BL/6 and Balb/c mice. *Med Microbiol Immunol.* 2004;193:141-147.
137. Frizelle S, Schwarz J, Huber SA and Leslie K. Evaluation of the effects of low molecular weight heparin on inflammation and collagen deposition in chronic coxsackievirus B3-induced myocarditis in A/J mice. *Am J Pathol.* 1992;141:203-209.
138. Okada I, Matsumori A, Tomioka N and Kawai C. Successive infection of coxsackievirus B3 and encephalomyocarditis virus: an animal model of chronic myocarditis. *J Pathol.* 1992;167:341-347.

139. Marijjanowski MM, Teeling P, Mann J and Becker AE. Dilated cardiomyopathy is associated with an increase in the type I/type III collagen ratio: a quantitative assessment. *J Am Coll Cardiol*. 1995;25:1263-1272.
140. Bardina SV, Michlmayr D, Hoffman KW, Obara CJ, Sum J, Charo IF, Lu W, Pletnev AG and Lim JK. Differential roles of chemokines CCL2 and CCL7 in monocytoysis and leukocyte migration during West Nile virus infection. *J Immunol*. 2015;195:4306-4318.
141. Afanasyeva M, Georgakopoulos D, Belardi DF, Bedja D, Fairweather D, Wang Y, Kaya Z, Gabrielson KL, Rodriguez ER and Caturegli P. Impaired up-regulation of CD25 on CD4<sup>+</sup> T cells in IFN- $\gamma$  knockout mice is associated with progression of myocarditis to heart failure. *Proc Natl Acad Sci*. 2005;102:180-185.

## 7. List of Figures

1.1. Development of viral causes of myocarditis over time.....	2
1.2. Different phases of Coxsackievirus-mediated myocarditis.....	3
1.3. Specific surface antigen expression of EMB-CardAPs.....	8
1.4. Three-dimensional blot showing the principal component analysis of EMB-CardAPs.....	8
2.1. EMB-CardAPs and EMB-CF differ in their proteoform expression.....	12
3.1. Isolation of CardAPs from an endomyocardial biopsy via outgrowth culture.....	21
3.2. Isolation of CardAPs from the right atrial appendage via outgrowth culture and subsequent immunomagnetic sorting.....	22
3.3. Experimental design for the evaluation of EMB-CardAPs and EMB-CF in acute Coxsackievirus B3-induced myocarditis mice.....	24
3.4. Experimental design for the evaluation of RAA-CardAPs in acute Coxsackievirus B3-induced myocarditis mice.....	25
3.5. Experimental design for the chronic Coxsackievirus B3-induced myocarditis model.....	25
3.6. Experimental design for the evaluation of RAA-CardAPs in chronic Coxsackievirus B3-induced myocarditis mice.....	26
3.7. Left panel depicts the left ventricle and the correct position of the conductance catheter, whereas the right panel illustrates the complete cardiac cycle represented by the pressure volume loop showing the points of opening and closing of the aortic and mitral valves. ....	27
3.8. Figure illustrates a conductance catheter of Millar system positioned in a 0.9% saline solution.....	27
3.9. Scheme illustrating the surgical procedure of the PV loop catheterization in an open chest mouse showing.....	29
3.10. Hemodynamic analysis at baseline.....	29
3.11. Hemodynamic analysis of saline.....	30
3.12. Hemodynamic analysis of occlusion.....	31
3.13. Illustration of A. the amplification curve for real-time PCR showing the threshold line and the Ct value and B. The delta C method for normalization.....	34
3.14. Principle of the Avidin-Biotin Complex (Dako guide 6th ed.).....	36
3.15. The Envision™ polymer-based method (Dako guide 6th ed.).....	37
4.1.1. Impact of intravenous injection of EMB-CardAPs and EMB-CF on the left ventricular function in acute Coxsackievirus B3-induced myocarditis mice.....	39
4.1.2. Impact of intravenous injection of EMB-CardAPs and EMB-CF on left ventricular collagen expression in acute Coxsackievirus B3-induced myocarditis mice.....	41
4.1.3. Impact of intravenous injection of EMB-CardAPs and EMB-CF on left ventricular chemokine mRNA expression in acute Coxsackievirus B3-induced myocarditis mice.....	42
4.1.4. Impact of intravenous injection of EMB-CardAPs and EMB-CF on left ventricular chemokine receptor mRNA expression in acute Coxsackievirus B3-induced myocarditis mice.....	43
4.1.5. Impact of intravenous injection of EMB-CardAPs and EMB-CF on left ventricular immune cell presence in acute Coxsackievirus B3-induced myocarditis mice.....	44
4.1.6. Impact of intravenous injection of EMB-CardAPs and EMB-CF on left ventricular cytokine mRNA expression in acute Coxsackievirus B3-induced myocarditis mice.....	45
4.1.7. Impact of intravenous injection of EMB-CardAPs and EMB-CF on left ventricular mRNA expression of apoptotic markers in acute Coxsackievirus B3-induced myocarditis mic.....	46

4.1.8. Impact of intravenous injection of EMB-CardAPs and EMB-CF on left ventricular Cxsackievirus B3 mRNA expression in acute Cxsackievirus B3-induced myocarditis mice.....	47
4.2.1. Cxsackievirus B3 infection does not hamper the viability of RAA-CardAPs.....	48
4.2.2. RAA-CardAPs reduce Cxsackievirus B3-induced apoptosis of DiO-labeled HL-1 cardiomyocytes.....	49
4.2.3. RAA-CardAPs do not decrease Cxsackievirus B3 mRNA expression in a co-culture of DiO-labeled HL-1 cardiomyocytes with RAA-CardAPs.....	49
4.3.1. Impact of intravenous injection of RAA-derived CardAPs on the left ventricular function in acute Cxsackievirus B3-induced myocarditis mice.....	50
4.3.2. Impact of intravenous injection of RAA-derived CardAPs on left ventricular collagen expression in acute Cxsackievirus B3-induced myocarditis mice.....	51
4.3.3. Impact of intravenous injection of RAA-derived CardAPs on left ventricular chemokine mRNA expression in acute Cxsackievirus B3-induced myocarditis mice.....	52
4.3.4. Impact of intravenous injection of RAA-derived CardAPs on left ventricular chemokine receptors mRNA expression in acute Cxsackievirus B3-induced myocarditis mice.....	53
4.3.5. Impact of intravenous injection of RAA-derived CardAPs on left ventricular immune cell presence in acute Cxsackievirus B3-induced myocarditis mice.....	54
4.3.6. Impact of intravenous injection of RAA-derived CardAPs on left ventricular cytokine mRNA expression in acute Cxsackievirus B3-infected mice.....	55
4.3.7. Impact of intravenous injection of RAA-derived CardAPs on left ventricular mRNA expression of apoptotic markers in acute Cxsackievirus B3-induced myocarditis mice.....	56
4.3.8. Impact of intravenous injection of RAA-derived CardAPs on left ventricular Cxsackievirus B3 mRNA expression in acute Cxsackievirus B3-induced myocarditis mice.....	56
4.4.1. Impact of Cxsackievirus B3 infection on the left ventricular function of NMRI mice at day 28 post infection.....	58
4.4.2. Impact of Cxsackievirus B3 infection on the left ventricular collagen expression in NMRI mice at day 28 post infection.....	59
4.4.3. Impact of Cxsackievirus B3 infection on the left ventricular chemokine mRNA expression in NMRI mice at day 28 post infection.....	60
4.4.4. Impact of Cxsackievirus B3 infection on the left ventricular mRNA expression of chemokine receptors in NMRI mice at day 28 post infection.....	60
4.4.5. Impact of Cxsackievirus B3 infection on left ventricular immune cell presence in NMRI mice at day 28 post infection.....	62
4.4.6. Impact of Cxsackievirus B3 infection on left ventricular cytokine mRNA expression in NMRI mice at day 28 post infection.....	62
4.4.7. Impact of Cxsackievirus B3 infection on left ventricular mRNA expression of apoptotic markers in NMRI mice at day 28 post infection.....	63
4.3.8. Impact of Cxsackievirus B3 infection on left ventricular Cxsackievirus B3 mRNA expression in NMRI mice at day 28 post infection.....	63
4.5.1. Impact of intravenous injection of RAA-CardAPs on the left ventricular function in Cxsackievirus B3-infected NMRI.....	65
4.5.2. Impact of intravenous injection of RAA-derived CardAPs on left ventricular collagen I expression in chronic Cxsackievirus B3-infected NMRI mice.....	66
4.5.3. Impact of intravenous injection of RAA-derived CardAPs on left ventricular chemokine mRNA expression in Cxsackievirus B3-infected NMRI mice.....	67
4.5.4. Impact of intravenous injection of RAA-derived CardAPs on left ventricular chemokine-receptors mRNA expression in Cxsackievirus B3-infected NMRI mice.....	68

4.5.5. Impact of intravenous injection of RAA-derived CardAPs on left ventricular immune cell presence in chronic Coxsackievirus B3-infected NMRI mice.....	68
4.5.6. Impact of intravenous injection of RAA-derived CardAPs on left ventricular mRNA expression of cytokines in Coxsackievirus B3-infected NMRI mice.....	69
4.5.7. Impact of intravenous injection of RAA-derived CardAPs on left ventricular mRNA expression of apoptotic markers in Coxsackievirus B3-infected NMRI mice.....	70
4.5.8. Impact of intravenous injection of RAA-derived CardAPs on left ventricular Coxsackievirus B3 mRNA expression in Coxsackievirus B3-infected NMRI mice.....	71

## 8. List of Tables

1.1. Comparison of EMB-CardAPs and RAA-CardAPs.....	11
3.1. Laboratory Equipment.....	13
3.2. Laboratory consumables.....	14
3.3. Chemicals and reagents.....	14
3.4. Reporter assays.....	16
3.5. Coxsackievirus B3 primers.....	17
3.6. Kits .....	17
3.7. Cell culture media and reagents.....	17
3.8. Cell culture medium composition.....	18
3.9. Antibodies for immunohistochemistry.....	19
3.10. Antibodies/kits for flow cytometry.....	19
3.11. Coxsackievirus B3.....	19
3.12. Software.....	20
3.13. Measured hemodynamic parameters.....	31
3.14. Reaction mixtures for cDNA reverse transcription.....	33
3.15. Real-time PCR reaction mixture with Taqman Universal PCR master mix.....	35
3.16. Coxsackievirus B3 Real-time PCR reaction mixture with Taqman Universal PCR master mix.....	35
3.17. Antibodies and dilutions used with the ABC method.....	37
3.18. Antibodies and dilutions used with the Envision™ method.....	38

## 9. Complete list of publications

### Monograph:

1. **M EI-Shafeey**, H EI-Adawi, D Al-Azhari, A Abd EI-Wahab and M Abdel-Mohsen. (2010): "Effect of Silymarin and Grape seed extracts on the recovery of fumonisin B1 toxicity in rats"- **M.Sc**

### Further publications:

#### 1) Publications with peer review process

- a) H EI-Adawi\*, D EI-Azhary\*, A Abd EI-Wahab, **M EI-Shafeey** and M Abdel-Mohsen (2011): Protective effect of milk thistle and grape seed extracts on fumonisin B1 induced hepatoandnephro-toxicity in rats. *Journal of Medicinal Plants Research*. 5(27):6316-6327
- b) **M EI-Shafeey\***, H EI-Adawi, D Al-Azhari, A Abd EI-Wahab and M Abdel-Mohsen (2012): Synergistic Effect of Milk Thistle and Grape Seed Extracts on the Recovery of Fumonisin b1Toxicity in Rats. *Egypt. Acad. J. Biolog. Sci., C. Physiology & Molecular Biology*. 4(1): 63-85
- c) K Miteva, K Pappritz, **M EI-Shafeey**, J Ringe, C Tschöpe\*, S Van Linthout\* (2016): Mesenchymal stromal cells modulate monocytes trafficking in Cocksackievirus B3-induced myocarditis. *Stem cells Translational medicine*. 6(4):1249-1261
- d) I Müller, K Pappritz, K Savvatis, K Puhl, F Dong, **M EI-Shafeey**, N Hamdani, I Hamann, M Noutsias, C Infante-Duarte, WA Linke, S Van Linthout\*, C Tschöpe\* (2017): CX3CR1 knockout aggravates Cocksackievirus B3-induced myocarditis. *PlosOne*. 12(8): e0182643
- e) TM Tamer\*, MA Hassan\*, AM Omer\*, WMA Baset, ME Hassan, **M EI-Shafeey**, MS Mohy Eldin (2016): Synthesis, characterization and antimicrobial evaluation of two aromatic chitosan Schiff base derivatives. *Process Biochemistry*TM Tamer\*, KValachova, MA Hassan, AM Omar, **M EI-Shafeey**, MS Mohy Eldin, L Soltes (2018): Chitosan/hyaluronan/edaravone membranes for anti-inflammatory wound dressing: *In vitro* and *in vivo* evaluation studies. *Materials Science and Engineering: C*. 51(10): 1721-1730
- f) K Miteva, K Pappritz, M Sosnowski, **M EI-Shafeey**, I Müller, F Dong, K Savvatis, J Ringe, C Tschöpe\*, S Van Linthout\* (2018): Mesenchymal stromal cells inhibit NLRP3 inflammasome activation in a model of Cocksackievirus B3-induced inflammatory cardiomyopathy. *Scientific Reports*. 8:2820

- g) **M El-Shafeey\***, K Pappritz\*, F Diedrichs, M Seifert, C Stamm, M Haag, M Sittinger, C Tschöpe, S Van Linthout: Cardioprotective and immunomodulatory effects of right atrial appendage-derived stromal cells in an acute model of Coxsackievirus B3-induced myocarditis (Manuscript in preparation).

## 2) Submitted publications with peer review process

- a) K Pappritz, J Grune, O Klein, F Dong, **M El-Shafeey**, J Lin, WM Kübler, U Kintscher, C Tschöpe, S Van Linthout (**Submitted**): Two-dimensional speckle-tracking echocardiography assesses time-dependent alteration of myocardial deformation in experimental diabetic cardiomyopathy.
- b) K Pappritz, F Dong, N Hamdani, O Klein, A Kovacs, K Miteva, **M El-Shafeey**; B Kerim, Li O'Flynn, SJ Elliman, C Tschöpe, S Van Linthout (**Submitted**): Impact of CD362+-selected mesenchymal stromal cells in db/db mice at an early onset of diabetic cardiomyopathy.

## 3) Abstracts and posters

- a) **M El-Shafeey**, K Pappritz, F Diedrichs, M Seifert, C Stamm, M Haag, M Sittinger, C Tschöpe, S Van Linthout: Cardioprotective and immunomodulatory effects of endomyocardial biopsy and atrial appendage-derived stromal cells in an acute model of Coxsackievirus B3-induced myocarditis. European Heart Journal, Volume 20, Issue suppl\_1, 517 May 2018, P1982.
- b) S Van Linthout, K Pappritz, J Lin, M Sosnowski, **M El-Shafeey**, C Tschöpe: Colchicine reduces NLRP3 inflammasome activity in murine Coxsackievirus B3-induced myocarditis. European Heart Journal, Volume 39, Issue suppl\_1, August 2018, P2845.
- c) K Pappritz, J Grune, O Klein, F Dong, **M El-Shafeey**, J Lin, C Tschöpe, S Van Linthout: Extracellular matrix turnover influences myocardial contraction behavior in diabetic cardiomyopathy assessed by two-dimensional speckle-tracking echocardiography. European Heart Journal, Volume 39, Issue suppl\_1, August 2018, P2842.

## 10. Acknowledgments

This study was carried out at the Berlin-Brandenburg Center for Regenerative Therapies (BCRT), Charité, Universitätsmedizin Berlin, during the years 2015-2019, funded by the Egyptian ministry of higher education-cultural affairs and missions sector.

First, I am very grateful to Professor Carsten Tschöpe for accepting me to work and perform my dissertation after 4 years of laboratory work in his group. It was my honor to do my doctoral thesis in such an international working group. I had the great chance to do research in the field of inflammatory cardiomyopathy.

I wish to express my deepest gratitude and thanks to my supervisor PD Dr. Sophie Van Linthout, for introducing me to the immunocardiology field, and for the great opportunity to write my dissertation at the Berlin-Brandenburg Center for Regenerative Therapies. Dr. Sophie's great research experience and profound knowledge of science helped me to achieve my dissertation in a good time. I would like to appreciate her time to listen, her valuable discussion, critical reading of the manuscript and continuous encouragement, which gave me more confidence.

My sincere thanks go to Professor Jens Kurreck, for his acceptance to enroll me for the Dr.rer.nat at the institute of Biotechnology, at faculty III of the TU.

My special thanks go to Dr Kathleen Pappritz, who helped from the start to integrate in the group, to achieve my *in vivo* work by training me in the *in vivo* lab. She also helped me in the analysis of data. She always had or took the time to answer my questions

I wish to express my gratitude and thanks to Dr Irene Muller, who helped me in the translation of the thesis abstract to German.

I am also greatly indebted to my group for the great time. They supported me both scientifically and morally right from the beginning. I would like to thank Kerstin Puhl, Annika Koschel, and Marzena Sosnowski, for their excellent technical assistance, constant support and training in the lab. I also would like to thank Fenqguan Dong for training me the hemodynamic measurement. I am so glad to have all such colleagues.

Finally, I want to thank my whole family. I would like to express my special thanks to my wife for the endless support during my entire doctoral thesis. My great thanks go to my mother, brothers and sisters in Egypt. They have supported me in every situation. Without the great support of my family, I would not have achieved it this far. Many thanks for my friends for their constant support and encouragement.

## **11. Declaration**

I hereby declare that I have written my own dissertation on the topic " Impact of stromal cells on Coxsackievirus B3-induced myocarditis" and have not already used it as a dissertation and resources used have been completely stated.

Muhammad El-Shafeey